

6  
4/75-13

LIBRARIES  
COLORADO STATE UNIVERSITY  
FORT COLLINS, COLORADO

VERIFICATION OF A MATHEMATICAL MODEL  
FOR WOOD JOIST FLOOR SYSTEMS

J.S. Liu  
J.R. Goodman  
M.E. Criswell  
J. Bodig  
E.G. Thompson  
M.D. Vanderbilt



Structural Research Report No. 11<sup>12</sup>  
Civil Engineering Department  
Colorado State University  
Fort Collins, Colorado 80523

August 1974

CER 74-75 JSL-JRG-MEC-JB-EQT-MDV

VERIFICATION OF A MATHEMATICAL MODEL  
FOR WOOD JOIST FLOOR SYSTEMS

J.S. Liu

J.R. Goodman

M.E. Criswell

J. Bodig

E.G. Thompson

M.D. Vanderbilt



Structural Research Report No. ~~41~~ 12  
Civil Engineering Department  
Colorado State University  
Fort Collins, Colorado 80523

August 1974

TA7

.CG

CER 74 / 75-13

## ABSTRACT OF THESIS

### VERIFICATION OF A MATHEMATICAL MODEL FOR WOOD JOIST FLOOR SYSTEMS

The primary objective of this study is to develop verification for the validity of a mathematical model for the behavior of wood joist floor systems under working loads. This complex, multi-layered structural system consists of joists acting in incomplete composite and two-way behavior with one or more layers of sheathing. This physical system is simulated by a crossing-beam model consisting of a perpendicular set of T-beams and sheathing strips in developing the mathematical model.

To allow the use of ordinary beam theory in evaluating the behavior of the T-beam elements, the effective flange width of the incomplete composite sheathing elements was required. An essential part of this study was the derivation and quantification of the effective flange width for a wide variety of parameters.

Two solution techniques are presented for the mathematical model, a finite difference method and a more versatile finite element procedure. Methods are developed to evaluate the effect of gaps in the sheathing layers and the results of the effective flange width study are utilized in the theoretical solutions.

A total of twenty-two full-scale floor tests are conducted as part of an experimental program to provide the necessary data for verification of the mathematical model. Generally excellent agreement was obtained between the computed and the measured results. An average algebraic error of +3.24 percent was obtained for the computed results as compared to the measured deflection for the

twenty-two specimens studied. As indicated, the predicted values from application of the mathematical model are generally conservative.

The verified mathematical model was used to evaluate extreme cases to assess individual effects of composite and two-way action of wood joist floors. In addition, parameter studies were conducted to isolate the effects of major variables. The verified model provides the basis for future development of improved design criteria for wood joist structural systems.

Jeong-Shwu Liu  
Civil Engineering Department  
Colorado State University  
Fort Collins, Colorado 80521  
August, 1974

## ACKNOWLEDGMENTS

The author wishes to thank Professors J. R. Goodman, E. G. Thompson, M. E. Criswell, J. Bodig and M. D. Vanderbilt for serving as members of his graduate committee. In particular, sincere appreciation is due to Professor Goodman for his continuous and inspiring guidance throughout the course of this study. Gratitude is also owed to Professors Vanderbilt and Thompson for their direction in use of computer programs.

Acknowledgment is also due to the National Science Foundation for their support of this research study and the author's graduate assistantship through their Grant No. GK-30853 entitled "A Rational Analysis and Design Procedure for Wood Joist Floor Systems."

Finally, a special thanks to the author's wife, Shun-Ying, for her devotion, sacrifice and continual encouragement during the years for the completion of the degree.

## TABLE OF CONTENTS

<u>Chapter</u>	<u>Page</u>
ABSTRACT . . . . .	iii
ACKNOWLEDGMENTS . . . . .	v
LIST OF TABLES . . . . .	ix
LIST OF FIGURES . . . . .	x
NOTATIONS . . . . .	xiii
1. INTRODUCTION AND LITERATURE REVIEW . . . . .	1
1.1 Introduction . . . . .	1
1.1.1 Purpose of Floor Project . . . . .	2
1.1.2 Phases of Floor Project . . . . .	4
1.2 Literature Review . . . . .	7
1.2.1 Experimental Investigations . . . . .	8
1.2.2 Theoretical Consideration . . . . .	11
2. THEORETICAL DEVELOPMENT . . . . .	16
2.1 Introduction . . . . .	16
2.2 Layered Beam Theory and Effective Flange Considerations . . . . .	17
2.2.1 Basic Derivation of Layered Beam Theory . . . . .	18
2.2.2 Derivation of Transformation for MOE of Plywood . . . . .	21
2.2.3 Development of the Theory of Effective Flange Width . . . . .	25
2.2.4 Effect of Gaps in the Analysis of Floors and the Solution by Finite Element Method . . . . .	37
2.3 Theoretical Development of Floor Analysis Method . . . . .	38
2.3.1 General Development of the Governing Equations of the Layered Beam Systems with Interlayer Slip . . . . .	39
2.3.2 Finite Difference Approach . . . . .	40
2.3.3 Finite Element Approach . . . . .	52
2.4 Implication and Limiting Cases for Floor Model . . . . .	63
3. EXPERIMENTAL STUDY . . . . .	68
3.1 Introduction . . . . .	68
3.2 Material Used for Floor Specimens . . . . .	72

<u>Chapter</u>	<u>Page</u>
3.3	Material Properties . . . . . 73
3.3.1	Joist Properties . . . . . 74
3.3.2	Sheathing Properties . . . . . 75
3.3.3	Connector Properties . . . . . 77
3.4	Construction of Floor Specimens . . . . . 79
3.5	Testing Equipment . . . . . 82
3.6	Testing Procedures . . . . . 84
3.7	Experimental Behavior of Floor Specimens . . . . . 87
3.7.1	Effect of Connectors . . . . . 88
3.7.2	Effect of Gaps in the Sheathing Layer . . . . . 90
3.7.3	Effect of Numbers of Sheathing Layers . . . . . 93
3.7.4	Nonlinear Behavior and Mode of Failure . . . . . 95
4.	VERIFICATION OF THE MATHEMATICAL FLOOR MODEL . . . 98
4.1	Introduction . . . . . 98
4.2	Mathematical Floor Model Used in the Verification Study . . . . . 98
4.3	Input Data of Floor Specimens . . . . . 99
4.4	Selection of the Values of Slip Modulus . . . 100
4.5	Comparison of Computed and Experimental Results . . . . . 104
5.	PARAMETER STUDIES AND DEMONSTRATIONS . . . . . 116
5.1	Introduction . . . . . 116
5.2	Example Floor Specimen Used in Parameter Study . . . . . 116
5.3	Effects of Parameters on Floor Behavior . . . . . 117
5.3.1	Effect of Slip Modulus . . . . . 118
5.3.2	Effect of Joist MOE . . . . . 121
5.3.3	Effect of Effective Flange Width . . . 121
5.4	Parameter Studies of Effective Flange Width . . . . . 125
5.4.1	Effect of Sheathing Thickness . . . . 128
5.4.2	Effect of Joist Depth . . . . . 130
5.4.3	Effect of Slip Modulus . . . . . 130
5.4.4	Effect of Sheathing MOE . . . . . 134
5.4.5	Effect of Available Flange Width . . . 137
6.	SUMMARY AND CONCLUSIONS . . . . . 143

Chapter

Page

REFERENCES . . . . .	147
APPENDIX A TABLE OF MOE TRANSFORMATION CONSTANT FOR PLYWOOD . . . . .	150
APPENDIX B DETAILED DATA OF FLOOR SPECIMENS . . .	152
APPENDIX C AVERAGE CONNECTOR SLIP MODULI VALUES .	161
APPENDIX D COMPUTED VERSUS MEASURED DEFLECTIONS OF FLOOR SPECIMENS . . . . .	163
APPENDIX E LISTING OF A COMPUTER PROGRAM FOR EVALUATING EFFECTIVE FLANGE WIDTH OF T-BEAM SYSTEMS . . . . .	182

LIST OF TABLES

<u>Table</u>		<u>Page</u>
3.1	General Data of Floor Specimens . . . . .	70
4.1	Values of Slip Modulus, $k$ . . . . .	105
4.2	Slip Modulus, $k$ , Used for Floor Specimens . . . . .	106
4.3	Comparison of Computed and Experimental Results . . . . .	113
5.1	Recommended Effective Flange Width for Uniform Load . . . . .	141

## LIST OF FIGURES

<u>Figure</u>		<u>Page</u>
2.1	Two Layered Beam System . . . . .	19
2.2	Original and Transformed Cross Sections of a Strip of Three-ply Plywood with Unit Width . . . . .	23
2.3	Strain and Stress Distributions Over the Transformed Cross Section of Plywood Subjected to Bending . . . . .	23
2.4	Strain and Stress Distributions Over the Transformed Cross Section of Plywood Subjected to Axial Force . . . . .	23
2.5	Layout and Sign Convention of T-beam . . . . .	27
2.6	Beam Element with Force and Moment Components .	31
2.7	Five-Layer Example of m-Layer System . . . . .	41
2.8	Physical Model of a Floor System . . . . .	44
2.9	Finite Difference Model and Boundary Conditions . . . . .	46
2.10	Finite Difference Model of Sheathing Beam . . .	51
2.11	Finite Element Model of Layered Beam . . . . .	54
2.12	Interlayer Slip Related to Deformation . . . . .	57
2.13	Example Floor for Parameter Studies . . . . .	64
2.14	Deflection Curves of Limiting Cases for an Example Floor . . . . .	65
3.1	Detail of Joist Header Construction . . . . .	76
3.2	Typical Load-Deflection Plot for MOE Test . . .	76
3.3	Nail Slip Modulus Test Specimens . . . . .	78
3.4	Typical Load-Slip Curve . . . . .	80
3.5	55-Kip MTS Loading Actuator and Support Frame . . . . .	83
3.6	The Configuration of Sheathing Gaps for Load Testing of Specimen F5-8D16-1 . . . . .	86

<u>Figure</u>		<u>Page</u>
3.7	Two Stages of Connection During Load Tests for Three-Layer Specimens . . . . .	89
3.8	Effect of Type of Connector . . . . .	91
3.9	Effect of Nail Spacing . . . . .	92
3.10	Effect of Gaps in the Sheathing . . . . .	94
3.11	Deflection Behavior of a Floor as a Function of Number of Layers . . . . .	96
4.1	Layout and Data of Specimen F2-8D16-1 . . . . .	101
4.2	Computed vs Measured Results of Specimen F2-8D16-1 . . . . .	102
4.3	Layout and Data of Specimens F6-8E16-1 and F6-8E16-2 . . . . .	103
4.4	Computed vs Measured Results of Specimen F6-8E16-1 . . . . .	109
4.5	Computed vs Measured Results of Specimen F6-8E16-2 (Nails of Top Layer Not Driven into Joist) . . . . .	110
4.6	Computed vs Measured Results of Specimen F6-8E16-2 (Nails of Top Layer Driven into Joist) . . . . .	111
5.1	Deflections vs Slip Modulus, k, Concentrated Load . . . . .	119
5.2	Deflections vs Slip Modulus, Uniform Load . . . . .	120
5.3	Joist MOE vs Deflections, Concentrated Load . . . . .	122
5.4	Deflections vs Joist MOE, Uniform Load . . . . .	123
5.5	Effective Flange Width vs Deflections, Concentrated Load . . . . .	124
5.6	Effective Flange Width vs Deflections, Uniform Load . . . . .	126
5.7	Effective Flange Width vs Sheathing Thickness, Concentrated Load . . . . .	127

<u>Figure</u>		<u>Page</u>
5.8	Effective Flange Width vs Sheathing Thickness, Uniform Load . . . . .	129
5.9	Effective Flange Width vs Joist Depth, Concentrated Load . . . . .	131
5.10	Effective Flange Width vs Joist Depth, Uniform Load . . . . .	132
5.11	Effective Flange Width vs Slip Modulus, Concentrated Load . . . . .	133
5.12	Effective Flange Width vs Slip Modulus, Uniform Load . . . . .	135
5.13	Effective Flange Width vs MOE of Sheathing, Concentrated Load . . . . .	136
5.14	Effective Flange Width vs MOE of Sheathing, Uniform Load . . . . .	138
5.15	Effective Flange Width vs Available Flange Width, Concentrated Load . . . . .	139
5.16	Effective Flange Width vs Available Flange Width, Uniform Load . . . . .	140

## NOTATIONS

- $A$  = Matrix of total forces applied on floor at nodal points  
 $A_g$  = Gross cross-sectional area of plywood  
 $A_i$  = Gross cross-sectional area of the  $i^{\text{th}}$  layer  
 $A_i^*$  = Transformed cross-sectional area of the  $i^{\text{th}}$  layer  
 $A_n$  = Constant coefficient of flange stress solution equation  
 $A_t$  = Transformed cross-sectional area of plywood  
 $AS$  = Matrix of total force on sheathing strips at nodal points  
 $AT$  = Matrix of total force on T-beams at nodal points  
 $B_n$  = Constant coefficient of flange stress solution equation  
 $C_i$  = Constant relating  $y$  and  $F$  solutions  
 $C_{i,i+1}$  = Centroidal distance between  $i^{\text{th}}$  and  $j^{\text{th}}$  layers  
 $C_n$  = Constant coefficient of flange stress solution equation  
 $C_p$  = Constant relating the elastic parameters and dimension of plywood  
 $D$  = Matrix of floor deflections at nodal points  
 $D_n$  = Constant coefficient of flange stress solution equation  
 $DS$  = Matrix of total sheathing strip deflections at nodal points  
 $DT$  = Matrix of total T-beam deflections at nodal points  
 $E$  = Percentage of effective flange width with respect to available flange width  
 $E_{1x}$  = MOE of first layer in x-direction  
 $E_{ea}$  = Effective MOE of plywood in axial loading  
 $E_{eb}$  = Effective MOE of plywood in bending

- $E_i$  = MOE of  $i^{\text{th}}$  layer  
 $E_{in}$  = MOE of inner ply of plywood  
 $E_o$  = MOE of outermost ply of plywood  
 $\{F\}$  = Vector of total vertical forces of floor at nodal point  
 $F_i$  = Axial force in  $i^{\text{th}}$  layer  
 $F_L$  = Axial force on the left side of a concentrated load  
 $f_n$  = Constant relating elastic parameters and dimensions of plywood  
 $F_n$  = Coefficient of the Fourier series expansion for moment  
 $G$  = Shear modulus  
 $g_n$  = Constant relating elastic parameters and dimensions of plywood  
 $[H]$  = Flexibility matrix of T-beam  
 $h_i$  = Depth of  $i^{\text{th}}$  layer  
 $H_n$  = Constant relating elastic parameters and dimensions of plywood  
 $I_g$  = Gross moment of inertia  
 $I_i$  = Moment of inertia of  $i^{\text{th}}$  layer  
 $I_t$  = Transformed moment of inertia  
 $J$  = Total energy of a layered beam system  
 $J^b$  = Energy due to bending action  
 $J^c$  = Energy due to interlayer slip  
 $J^q$  = Energy due to external loading  $q$   
 $J^u$  = Energy due to axial deformation  
 $\delta J$  = Variation of total energy  $J$

- $k$  = Slip modulus of connector  
 $K^*$  = Transformation constant of MOE for plywood  
 $[K]$  = Total stiffness matrix of finite element formulation of layered beam system  
 $L$  = Span of beam  
 $M_i$  = Bending moment in the  $i^{\text{th}}$  layer  
 $M_T$  = Total moment on a cross-section  
 $n$  = Number of rows of connectors across the joist width  
 $n_L$  = Number of layers of a layered beam system  
 $[N_u]$  = Shape functions of the axial deformations of a layered beam system  
 $[N_y]$  = Shape functions of the deflections and slopes of a layered beam system  
 $P$  = Concentrated load  
 $Q$  = Shear force transmitted by each connector  
 $q$  = Uniform load  
 $q_{i,i+1}$  = Shear flow transmitted between the  $i^{\text{th}}$  and  $(i+1)^{\text{th}}$  layers  
 $r_i$  = Distance from the centroid of beam to the centroid of  $i^{\text{th}}$  layer  
 $r_n$  = Constant relating the elastic parameters and dimensions of plywood  
 $s$  = Connector spacing along joist length  
 $\Delta s$  = Interlayer slip  
 $\{S\}$  = Vector of axial deformations, deflections and slopes at the nodal points of a beam system  
 $s_n$  = Constant relating the elastic parameters and dimensions of plywood  
 $t_i$  = Thickness of  $i^{\text{th}}$  ply of a strip of plywood  
 $T.C.$  = A transfer constant relating  $I_s$  and the summation of  $I$

- $u$  = Deformation in x-direction  
 $\{U_i\}_j$  = Vector of the axial deformations of the  $i^{\text{th}}$  layer at the  $j^{\text{th}}$  nodal point  
 $V$  = Shear force on the cross-section of a beam  
 $w$  = Deformation in z-direction  
 $w_e$  = Effective flange width  
 $w_i$  = Width of the first layer  
 $x$  = Distance along the beam length  
 $y$  = Beam deflection  
 $y_L$  = Beam deflection on the left-hand side of a concentrated load  
 $y_R$  = Beam deflection on the right-hand side of a concentrated load  
 $y_s$  = Beam deflection of a rigidly connected layered beam system  
 $\{Y\}_j$  = Vector of the beam deflections at  $j^{\text{th}}$  nodal point  
 $Z_n$  = Coefficient of the Airy stress function  
 $\epsilon$  = Normal strain  
 $\gamma$  = Shear strain  
 $\nu$  = Poisson's ratio  
 $\sigma$  = Normal stress  
 $\tau$  = Shear stress  
 $\Delta$  = Deformation  
 $\phi$  = Airy stress function  
 $\omega_n$  = Constant relating to number of term in the Airy stress function and the beam length  
 $\lambda_i$  = Constant relating the elastic parameters of plywood  
 $\alpha$  = Constant relating the elastic parameters of plywood  
 $\beta$  = Constant relating the elastic parameters of plywood  
 $\eta$  = Constant relating the elastic parameters of plywood

## CHAPTER 1

### INTRODUCTION AND LITERATURE REVIEW

#### 1.1 Introduction

The rapidly growing demand for quality housing in the United States and throughout the world presents a great challenge. Wood has long been used as the traditional material for residential floor construction in U.S. and approximately three-fourths of all residential housing is currently constructed with wood.

In spite of wide use, large quantity and great economic importance of wood construction, the current methods used for the analysis and design of light frame wood structures lag behind the modern design methods available for other building materials such as steel and reinforced concrete. The current practice in the structural design of the wood floor construction is based on generally conservative, oversimplified assumptions and has changed little during the past century. Because of the previous lack of knowledge of the incomplete composite action between layers of floor due to interlayer slip and the load sharing ability of joists through the two-way action of the flooring members, it is normally assumed that joists carry all the load. Furthermore, due to the wide variation in material properties of each component of the floor, design has generally been based on allowable stress obtained by a five percent exclusion method (3). Therefore, the stiffness and the load-carrying capacity of wood joist as the result of the five percent limit result in overdesign of floor systems. Such overdesign means that construction materials have not been fully utilized to achieve the most economical result. Improved

design procedure for wood house construction can bring about a significant reduction of timber consumption or increased utilization of lower quality material.

The limitations of the conventional design procedures used in wood house construction have long been recognized (4, 5, 7, 16). Efforts have been made by several researchers to develop more precise methods analyzing the behavior and design of wood joist floor systems with the hope that the timber resource can be more wisely and efficiently used.

A research project on the behavior of wood joist floor systems has been developed by a group of researchers at Colorado State University. The long-term goal of this project is to develop a rational, unified design procedure of wood joist floor systems. The final output of this and future projects can help minimize the building cost of housing while simultaneously meeting the necessary requirements of consumer protection.

#### 1.1.1 Purpose of Floor Project

The purpose of the wood floor research project is to derive a mathematical model of wood joist floor systems which can accurately analyze the load-resisting behavior of wood floor construction incorporating the following aspects:

1. Composite behavior due to interlayer slip

The wood joist floor is a layered system composed of a flooring plate reinforced by a set of parallel and usually constantly spaced wood joists. The flooring plate is usually plywood or particle board joined to the wood joists by connectors, such as nails and/or glue. Since the connection

between the sheathing plate and the joists is not perfectly rigid, relative movement occurs between layers, which is termed interlayer slip. Because of the interlayer slip of the floor system, the composite action between the joists and the sheathing falls somewhere between a complete composite action with perfectly rigid connection and no composite action at all where layers are loosely overlapped only, and is therefore termed incomplete composite action. The mathematical floor model must be able to account for the effect of the incomplete composite action between layers due to interlayer slip.

## 2. Two-way action

The conventional procedures used for the design of wood joist floor structures generally ignore the existence of the flooring materials. Also neglected is the two-way action of the sheathing across the joists except for allowing a stress increase for repetitive loading. In reality, external load applied at one joist can affect the deflections of the neighboring joists and the sheathing layer can spread out the applied load to the other joists. A stiffer joist in the floor can help the neighboring less-stiff joists by sharing the external load. The load sharing action of the joists through the continuous beam effect of the sheathing layer is termed two-way action. A properly developed mathematical floor model must be able to take into consideration this two-way action.

## 3. Variable properties of material

The wood joist floor is an assembly of many components with different material properties which make the floor a highly non-uniform, nonhomogeneous structure. A realistic and useful

mathematical floor model must be able to handle this nonuniformity and nonhomogeneity.

#### 4. Gaps in sheathing

Due to the limited size of plywood and other sheathing materials, the sheathing layer is built piece by piece. The existence of gaps between pieces of sheathing layer is, therefore, unavoidable. Gaps represent discontinuities in sheathing layer(s) and thus reflect additional difficulty for the analysis of the floor behavior. A complete mathematical floor model must be able to cope with the discontinuities in sheathing caused by gaps.

#### 1.1.2 Phases of Floor Project

To achieve the above stated objectives, several phases of the wood floor research project have been or are being studied by the research team at Colorado State University. A brief description of each of the phases of study of the wood floor research project are as follows:

1. Development of the theory for layered beam systems with interlayer slip.

Layered beam theory including interlayer slip is the foundation of the mathematical floor model. Based on this beam theory, the theory of floor is developed. Goodman (9, 10, 11) developed the beam theory for three-layered wood beam systems with equal layer width and with interlayer slip. An intensive study on two- and three-layered wood beam systems with interlayer slip was done by Ko (17). Both closed form solutions and finite difference solutions were presented for concentrated and uniform

loads. The general governing equation for any number of layered system subjected to uniform load was also proposed. A more sophisticated solution which can efficiently handle the nonuniform material properties and the gaps in the sheathing of a layered beam system was worked out later by Thompson (36) using energy methods and the finite element technique.

2. Development of the testing techniques to determine material and fastener properties.

To verify the predicted behavior of wood joist floor systems, the material properties of each of the floor components and the connector properties must be obtained before the floor is constructed. To measure these material properties, full-sized nondestructive testing techniques were developed for each floor component.

The MOE (modulus of elasticity) values of joists were determined by continuous load-deflection tests with a 3-foot span loaded at midspan as a plank. The specimen was fed through a continuous deflection machine developed by the Wood Science Laboratory. The MOE values at each one foot interval, along the length were determined and an average MOE value was used for the specimen. Joists were also tested for edgewise MOE, in place, prior to being used as T-beam or floor elements. More detailed description of the testing procedure is discussed in Sec. 3.3.1. A total of 412 joists of various sizes, species and grades were tested.

Figure 2.12: Interlayer Slip Related to Deformation

The testing techniques used to determine the in-plane static MOE and dynamic MOE values of the full size wood

composite panels has been developed by McLain (20). The in-plane elastic parameters of five types of sheathing materials were tested in the Wood Science Laboratory of Colorado State University. A total of 219 pieces of 4 feet by 8 feet panels of 3/4 inch and 1/2 inch Douglas-fir plywood, Engelmann spruce plywood and 1/2 inch Douglas-fir particle board were selected for the testing.

To assess the degree of incomplete composite action in a wood joist floor, the stiffness of the interlayer connection between the joists and the sheathing must be evaluated. Double-shear tests of nailed and glued connections were conducted to assess the interlayer slip properties. The result of these tests provided the values for the interlayer connection stiffness (slip modulus). The double shear tests of connections composed of the materials used in the floor construction were conducted by Patterson (26). The effects of MOE, specific gravity of the lumber, direction of loading with respect to the lumber, species of plywood, and number of nails on the load-slip relationship of the joints were reported.

### 3. Conducting load tests of T-beam and floor specimens.

To confirm the layered beam theory developed by Goodman (9, 10, 11) and to check the solutions presented by Ko (17) and Thompson (36), a series of T-beams have been constructed on which load tests were performed by Penner (27) and Kuo (19). The experimental load-deflection curves were recorded and compared with those predicted by the theoretical solutions. Good agreement between the experimental results and the theoretical

values of the layered beam systems were reported. The details of the testing equipment, construction procedure and testing process of the T-beams have been comprehensively presented by Penner (27) and Kuo (19).

With the assurance of the reliability of the layered beam theory including interlayer slip, testing was developed for wood joist floors to check the accuracy of the mathematical floor model. Four wood floors were built and tested under concentrated load by Penner (27). Seven additional basic wood floors were constructed and load tests performed as part of the work of this dissertation. Several of these floors were tested first as two-layer floors and then by adding an additional layer of sheathing to provide three-layer floors. The details of the construction and testing of the wood floor specimens will be presented in Chapter 3 and the verification of the validity of the mathematical floor model will be reported in Chapter 4 in this study.

## 1.2 Literature Review

Layered beam systems constructed with nails or nails and glue have been studied both theoretically and experimentally by several investigators. For recent developments on layered beam systems, refer to the studies reported by Goodman (9, 10, 11), Henghold (14, 15), Penner (27), Ko (17) and Kuo (19).

The study reported herein concerns itself primarily with floor system behavior. A general review of the state-of-the-art of research on the wood joist floor systems was presented by Onysko (25). The major developments that related to the study of the behavior of the

wood joist floor systems are examined in the following two categories, experimental investigations and theoretical considerations.

### 1.2.1 Experimental Investigations

Traditional design practice of wood joist floors is based on the assumption that a set of independently acting joists can be assumed to predict floor behavior. Therefore, the design of floor can be accomplished by analyzing and designing the joists comprising the floor. Floors with excessive load capacity often result by neglecting the load sharing ability of the floor through the two-way and composite action of the floor sheathing. This has been investigated and recognized by several researchers in the literature (4, 5, 7, 16, 25).

Colville et al. (7) and Angleton et al. (5) studied the effect of two-way action on load sharing and on the stiffness of floors in the working load range. Increases in stiffness of floors up to 25 percent greater than the individual joist stiffness were reported.

A series of load tests were conducted by Kloot and Schuster (16) on the load distribution of a set of joists connected by a single strip of flooring material. It is reported that the theoretical results obtained by assuming the condition of beam on elastic foundation could well describe the sheathing and joists interaction under conditions of concentrated load. It was also shown, that for joists crossed at their mid-span by a single piece of flooring, the actual load distribution of a concentrated load could be calculated from simple beam theory according to the measured deflections at the crossing points.

Load tests were conducted on forty-four nailed wood joist floors by Polensek et al. (32) to investigate the floor response to static load. It was reported that about two-thirds of a concentrated load applied at

a joist mid-span was distributed to the six adjacent joists, three on each side. For uniform load tests, generally uniform deflection throughout the floor was noted due to the two-way action of the 1/2 inch plywood floor covering. The tested floors were reported to be stronger and stiffer than predicted by conventional beam analysis based on the mechanical properties of joists alone.

Altherton and Corder (4) compared the first-break load of floors subjected to uniform load with the first-break load of the side-matched joists in eleven test floors. The first-break load for floors was found higher by up to 3.6 time of those found in matched joists. The substantial increase of the first-break load was considered as a result of the load sharing effect and some composite action between the flooring and joists.

The degree of composite action between layers has been recognized to have a striking effect on the behavior of wood joist floor systems. Characteristics of the joints which connect the layers determines the degree of composite action between the layers. Tests on the load-slip properties of nailed-joints between the lumber joist and the plywood sheathing members were conducted by Patterson (26). Several factors which might influence the load-slip relationship of the nailed joints were investigated. It was reported that the material properties of both the joist and the sheathing member could affect the joint behavior. The lateral load capacity was found, as expected, to be larger when the lateral load was applied parallel to the grain of the joist as opposed to the perpendicular to the grain test. The maximum load per nail decreased with increasing number of nails in a fixed length of joint.

The use of the elastomeric adhesives in recent years for the construction of wood joist floors has greatly increased. Field-glued plywood T-beams and floors were tested by Rose (35). Test results showed an increase of stiffness of the glued specimens up to 66 percent as compared to the stiffness of the joists alone; while only up to five percent increase was found for the nailed specimens.

The NAHB Research Foundation (22) completed tests on thirteen glued floors and two conventional nailed floors. The stiffness of the glued floors was reported varying approximately from 75 percent to 90 percent of the stiffness of the corresponding floor with presumed rigid interlayer connections. The calculated bending stresses from the measured strains for the glued composite floors varied from 0.64 to 0.84 of the bending stresses of the joists alone under the same bending loads. It was also reported that the glued floors tend to act more as a single unit under vibration as opposed to the nailed floors which provide some internal damping.

The static and dynamic properties of glued wood joist floors were also investigated by Polensek (30). He conducted tests on one nailed and three glued wood floors. Strength, stiffness, natural frequency and damping capacity were determined for each floor. It was reported that the glued floor was stiffer than the nailed one only when subjected to uniform distributed load and the two were equally stiff when loaded with concentrated load. It was also concluded that the glued floors appeared to be more acceptable as to human response to vibration than the nailed floor. However, it was noted that gluing had only minor effect on damping capacity of the wood joist floors.

Four floors and two T-beams, all nailed were tested to failure under concentrated loads by Penner (27). The load corresponding to the allowable deflection was reported up to 300 percent higher than the allowable load computed with the conventional design procedure. Load corresponding to the first joist failure was found to be four to 21 times the allowable joist load computed on the basis of allowable stresses and using current design assumptions.

The research reported previously has been primarily experimental and has not been generally aimed at verification of a formulated mathematical model. Since, in many cases, material properties were not measured prior to floor testing, the various tests do not relate well to each other.

#### 1.2.2 Theoretical Considerations

The theories for predicting the behavior of wood joist floors are essentially based on the theory of layered beam systems. Goodman (9) showed that the governing equations of the composite action of the layered beam systems with interlayer slip, established by Granholm (13), Pleshkov (29) and Newmark et al. (23), were in fact equivalent for one to another. The theory was extended by Goodman to three equal layered wood beam systems and good agreement was obtained between the theoretical and the experimental results.

Additional theoretical studies on layered wood beam systems were carried out by Ko (17) and Henghold (14, 15) based on Goodman's previous work (9). The general case of a m-layered beam was first investigated and governing equations for the layer axial forces and the deflection of the system were derived. Two and three layered systems of unequal layers were then investigated intensively.

Governing equations were established and both closed form and finite difference solutions were presented. The predicted results were closely confirmed by experimental results. The theoretical formulation will be examined in more detail in the next chapter.

Amana and Booth (1) studied the effect of the shear lag phenomenon on the effective flange width of the single-rib T-beams and of double-skinned stress-skin panels with interlayer slip. A plane stress elasticity problem was assumed for the orthotropic skin plate member. A fourth order partial differential governing equation of the flange stresses in terms of Airy Function,  $\phi$ , was derived from the field equations of elasticity. A series solution of Levy type, which satisfied part of the stress boundary conditions, was employed to solve the fourth order partial differential equation. The compatibility condition that the interlayer slip per unit length was equal to the net strain of the contacting surfaces of layers was utilized to relate the connectors' properties to the internal resisting axial force and moment of the layers. From the assumption that each layer deflects the same amount, the internal resisting axial force and moment of each layer were expressed in terms of the external total moment, which was also transformed into series form. Using the proper stress and strain boundary conditions, the deflection of the system and the effective flange width were obtained. It was concluded that the effective flange width varied along the span and its magnitude depended on the type of loading with the smallest effective width at the point of maximum bending moment.

Frequency analysis of wood joist floors was investigated by Polensek (31). In his study, the following assumptions were made:

1. The system remains in the elastic range,
2. Damping is not included in the calculation,
3. The contribution of blocking and headers to the distribution of forces in the direction across the joists is ignored,
4. Rigidity and mass distribution are constant along each joist,
5. Rigidity and mass distribution per unit area of floor are constant.

Bleich's method was used in the development of the frequency analysis. The complex wood floor system was first transformed into a set of statically determinate beam system by releasing the continuity moments in the sheathing where it crossed the joists and adding the sheathing mass proportionally to the joist masses. The frequency and modal shapes were determined for the statically determinate beam system. The influence of the redundant continuity moments were evaluated and added to the above analysis to form a governing frequency equation of the wood joist floor system. Good correspondence was reported between the calculated frequencies and those acquired from the tests with the largest discrepancy less than two percent occurred at the first mode. Measured stiffness at nodes were used in the frequency analysis.

A finite element method was later employed by Polensek (33) for the static and dynamic analysis of wood joist floor systems. The model representing the joist floor consisted of an assembly of rectangular two-dimensional plate elements and single dimensional beam elements connected at nodal points. Elemental stiffness

$[M_s]$  = system mass matrix,

$\{X\}$  = eigenvector corresponding to  $\{w_s\}$  and  $\omega^2$ .

The equation of motion was expressed in terms of acceleration,  $\{\ddot{w}_s\}$ , velocity,  $\{\dot{w}_s\}$ , and displacement,  $\{w_s\}$ , as

$$[M_s] \{\ddot{w}_s\} + [C_s] \{\dot{w}_s\} + [K_s] \{w_s\} = \{P_s\} \quad (1.3)$$

where,

$[C_s]$  = system damping matrix.

It was concluded that the theoretical results agreed closely to the experimental data.

Thompson (36) also investigated the static behavior of the wood joist floor systems using energy methods by a finite element technique. The floor system was simulated by two sets of beams crossing each other at right angles. An energy method was used to evaluate the deflection at each nodal point along every beam. The compatibility condition applied to each nodal point at which two beams intersect required each beam to deflect the same amount at the point. The details of this theoretical development are discussed in the next chapter.

## CHAPTER 2

### THEORETICAL DEVELOPMENT

#### 2.1 Introduction

The wood joist floor is a layered repetitive-member system in which the joists and sheathing act together through partially composite and two-way action to share the applied load. The sheathing members are usually one or two layers of sheathing panels, usually plywood or particle board, with T & G (tongue-and-groove), butted, or open joints, fastened to the joists by nailing or nailing and gluing to form a complicated composite floor structure.

For the convenience of analysis, the wood joist floor system may be idealized as two sets of crossing beams. One set consists of the T-beams; the other set is the sheathing acting as a beam. The crossing points of the two sets of beams are the nodal points. The analysis of the floor structure is therefore simulated from the analysis of the crossing beam system.

The layered beam theory, is then applied to each beam. The incomplete composite action due to interlayer slip of the floor is considered through the process of solving each set of beams. The two-way action of the floor is included by consideration of the sheathing beams. Compatibility, requiring that at each nodal point the two crossing beams deflect the same amount at that point, is employed together with the statics of the floor structure to solve for the resisting forces at each nodal point. Once the resisting forces at each nodal point are known, the floor deflections at each nodal point in turn can be calculated.

In addition to the consideration of the incomplete composite action and two-way action, a special problem arises if plywood is used for sheathing. The plywood is a compound member constructed by press-gluing several layers of veneer with different material properties together. Due to the difference in stress distributions over the cross section of the plywood in bending or axial load, the effective MOE for bending is different from the effective MOE for axial load based on the gross geometrical dimensions of the cross section. Therefore, if the effective MOE for bending is also to be used for the effective MOE for axial load, a transformation constant,  $K^*$ , must be applied.

The thickness of the sheathing member is generally small compared to the depth of the joists. When the floor is subjected to external load, because of the shear lag effect, the compressive stresses in the sheathing layer parallel to the longitudinal direction of the joists may not be uniformly distributed as predicted by the beam theory. Therefore, when the idealized physical floor model with two sets of crossing beams is used for the analysis of the floor structure, the effective flange width of the T-beams must be predetermined and used for the T-beams so that beam theory can be properly applied.

## 2.2 Layered Beam Theory and Effective Flange Considerations

The layered beam theory including interlayer slip used by Ko (17) is briefly reviewed in this section. The derivation of the governing equations of a two-layered system is examined. The derivations of the MOE transformation constant for plywood,  $K^*$ , and the effective flange width of the T-beams,  $w_e$ , is also developed in this section along with a discussion of the effect of gaps in the sheathing.

### 2.2.1 Basic Derivation of Layered Beam Theory

A general two-layered beam system subjected to uniformly distributed load,  $q$ , as shown in Fig. 2.1, serves as an example for the review of the derivation of the governing equations. The assumptions employed by Goodman (9, 10, 11) and Ko (17) are as follows:

1. The shear connection between layers is continuous along the length; i.e., discrete deformable connections are assumed to be replaced by a continuous shear connection.
2. The amount of slip at a connector is directly proportional to the load.
3. The distribution of strain through the depth of a given individual layer is linear.
4. At every section of a beam, each layer deflects the same amount and no buckling of the layers occurs.
5. Friction between the layers is negligible.

Applying the equilibrium conditions of statics to the force components acting on a beam element as shown in Fig. 2.1(d), yields

$$\text{from } \Sigma F_x = 0, \quad F_1 = -F_2 = F \quad (2.1)$$

The total moment at a certain cross section is:

$$M_T = \sum_1^2 M_i + C_{12} \cdot F \quad (2.2)$$

where

$F_1, F_2$  = the axial forces in the first and second layer,  
respectively, lb.,

$M_i$  = the resisting moment of  $i^{\text{th}}$  layer, lb-in.,

$M_T$  = the total external moment, lb-in.,

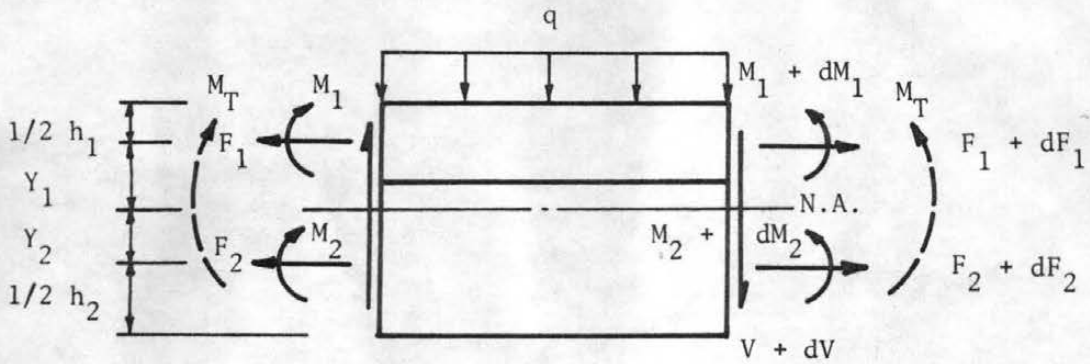
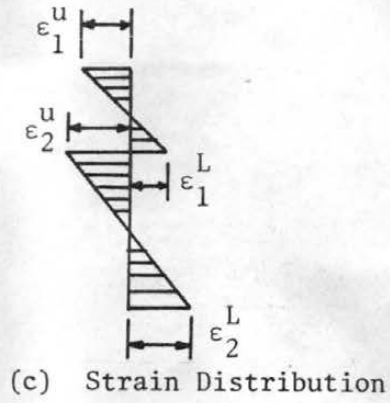
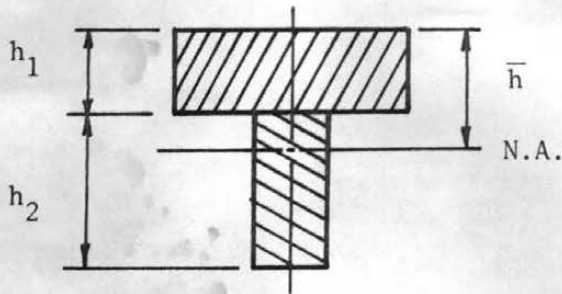
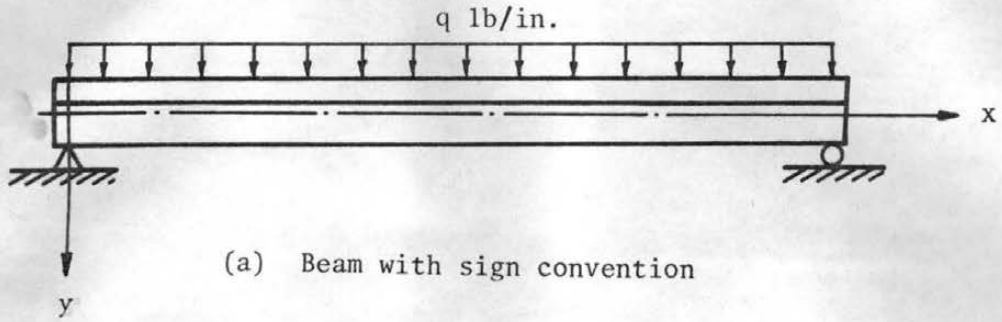


Figure 2.1 Two-Layer Beam System

- $C_{12} = 1/2 (h_1 + h_2)$ , in.,  
 $x$  = the beam length, in.,  
 $y$  = the deflection of beam, in.

If it is assumed that each layer has the same curvature and deflects the same amount, then

$$M_i = -E_i I_i \frac{d^2 y}{dx^2} \quad (2.3)$$

Substituting Eq. (2.3) into Eq. (2.2) yields

$$\frac{d^2 y}{dx^2} = \frac{-M_T + C_{12} F}{\sum_1 E_i I_i} \quad (2.4)$$

where

$E_i$  = the MOE of  $i^{\text{th}}$  layer, lb/in<sup>2</sup>.,

$I_i$  = the moment of inertia of the  $i^{\text{th}}$  layer about its own neutral axis, in<sup>4</sup>.

To relate the axial force,  $F$ , to the beam deflection,  $y$ , the compatibility condition that the slip of the connectors per unit length of beam is equal to the net strain of the contacting surface of layers must be utilized and the following relation is found:

$$\frac{s}{kn} \frac{d^2 F}{dx^2} = \left( \frac{1}{E_2 A_1^*} + \frac{1}{E_2 A_2} \right) F - \frac{M_1}{E_2 I_1^*} \frac{h_1}{2} - \frac{M_2}{E_2 I_2} \frac{h_2}{2} \quad (2.5)$$

where

$A_1^*$  = the transformed cross-sectional area for axial load of the first layer based on  $E_2$ , in.<sup>2</sup>,

$I_1^*$  = the moment of inertia of  $A_1^*$  about its neutral axis, in<sup>4</sup>.,

$s$  = the connector spacing along the beam length, in.,

$k$  = the connector slip modulus per connector, lb/in.,

$n$  = the number of connectors per row in the transverse direction of the beam length.

Substituting Eq. (2.4) into Eq. (2.5) gives

$$\frac{d^2F}{dx^2} - C_1 F = - C_2 M_T(x) \quad (2.6)$$

where

$$C_1 = \frac{kn}{sE_2} \left( \frac{1}{A_1^*} + \frac{1}{A_2} \right) \text{ (T.C.)}$$

$$C_2 = \frac{kn}{sE_2} \frac{C_{12}}{I_1^* + I_2}$$

$$\text{T.C.} = \frac{I_s}{I_1^* + I_2} = 1 + \frac{C_{12}^2}{(I_1^* + I_2) \left( \frac{1}{A_1^*} + \frac{1}{A_2} \right)}$$

Since the external load condition is known,  $M_T(x)$  can be expressed in terms of  $x$ , and hence the layer axial force  $F$  along the beam can be obtained by solving Eq. (2.6).

From Eq. (2.4) and Eq. (2.6), the deflection equation may be rewritten as

$$\frac{d^2y}{dx^2} = \frac{d^2y_s}{dx^2} + \frac{1}{C_1} \frac{C_{12}}{E_2(I_1^* + I_2)} \frac{d^2F}{dx^2} \quad (2.7)$$

Integrate Eq. (2.7) twice to obtain the deflection as

$$y = y_s + \frac{1}{C_1} \frac{C_{12}}{E_2(I_1^* + I_2)} F \quad (2.8)$$

where  $y_s$  is the deflection of the assumed rigidly connected beam.

### 2.2.2 Derivation of Transformation Constant for MOE of Plywood

It was pointed out previously that the MOE of bending is different from the MOE of axial deformation for plywood. A transformation

constant,  $K^*$ , is therefore required in order that the effective MOE of bending can be properly transformed into the effective MOE of axial deformation of plywood for the gross cross section in the direction either parallel or perpendicular to the face grain. Usually, cross-laminated veneer is used in plywood for each neighboring ply. Consider a strip of three-ply plywood of unit width, as shown in Fig. 2.2(a), with  $E_o$  and  $E_{in}$  being the MOE values in the longitudinal direction of the outer plies and inner ply, respectively. The original cross-section and the transformed cross section based on  $E_o$  are shown in Fig. 2.2(b) and Fig. 2.2(c). The strain and stress distributions of the plywood strip due to bending and axial compression are shown in Fig. 2.3 and Fig. 2.4, respectively. For the case of bending loading only, the effective MOE based on the original cross sectional dimensions is

$$E_{eb} = E_o \left[ \frac{2t_1}{2t_1 + t_2} + \frac{4t_1 t_2}{(2t_1 + t_2)^2} - \frac{t_2(4t_1^2 - t_2^2 \frac{E_{in}}{E_o})}{(2t_1 + t_2)^3} \right] \quad (2.9)$$

For the case of axial compression only, the effective MOE based on the original cross section is

$$E_{ea} = E_o \left[ 1 - \frac{t_2}{2t_1 + t_2} \left( 1 - \frac{E_{in}}{E_o} \right) \right] \quad (2.10)$$

From Eqs. (2.9) and (2.10), it is seen that the MOE of bending and the MOE for axial deformation are not the same for plywood.

To derive the transformation constant,  $K^*$ , for transforming effective MOE of bending to the effective MOE of axial deformation, the following notations will be used:

$$E_o = \text{MOE of the outer most plies of plywood in longitudinal direction, lb/in.}^2,$$

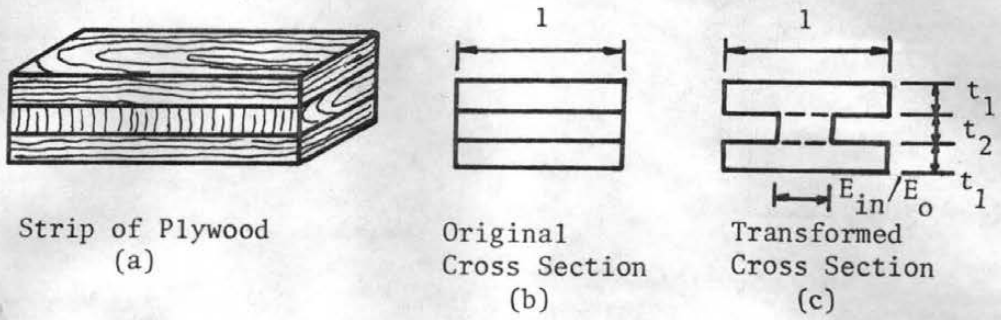


Figure 2.2 Original and Transformed Cross Sections of a Strip of 3-ply Plywood with Unit Width

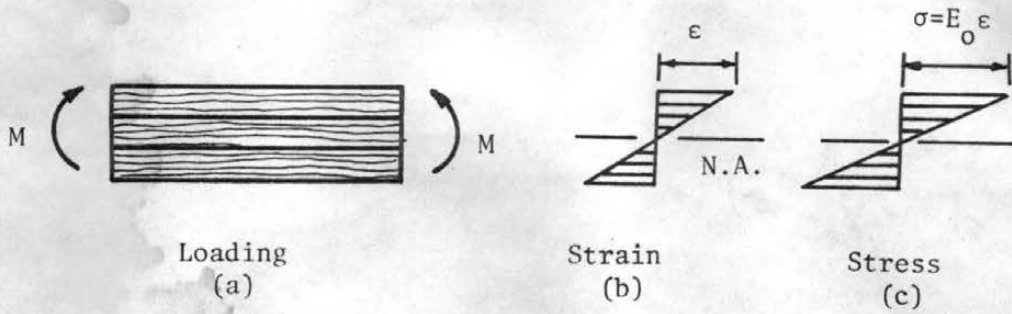


Figure 2.3 Strain and Stress Distributions Over the Transformed Cross Section of Plywood Subjected to Bending

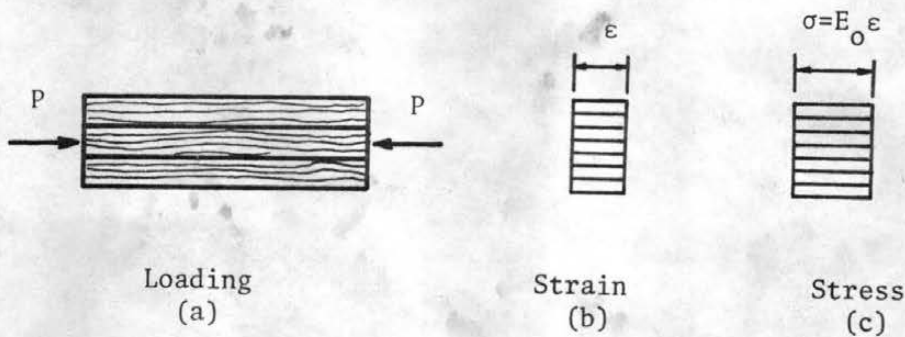


Figure 2.4 Strain and Stress Distributions Over the Transformed Cross Section of Plywood Subjected to Axial Compression

$A_t$  = transformed cross section area of plywood board based on  $E_o$ , in.<sup>2</sup>,

$A_g$  = gross cross section area of the plywood board, in.<sup>2</sup>,

$E_{eb}$  = effective MOE of bending based on  $A_g$ , lb/in.<sup>2</sup>,

$E_{ea}$  = effective MOE of axial deformation based on  $A_g$ , lb/in.<sup>2</sup>,

$I_t$  = moment of inertia based on  $A_t$ , in.<sup>4</sup>,

$I_g$  = moment of inertia based on  $A_g$ , in.<sup>4</sup>.

Since  $K^*$  is defined as the constant to be multiplied by  $E_{eb}$  to yield  $E_{ea}$ , we have

$$E_{ea} = K^* E_{eb} \quad (2.11)$$

To obtain the same bending or axial deformation effect based on either  $A_t$  or  $A_g$ , the following relationships must be true:

$$E_{ea} \cdot A_g = E_o A_t \quad (2.12a)$$

$$E_{eb} I_g = E_o I_t \quad (2.12b)$$

Substitute Eq. (2.11) into Eq. (2.12a) and divide by Eq. (2.12b) to solve for  $K^*$  as

$$K^* = \frac{I_g}{I_t} \cdot \frac{A_t}{A_g} \quad (2.13)$$

Therefore,  $K^*$  depends not only on the geometry of the cross section but also on the material property of each ply. The values of  $K^*$  of the various types of plywood used in the experimental phase of this study are tabulated in Appendix A.

### 2.2.3 Development of the Theory of Effective Flange Width

Due to the small thickness of the sheathing and the relatively large spacings between joists, shear lag effects may take place. The normal stresses in the sheathing acting in the longitudinal direction of joists do not distribute uniformly and thus can not be correctly predicted by elementary beam theory. For the convenience of analysis, a reduced flange width is introduced for the T-beams such that when elementary beam theory is applied to the transformed T-beam sections, the effective flange may be considered to have a uniform normal stress in the sheathing layer. This uniform stress is, thus, equal to the maximum normal stress of the nonuniformly distributed normal stresses across the sheathing layer cross section and will result in the same total normal force effect. The reduced flange width concept (effective flange width) was first introduced by Pietzker (28) in 1914 in his study of the buckling resistance of stiffened plates. The theory of evaluating effective flange width was first developed by von Kármán (39). Investigations of effective flange width were also done by Girkmann (8) and Reissner (34). A more extensive numerical evaluation of effective flange width were made by Metzger (21) and Chwalla (6).

While considerable work on this problem has been done, particularly by Amana and Booth (1, 2), no quantification of the effects of the key parameters on effective flange width has been made for wood joist systems. Thus, a thorough evaluation of the effective flange width problem was necessary to allow proper use of the basic crossing-beam physical model for wood joist floors.

#### A. Mathematical Formulation of the Flange Stress Covering Equation

Since the thickness of the sheathing for wood layered beam systems is usually small compared to the flange width and the joist depth, the

stress distribution in the flange can be considered as a plane stress problem and the effect due to bending action can be neglected without introducing substantial degree of error. It is also assumed that the stresses are in the elastic range in this study.

For the sign convention shown in Fig. 2.5 and applying the strain-displacement equations of elasticity for the flange, results in

$$\epsilon_x = \frac{\partial u}{\partial x} \quad (2.14a)$$

$$\epsilon_z = \frac{\partial w}{\partial z} \quad (2.14b)$$

$$\gamma_{xz} = \frac{\partial u}{\partial z} + \frac{\partial w}{\partial x} \quad (2.14c)$$

Applying the equilibrium equation of elasticity to the flange and neglecting body forces leads to

$$\frac{\partial \sigma_x}{\partial x} + \frac{\partial \tau_{xz}}{\partial z} = 0 \quad (2.15a)$$

$$\frac{\partial \sigma_z}{\partial z} + \frac{\partial \tau_{xz}}{\partial x} = 0 \quad (2.15b)$$

From Eqs. (2.15a) and (2.15b) we obtain

$$\frac{\partial^2 \sigma_x}{\partial x^2} + \frac{\partial^2 \sigma_z}{\partial z^2} = -2 \frac{\partial^2 \tau_{xz}}{\partial x \partial z} \quad (2.15c)$$

Applying the stress-strain equation of elasticity to the flange and utilizing the constitutive law for an orthogonal plate yields

$$\epsilon_x = \frac{1}{E_x} (\sigma_x - \nu_{xz} \sigma_z) \quad (2.16a)$$

$$\epsilon_y = \frac{\sigma_z}{E_z} - \frac{\nu_{xz}}{E_x} \sigma_x \quad (2.16b)$$

$$\gamma_{xz} = \tau_{xz} / G_{xz} \quad (2.16c)$$

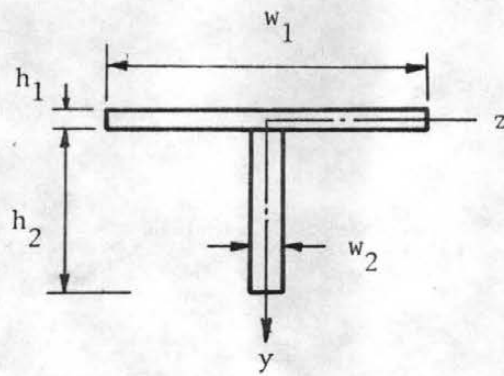
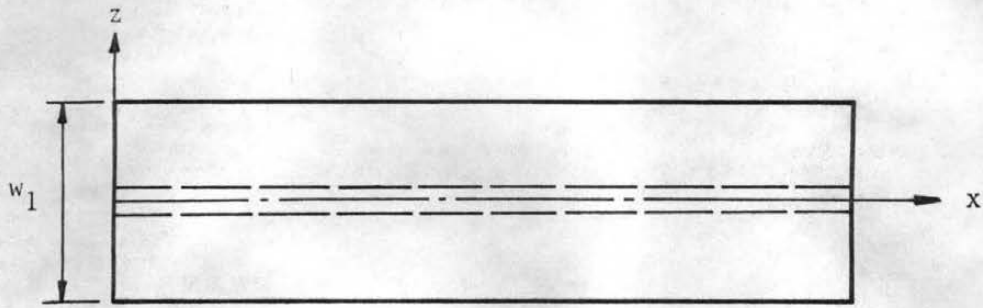
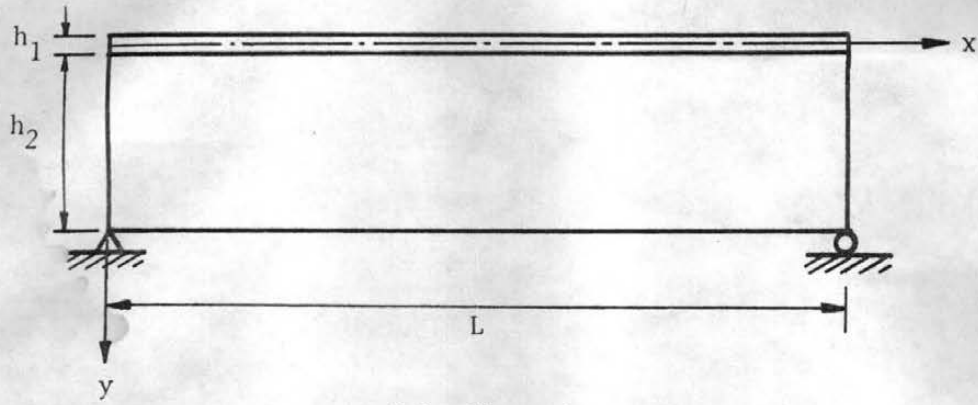


Figure 2.5 Layout and Sign Convention of T-Beam

Substituting Eqs. (2.15c) and (2.16) into Eq. (2.14) gives

$$\frac{\partial^2 \sigma_x}{\partial z^2} + \frac{E_x}{E_z} \frac{\partial^2 \sigma_z}{\partial x^2} - 2 \left( \frac{E_x}{G_{xz}} - \nu_{xz} \right) \frac{\partial^2 \tau_{xz}}{\partial x \partial z} = 0 \quad (2.17)$$

Introduce the Airy stress function,  $\phi$ , defined such that

$$\sigma_x = \frac{\partial^2 \phi}{\partial z^2} \quad (2.18a)$$

$$\sigma_z = \frac{\partial^2 \phi}{\partial x^2} \quad (2.18b)$$

$$\tau_{xz} = \frac{\partial^2 \phi}{\partial x \partial z} \quad (2.18c)$$

Substituting Eq. (2.18) into Eq. (2.17) yields the following governing equation for flange plane stresses:

$$\frac{\partial^4 \phi}{\partial z^4} + 2\alpha \frac{\partial^4 \phi}{\partial x^2 \partial z^2} + \beta \frac{\partial^4 \phi}{\partial x^4} = 0 \quad (2.19)$$

where,

$$\alpha = \frac{E_x}{2G_{xz}} - \nu_{xz}, \quad \beta = E_x/E_z$$

#### B. Solution to the Flange Stress Governing Equation

To solve Eq. (2.19), a series solution of the Levy type is assumed for the Airy stress function, i.e.,

$$\phi = \sum_{n=1}^{\infty} Z_n \sin \omega_n x \quad (2.20)$$

where  $Z_n$  is a function of  $z$  only and

Eq. (2.20) satisfies the stress boundary condition

$$\sigma_x = 0 \quad \text{at} \quad x = 0 \quad \text{and} \quad x = L$$

However, the boundary condition requiring that the shear stresses at ends are zero is not satisfied. By Eq. (2.18c), that is,

$$\tau_{xz} = \sum_{n=1}^{\infty} \omega_n \frac{\partial Z_n}{\partial z} \cos \omega_n x \neq 0 \text{ at } x = 0 \text{ and } x = L,$$

it is noted, however, that according to St. Venant's principle, the shear stress acting at ends has only local effect, at least for the usual dimensions involved in wood joist systems.

Substituting Eq. (2.20) into Eq. (2.19) leads to

$$(D^4 - 2\alpha\omega_n^2 D^2 + \beta\omega_n^4) Z_n = 0 \quad (2.21)$$

where  $D = \frac{d}{dx}$

Solving Eq. (2.21) gives a general solution as follows:

$$\begin{aligned} \phi = \sum_{n=1}^{\infty} (A_n \cosh \lambda_1 \omega_n z + B_n \cosh \lambda_2 \omega_n z \\ + C_n \sinh \lambda_1 \omega_n z + D_n \sinh \lambda_2 \omega_n z) \sin \omega_n x \end{aligned} \quad (2.22)$$

where

$$\lambda_1 = \sqrt{\alpha + \sqrt{\alpha^2 - \beta}}$$

$$\lambda_2 = \sqrt{\alpha - \sqrt{\alpha^2 - \beta}}$$

Eq. (2.22) has four unknown coefficients  $A_n$ ,  $B_n$ ,  $C_n$  and  $D_n$  which have to be solved from boundary conditions.

### C. Mathematical Formulation of Governing Equation of Axial Force in the Flange

Throughout the derivation, the following notations are used:

$s$  = connector spacing, inch,

$\Delta s$  = Slip of connector, inch,

$Q$  = shear force transmitted by each connector, lb/connector,

$n$  = number of rows of connectors,

$k$  = slip modulus of connector, lb./in./connector.

Referring to previous work by Goodman (9, 10, 11) and Ko (17), the shear flow per unit length transmitted by the connectors is

$$q_{12} = \frac{nQ}{s} \quad (2.23)$$

The slip modulus of connector is, by definition,

$$k = \frac{Q}{\Delta s} = \frac{q_{12} \cdot s}{n \cdot \Delta s} \quad (2.24)$$

Referring to Fig. 2.6, the shear flow,  $q_{12}$ , can be expressed, by statics, as

$$q_{12} = \frac{dF}{dx} \quad (2.25)$$

Substitute Eq. (2.25) into Eq. (2.24) obtaining

$$\Delta s = \frac{s}{nk} \frac{dF}{dx} \quad (2.26)$$

By the principle of compatibility, the connector's slip per unit length of beam has to be equal to the net interlayer strain. The relation can be expressed as

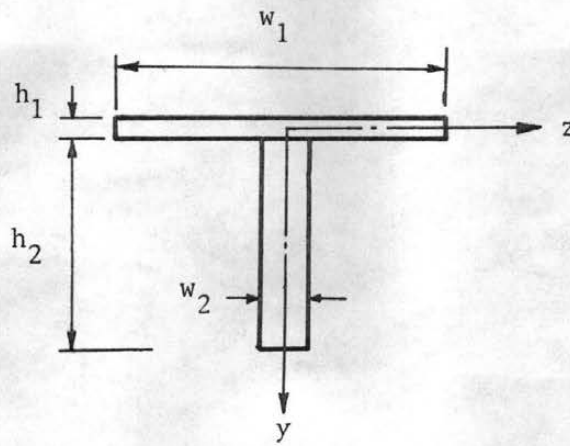
$$\frac{d\Delta s}{dx} = (\epsilon_2)_{z=0} - (\epsilon_1)_{z=0} \quad (2.27)$$

where,

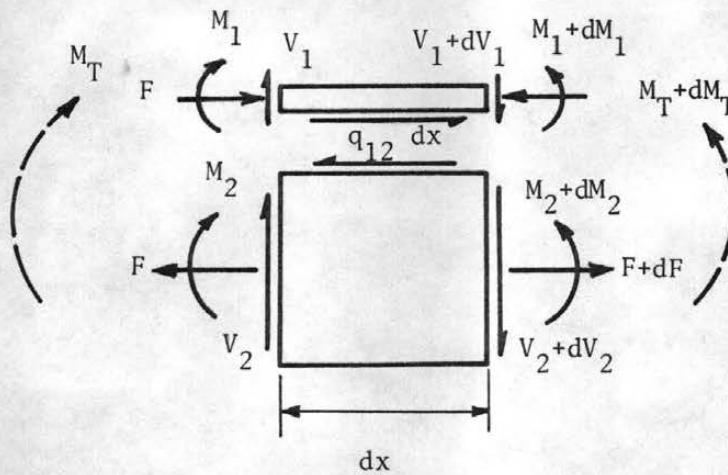
$(\epsilon_i)_{z=0}$  = the strain of the  $i^{\text{th}}$  layer at the interlayer surface and evaluated at  $z = 0$ , in./in.

Differentiation of Eq. (2.26) leads to,

$$\frac{d\Delta s}{dx} = \frac{s}{nk} \frac{d^2 F}{dx^2} \quad (2.28)$$



(a) Cross sectional dimensions



(b) Force components of a beam element

Figure 2.6 Beam Element with Force and Moment Components

Using Eqs. (2.27) and (2.28), yields

$$\frac{s}{nk} \frac{d^2 F}{dx^2} = (\epsilon_2)_{z=0} - (\epsilon_1)_{z=0} \quad (2.29)$$

Referring to Fig. 2.6, the strains in Eq. (2.29) can be evaluated as

$$(\epsilon_2)_{z=0} = \frac{F}{A_2 E_2} - \frac{M_2 h_2}{2 E_2 I_2} \quad (2.30a)$$

$$(\epsilon_1)_{z=0} = - (\epsilon_1)_F|_{z=0} + \frac{M_1 h_1}{2 E_{1x} I_1} \quad (2.30b)$$

where

$-(\epsilon_1)_F|_{z=0}$  = strain in the first layer at the interlayer surface  
evaluated at  $z = 0$ ,

$A_2$  = cross-section area of the second layer, in.,

$I_2$  = moment of inertia of the second layer, in.<sup>4</sup>,

$E_2$  = MOE of the second layer along the length, psi,

$I_1$  = moment of inertia of the first layer, in.<sup>4</sup>,

$E_{1x}$  = MOE of the first layer in x-direction, psi.

Substitute Eqs. (2.30a) and (2.30b) into Eq. (2.29) to obtain

$$\frac{s}{nk} \frac{\partial^2 F}{\partial x^2} = (\epsilon_1)_F|_{z=0} + \frac{F}{A_2 E_2} - \frac{M_2 h_2}{2 E_2 I_2} - \frac{M_1 h_1}{2 E_{1x} I_1} \quad (2.31)$$

Assume that each layer deflects the same amount and has the same curvature, from the study of layered beam system by Goodman (9, 10, 11) and Ko (15), the following equation is obtained:

$$\frac{M_2}{E_2 I_2} = \frac{M_1}{E_{1x} I_1} = \frac{M_T - C_{12} F}{EI} \quad (2.32)$$

where

$$C_{12} = \frac{1}{2} (h_1 + h_2)$$

$$EI = E_2 I_2 + E_{1x} I_1$$

Substituting Eq. (2.32) into Eq. (2.31), we can obtain the governing equation of layer axial force,  $F$ , as

$$\frac{s}{nk} \frac{\partial^2 F}{\partial x^2} = (\epsilon_1)_F|_{z=0} + F \left( \frac{1}{A_2 E_2} + \frac{C_{12}^2}{EI} \right) - \frac{M_T C_{12}}{EI} \quad (2.33)$$

with

$$(\epsilon_1)_F|_{z=0} = \frac{1}{E_{1x}} \left( \frac{\partial^2 \phi}{\partial z^2} - \nu_{xy} \frac{\partial^2 \phi}{\partial x^2} \right) |_{z=0} \quad (2.34)$$

$$F = 2h_1 \int_0^{w_1/2} \sigma_x dz = 2h_1 \left. \frac{\partial \phi}{\partial z} \right|_{z=0}^{z=w_1/2} \quad (2.35)$$

The total force,  $F$ , across the flange width must be related to the external load, and is developed subsequently.

#### D. Solution of the T-beam System with Interlayer Slip

The boundary conditions of the flange plate which have to be satisfied for the T-beam system with loads applied on x-axis are:

$$1. \quad \sigma_z = \frac{\partial^2 \phi}{\partial x^2} = 0 \quad \text{at } z = w_1/2$$

$$2. \quad \tau_{xz} = \frac{\partial^2 \phi}{\partial x \partial z} = 0 \quad \text{at } z = w_1/2$$

$$3. \quad w = 0 \quad \text{at } z = 0$$

where  $w$  is displacement in  $z$ -direction.

Substituting the general solution of Eq. (2.22) into the first boundary condition gives

$$\begin{aligned} \frac{A_n}{D_n} \cosh \frac{\lambda_1 \omega_n w_1}{2} + \frac{B_n}{D_n} \cosh \frac{\lambda_2 \omega_n w_1}{2} + \frac{C_n}{D_n} \sinh \frac{\lambda_1 \omega_n w_1}{2} \\ = - \sinh \frac{\lambda_2 \omega_n w_1}{2} \end{aligned} \quad (2.36)$$

Substituting the general solution of Eq. (2.22) into the second boundary condition yields

$$\begin{aligned} \frac{A_n}{D_n} \lambda_1 \sinh \frac{\lambda_1 \omega_n w_1}{2} + \frac{B_n}{D_n} \lambda_2 \sinh \frac{\lambda_2 \omega_n w_1}{2} + \frac{C_n}{D_n} \lambda_1 \cosh \frac{\lambda_1 \omega_n w_1}{2} \\ = - \lambda_2 \cosh \frac{\lambda_2 \omega_n w_1}{2} \end{aligned} \quad (2.37)$$

From the third boundary condition, by applying the strain-displacement equation, results

$$\gamma_{xz} \Big|_{z=0} = \frac{\partial u}{\partial z} \Big|_{z=0}$$

or

$$\left( \frac{\partial \epsilon_x}{\partial z} - \frac{\partial \gamma_{xz}}{\partial x} \right) \Big|_{z=0} = 0 \quad (2.38)$$

Substituting Eqs. (2.16) and (2.18) into Eq. (2.38) leads to

$$\frac{\partial^3 \phi}{\partial z^3} + \left( \frac{E_{1x}}{G_{xz}} - \nu_{xz} \right) \frac{\partial^3 \phi}{\partial x^2 \partial z} \Big|_{z=0} = 0 \quad (2.39)$$

Substitute Eq. (2.22) into Eq. (2.39) to obtain

$$\frac{C_n}{D_n} \frac{\lambda_1}{\lambda_2} \left( \frac{\lambda_1^{2-\eta}}{\lambda_2^{-\eta}} \right) = -1 \quad (2.40)$$

where

$$\eta = \frac{E_{1x}}{G_{xz}} - \nu_{xz}$$

$$(\epsilon_1)_F|_{z=0} = \frac{1}{E_{1x}} \sum_{n=1}^{\infty} D_n r_n \sin \omega_n x \quad (2.43)$$

$$F = 2h_1 \sum_{n=1}^{\infty} D_n s_n \sin \omega_n x \quad (2.44)$$

where

$$r_n = \omega_n^2 [(\lambda_1^2 + \nu_{xz})f_n + (\lambda_2^2 + \nu_{xz})g_n]$$

$$s_n = \omega_n [\lambda_1 f_n \sinh p_n + \lambda_2 g_n \sinh q_n - \frac{\lambda_2}{C_p} \cosh p_n + \lambda_2 \cosh q_n + \frac{\lambda_1}{C_p} - \lambda_2]$$

Substitute Eqs. (2.43) and (2.44) into Eq. (2.33) to obtain

$$\frac{C_{12} M_T}{EI} = \sum_{n=1}^{\infty} D_n \left\{ \frac{r_n}{E_{1x}} + 2h_1 s_n \left[ \frac{1}{A_2 E_2} + \frac{C_{12}^2}{EI} + \omega_n^2 \right] \right\} \sin \omega_n x \quad (2.45)$$

Writing the total moment  $M_T$  due to external load in Fourier series form yields

$$M_T = \sum_{n=1}^{\infty} F_n \sin \omega_n x \quad (2.46)$$

Substituting Eq. (2.46) into Eq. (2.45) and solve for  $D_n$  in terms of  $F_n$  results in

$$D_n = H_n F_n \quad (2.47)$$

where

$$H_n = \frac{C_{12}}{EI \left[ \frac{r_n}{E_{1x}} + 2h_1 s_n \left( \frac{1}{A_2 E_2} + \frac{C_{12}^2}{EI} + \omega_n^2 \right) \right]} \quad (2.48)$$

With the constant  $D_n$  being defined as above, it is possible to evaluate the effective flange width by definition as

$$w_e = \frac{F}{h_1 \sigma_x |_{z=0}} = 2 \cdot \frac{\sum_{n=1}^{\infty} H_n F_n s_n \sin \omega_n x}{\sum_{n=1}^{\infty} H_n F_n \omega_n^2 (f_n \lambda_{n1}^2 + g_n \lambda_{n2}^2)} \quad (2.49)$$

A computer program was developed from the above results for the evaluation of the effective flange width. A listing of the program is presented in Appendix E.

#### 2.2.4 Effect of Gaps in the Analysis of Floors and the Solution by Finite Element Method

As mentioned previously, the floor sheathing of a wood joist floor system is generally composed of several pieces of plywood or particle board, which are built on one by one, interlocked by T & G joints, butted, or open joints. Gaps between pieces of sheathing board are therefore inevitable. Only on some occasions are the gaps filled with glue. It has been a common construction practice to leave the gaps open and unglued.

The discontinuity in the sheathing layers caused by the gaps or the gaps filled with glue results in a very abrupt reduction in the stiffness of the sheathing layer which can not be easily treated by the closed-form solution of the finite difference techniques. Fortunately, this difficulty can be overcome by using finite element solution technique. The floor structure is treated as an assemblage of a finite number of structural elements interconnected at discrete nodal points. The variable material properties of the floor components can be included by assigning different material properties to the structural elements. Tightly butted gaps or gaps filled with glue can be coped with very easily by asserting pseudo nodal points, as many as the number of gaps, with zero element length and very low

stiffness of materials. Open gaps in sheathing can be handled by approximating the axial deformations with a discontinuous linear function and the deflections with a continuous third order function.

### 2.3 Theoretical Development of Floor Analysis Method

The wood floor system is a highly indeterminate and nonhomogeneous structure. To analyze the floor structure efficiently and yet not introduce significant error, simplifications are made as follows:

1. The floor system can be simulated physically by two sets of simply supported beams crossing each other at right angles. One set is the T-beams consisting of the wood joist connected to a flange of sheathing with an effective flange width; the other set is the sheathing beams consisting of the sheathing layer(s) only, with an assumed width equal to any convenient distance for the analysis.
2. Effects of torsional stiffness in the floor system can be neglected.

With the above simplifications, the floor can be divided into a set of T-beams, one for each joist and a set of sheathing beams with the number of beams dependent on the beam width chosen. The width of the sheathing beams is usually chosen such that there are no longitudinal gaps along the beam length.

The solution of the layered beam theory can then be applied to each beam to compute the deflection at each nodal point along the beam in terms of the vertical interaction forces between layers at the nodal points. The geometrical compatibility at each nodal point for the two sets of crossing beams is utilized to solve the vertical interaction forces between layers at each nodal point. From the vertical interaction forces, the deflection at each nodal point can in turn

be computed. Both finite difference and finite element methods can be employed for developing solutions and each will be discussed in detail.

### 2.3.1 General Development of the Governing Equations of the Layered Beam Systems with Interlayer Slip

Since the analysis of floor behavior is based on layered beam theory, further review of this theory is necessary. The derivation of the governing equations of a two-layer beam system subjected to uniformly distributed loading has been presented in Section 2.2.1. The governing equations of layered beam systems for different loading conditions and any number of layers will be reviewed briefly in this section. For the complete details of the derivations, reference is made to Goodman (9, 10, 11), Henghold (14, 15) and Ko (17).

By following the same procedure employed in Sec. 2.2.1, the final governing equation for the layer axial force,  $F$ , for a two layered beam system subjected to a concentrated load  $P$ , can be written as

$$\frac{d^2 F}{dx^2} - C_1 F = - C_2 M_T \quad (2.50)$$

Eq. (2.50) assumes the same form as Eq. (2.6) except the total moment  $M_T$  is, in this case, the result of a concentrated load. The governing equations for deflection are similar to Eq. 2.8 but must be rewritten as two equations to describe the deflections on each side of the concentrated load since different expressions for  $M_T$  are necessary on each side of the concentrated load. Thus,

$$Y_L = (Y_S)_L + \frac{C_{12}}{E_2(I_1^* + I_2)} \cdot \frac{1}{C_1} F_L \quad (2.51a)$$

$$Y_R = (Y_S)_R + \frac{C_{12}}{E_2(I_1^* + I_2)} \quad (2.51b)$$

For an  $m$ -layer beam system subjected to a uniformly distributed load,  $q$ , (Fig. 2.7 shows a five-layer example), the solution procedure is essentially the same as in previous examples. The final governing equations can be written as

$$\sum_{i=1}^m \frac{dF_i}{dx} = 0 \quad (2.52)$$

$$\sum_{i=1}^m EI_i \frac{d^4 y}{dx^4} - \sum_{i=1}^m r_i \frac{d^2 F_i}{dx^2} = q \quad (2.53)$$

and

$$-\left(\frac{s}{kn}\right)_{i,i+1} \cdot \frac{d^2 F_i}{dx^2} = \frac{F_{i+1}}{EA_{i+1}^*} - \frac{F_i}{EA_i^*} + C_{i,i+1} \frac{d^2 y}{dx^2} \quad (2.54)$$

where  $C_{i,i+1} = \frac{1}{2} (h_i + h_{i+1})$

The notations used are:

$h_i$  = thickness of the  $i^{\text{th}}$  layer, in.,

$r_i$  = the distance from the centroid of the transformed cross-section to the centroid of the  $i^{\text{th}}$  layer, in.,

$F_i$  = the axial force in the  $i^{\text{th}}$  layer, lb.,

$A_i^*$  = the transformed area of the  $i^{\text{th}}$  layer, lb, in<sup>2</sup>.

There are  $m + 1$  unknowns ( $m$   $F$  values and one value of  $y$  for any beam distance  $x$ ) in an  $m$ -layer beam system. The  $m + 1$  equations which are necessary to solve for the unknowns are provided with two equations from Eqs. (2.52), (2.53) and the remainder of the required  $m - 1$  equations obtained from Eq. (2.54).

### 2.3.2 Finite Difference Approach

The floor system can be represented physically by two sets of crossing beams under the previously stated simplifications. The

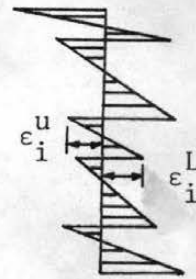
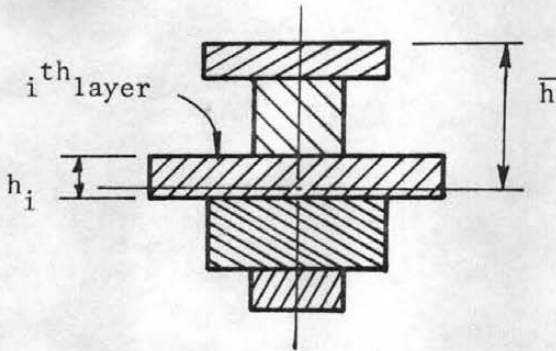
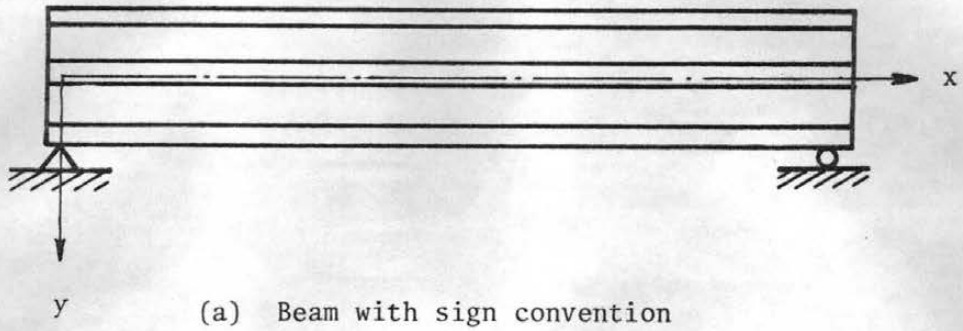
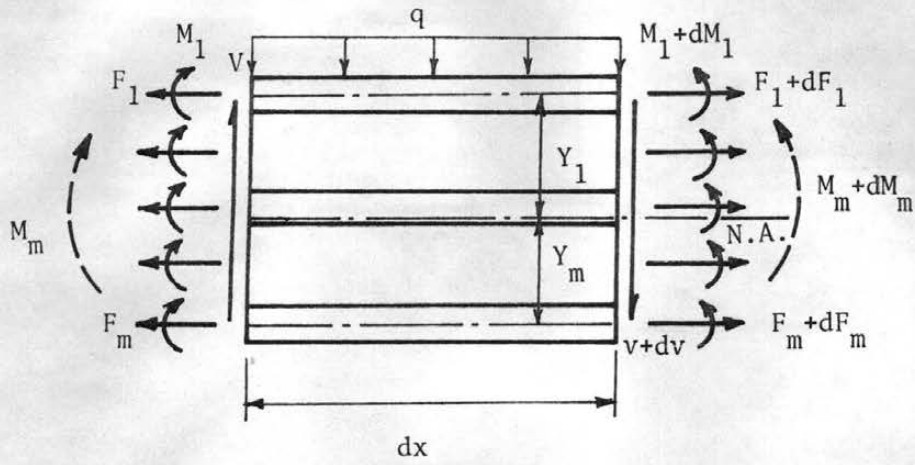
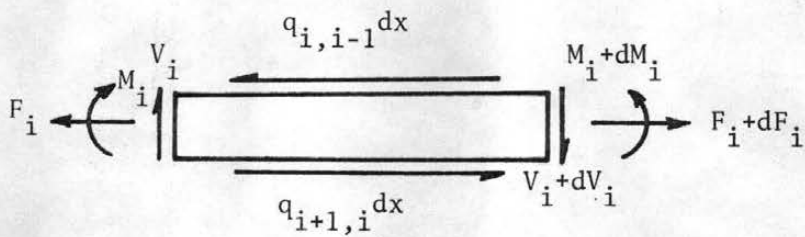


Figure 2.7 Five-Layer Example of m-Layer System



(d) Beam element



(e)  $i^{\text{th}}$  layer element

Figure 2.7 Five-Layer Example of  $m$ -Layer System (continued)

analysis of the floor structure is, therefore, reduced to the solving of an indeterminate structural system of crossing beams.

The flexibility method was employed by Vanderbilt and Goodman et al. (12, 38) in a finite difference approach to the analysis of a floor system. The basic mathematical model was developed in a series of steps using matrix theory. For a more detailed discussion of matrix analysis of structural mechanics, reference is made to a publication by Vanderbilt (38).

A general physical model for a floor system is presented in Fig. 2.8. First, consider the set of T-beams acting alone. The load-deflection relationship of the T-beams is given by

$$DT = FT * AT \quad (2.55)$$

where

DT = the matrix of deflections of T-beams at the nodal points,

FT = the flexibility matrix of T-beams at the nodal points,

AT = the matrix of loads carried by joists.

Similarly, for the set of sheathing beams acting alone, the load-deflection relationship is

$$DS = FS * AS \quad (2.56)$$

Static equilibrium requires that

$$AT + AS = A \quad (2.57)$$

where A is the matrix of external loads applied at nodal points.

To satisfy the geometrical compatibility condition, the two beams crossing at each node point must deflect the same amount. Therefore, it is required that

$$DS = DT = D \quad (2.58)$$

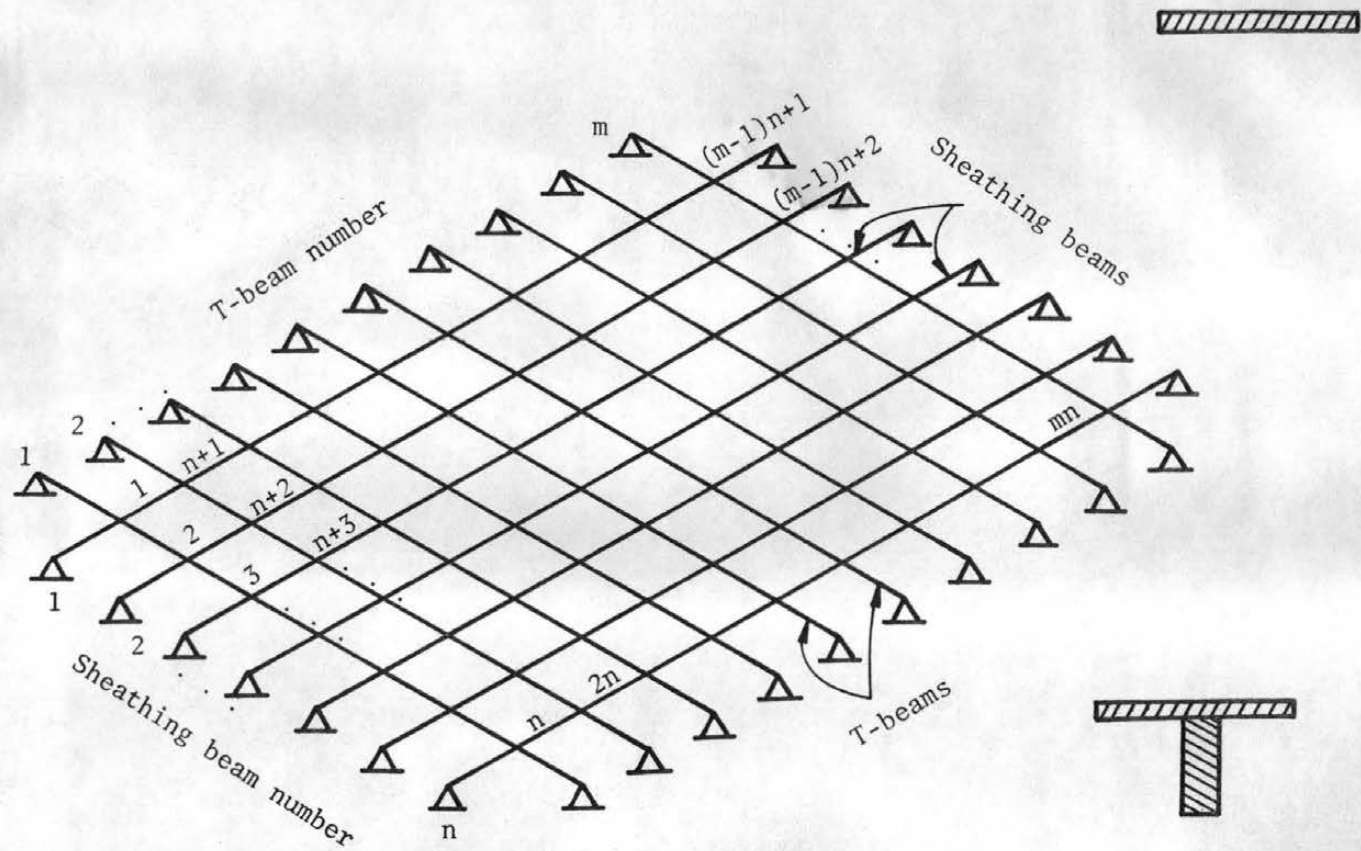


Figure 2.8 Physical Model of a Floor System

where  $D$  is the matrix of the nodal point deflections of the entire floor.

Substituting Eqs. (2.55), (2.56) and (2.57) into Eq. (2.58) and simplifying gives

$$(F_T + F_S) * A_T = F_S * A \quad (2.59)$$

from which

$$A_T = (F_T + F_S)^{-1} * F_S * A \quad (2.60)$$

Finally, the floor deflections at the nodal points,  $D$ , can be computed from Eq. (2.55) after  $A_T$  has been determined from Eq. (2.60).

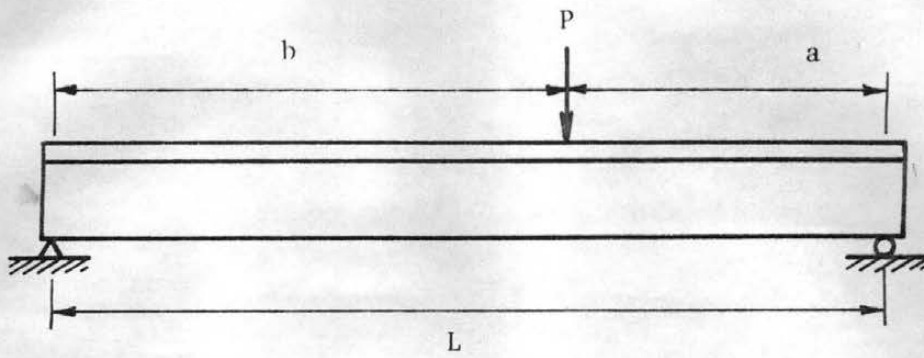
Closed form solutions are generally handicapped by the assumption that uniform cross-sectional, material and mechanical properties must be retained along the length of the beam. Consequently, to evaluate  $F_T$  and  $F_S$  including the varying section properties, connector modulus and spacings and to perform the computations of Eqs. (2.59), (2.60) and (2.55) efficiently, numerical solution with the application of high speed digital computer must be employed.

The two-layer floor system shown in Fig. 2.9 will be selected as an example to be solved by the finite difference technique. Since the uniformly loaded case can be approximated by a series of equally spaced concentrated loads, only the concentrated loading case need be considered.

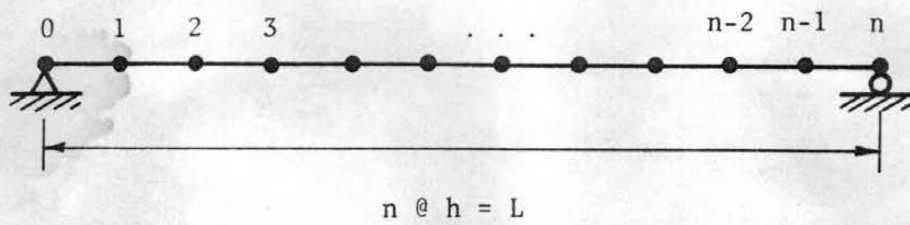
The solution procedure starts by solving Eq. (2.50) for  $F$  at the nodal points along the T-beams. Eq. (2.50) is rewritten below:

$$\frac{d^2 F}{dx^2} - C_1 F = - C_2 M \quad (2.50)$$

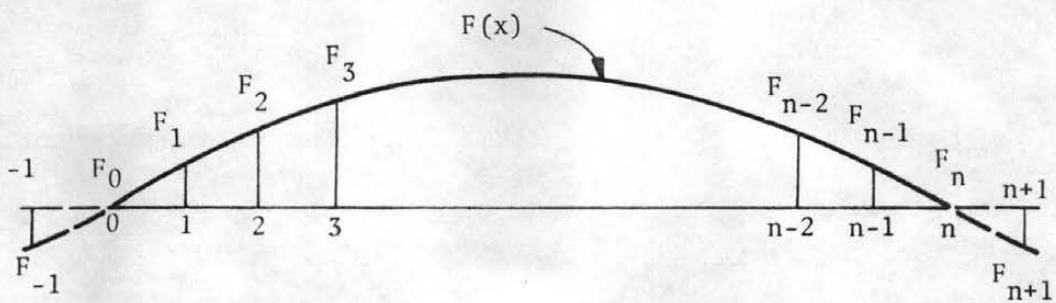
with the boundary conditions that the axial forces and the moments are zero at the ends since the T-beams are simply supported. From



(a) Real T-beam



(b) Finite difference model



(c) Boundary conditions of F

Figure 2.9 Finite Difference Model and Boundary Conditions

Eq. (2.50) it is noted that the second derivative of axial force at the ends of T-beams are also zero. If each T-beam is divided into  $n$  elements connected by  $n + 1$  discrete nodal points, as indicated in Fig. 2.9b, application of end conditions requires

$$\left. \begin{aligned} F_0 &= \frac{d^2 F_0}{dx^2} = 0 && \text{at } x = 0 \\ F_n &= \frac{d^2 F_n}{dx^2} = 0 && \text{at } x = L \end{aligned} \right\} \quad (2.61)$$

Based on a three-term finite difference expansion for the second derivative of  $F$ , the first boundary condition of Eq. (2.61) implies

$$\frac{d^2 F_0}{dx^2} = \frac{1}{h^2} (F_{-1} - 2F_0 + F_1) = 0$$

and since  $F_0$  is zero, it yields

$$F_{-1} = -F_1 \quad (2.62)$$

the second boundary condition implies

$$\frac{d^2 F_n}{dx^2} = \frac{1}{h^2} (F_{n-1} - 2F_n + F_{n+1}) = 0$$

since  $F_n$  is zero, it gives

$$F_{n+1} = -F_{n-1} \quad (2.63)$$

The boundary conditions for the axial force  $F$  are depicted in Fig. 2.9c.

For convenience, a dimensionless variable,  $z$ , is introduced as follows:

$$z = \frac{x}{L}, \quad 0 \leq z \leq 1 \quad (2.64)$$

and consequently the differential operators are

$$\frac{d}{dx} = \frac{1}{L} \frac{d}{dz}, \quad \frac{d^2}{dx^2} = \frac{1}{L^2} \frac{d^2}{dz^2} \quad (2.65)$$

and boundary conditions in terms of  $z$  become

$$\left. \begin{aligned} F_o &= 0 \quad \text{at } z = 0, \quad (\text{or } x = 0) \\ F_n &= 0 \quad \text{at } z = 1, \quad (\text{or } x = L) \end{aligned} \right\} \quad (2.66)$$

Using a five point finite difference expansion for the following operator is obtained (for detailed development reference is made to the work by Ko (17)).

$$\frac{d^2 F}{dx^2} = \frac{1}{L^2} \frac{d^2 F}{dz^2} = \frac{1}{12h^2} [ \textcircled{-1} - \textcircled{16} - \overset{\downarrow}{\textcircled{-30}} - \textcircled{16} - \textcircled{-1} ] F \quad (2.67)$$

where the error of the finite difference operator is of order  $h^4$ .

Substituting Eq. (2.65) into Eq. (2.50) for the  $i^{\text{th}}$  nodal point yields

$$\frac{d^2 F_i}{dz^2} - C_1 L^2 F_i = - C_2 L^2 M_i \quad (2.68)$$

where

$$M_i = M_{Li} = Pbz_i \quad \text{for } 0 \leq z \leq a/L$$

$$M_i = M_{Ri} = Pa(1-z_i) \quad \text{for } a/L \leq z \leq 1$$

Substituting Eq. (2.67) into Eq. (2.68) yields

$$\begin{aligned} -F_{i-2} + 16F_{i-1} + (-30 - 12C_1 h^2 L^2)F_i + 16F_{i+1} - F_{i+2} \\ = -12C_2 h^2 L^2 M_i \end{aligned} \quad (2.69)$$

or it may be written in operator form as

$$\text{FT} = \begin{bmatrix} \text{FT}_1 \\ \text{FT}_2 \\ \dots \\ \text{FT}_j \\ \dots \\ \text{FT}_m \end{bmatrix} \quad (2.74)$$

mnxmn

where

$m$  = the number of T-beams

$n$  = the number of sheathing beams.

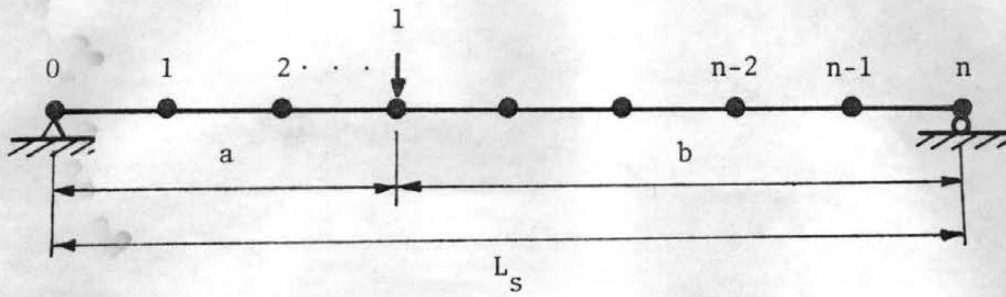
The flexibility matrix of the sheathing beams can be obtained from the load-deflection relationship of a simple beam since the sheathing beams are single-layered (for a two-layer floor) and simply supported. For a sheathing beam loaded by a unit concentrated load as indicated in Fig. 2.10, the deflection at the  $i^{\text{th}}$  nodal point is

$$y_i = \frac{ib/n}{6EI} [L_s^2 - (\frac{i}{n} L_s)^2 - b^2] \quad \text{for } 0 \leq \frac{i}{n} L_s < a \quad (2.75a)$$

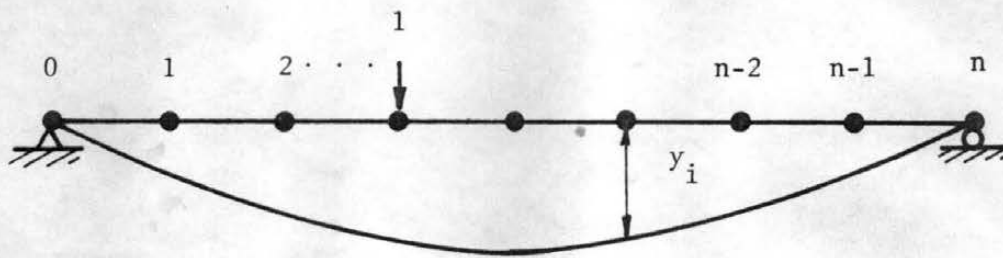
$$y_i = \frac{b}{6EI} \left[ \frac{1}{b} (\frac{i}{n} L_s - a)^3 + \frac{i}{n} (L_s^2 - b^2) - (\frac{i}{n})^3 L_s^2 \right]$$

for  $a \leq \frac{i}{n} L_s \leq L_s$  (2.75b)

The flexibility matrix of the  $q^{\text{th}}$  sheathing beam,  $\text{FS}_q$ , can be obtained by placing the unit load on each nodal point except the end points of the  $q^{\text{th}}$  sheathing beam and computing the deflections at each nodal point. Repeating the same procedure stated above for each sheathing beam and combining the individual flexibility matrix allows the formation of the complete flexibility matrix for all the sheathing beams as shown in Eq. (2.76).



(a) Sheathing beam subjected to unit load



(b) Deflection curve

Figure 2.10 Finite Difference Model of Sheathing Beam



Again, the physical model of a layered floor was simplified as two sets of crossing beams, i.e., T-beams and sheathing beams, as indicated previously in Fig. 2.8. Each set of beams is treated as a layered beam. The deflection and axial deformation of the layered beams can be approximated by the finite element form of the Rayleigh-Ritz procedure. The tightly butted or glued gaps in the sheathing layer(s) can be approximated by inserting a pseudo element with zero length and a small stiffness. The open gaps in sheathing are accounted for by using discontinuous functions to approximate axial displacements but continuous function for deflections.

The energy method was used to formulate the finite element solution procedure. The potential energy of a layered beam was considered as composed of four distinct parts due to:

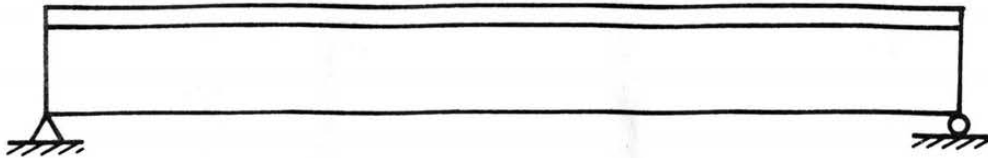
1. pure bending of each layer,
2. axial elongation of each layer,
3. the interlayer slip of connectors between each layer,
4. the external loads on the beam.

To form the finite element model, the beam is divided into a series of one dimensional elements as shown in Fig. 2.11. The energy of the beam system is the sum of the energy of all the elements. With the assumption that each layer of the beam deflects the same amount, the energy due to pure bending can be written as

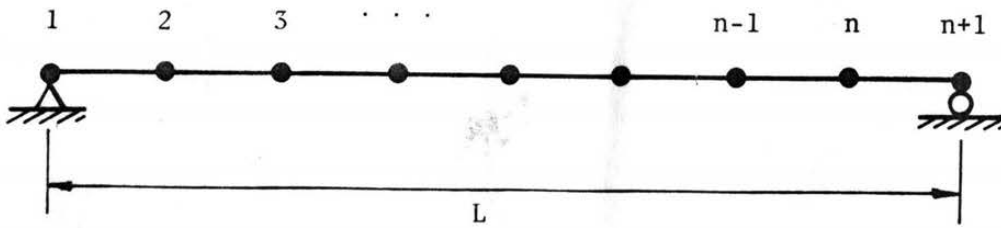
$$J^b = \frac{1}{2} \sum_{i=1}^{n_L} \int_0^L E_i I_i \left( \frac{d^2 y}{dx^2} \right)^2 dx \quad (2.77)$$

and the energy due to the external loads is

$$J^q = - \int_0^L q y dx \quad (2.78)$$



(a) Real T-beam or sheathing beam



(b) Finite element model

Figure 2.11 Finite Element Model of Layered Beam

where

- $J^b$  = energy due to pure bending, lb-in.,  
 $E_i$  = modulus of elasticity of  $i^{\text{th}}$  layer, psi,  
 $I_i$  = moment of inertia of  $i^{\text{th}}$  layer, in.<sup>4</sup>,  
 $y$  = deflection of beam, in.  
 $x$  = coordinate along length of beam, in.,  
 $n_L$  = number of layers,  
 $J^q$  = energy due to external loads, lb-in.,  
 $q$  = loading on beam, lb/in.,  
 $L$  = length of beam, in.

The total energy due to the axial deformation of each layer is

$$J^u = \sum_{i=1}^{n_L} \frac{1}{2} \int_0^L E_i A_i \left( \frac{du_i}{dx} \right)^2 dx \quad (2.79)$$

where

- $J^u$  = energy due to axial deformation, lb-in.,  
 $A_i$  = cross sectional area of  $i^{\text{th}}$  spacing layer, in.<sup>2</sup>,  
 $u_i$  = axial deformation of the  $i^{\text{th}}$  layer at middepth, in.

The energy due to the interlayer slip deformation of the connectors

is

$$J^c = \sum_{i=1}^{n_L-1} \frac{1}{2} \int_0^L \left( \frac{k_i n_i}{s_i} \right) (\Delta s_i)^2 dx \quad (2.80)$$

where

- $J^c$  = energy due to interlayer slip of the connectors, lb-in.,  
 $k_i$  = slip modulus of the connectors between  $i^{\text{th}}$  and  $(i+1)^{\text{th}}$  layers, lb/in.,  
 $n_i$  = number of rows of connectors across the beam between  $i^{\text{th}}$  and  $(i+1)^{\text{th}}$  layers,

$s_i$  = spacing of connectors along the beam between  $i^{\text{th}}$  and  $(i+1)^{\text{th}}$  layers,

$\Delta s_i$  = the interlayer slip between  $i^{\text{th}}$  and  $(i+1)^{\text{th}}$  layer interface.

The interlayer slip,  $\Delta s_i$ , can be expressed in terms of the beam deflection and the axial displacements of the  $i^{\text{th}}$  and  $(i+1)^{\text{th}}$  layers. The relation is depicted in Fig. 2.12 and with the assumption that the slope of the beam is small compared to unity can be stated as

$$\begin{aligned}\Delta s_i &= (u_{i+1} - \frac{h_{i+1}}{2} \frac{dy}{dx}) - (u_i + \frac{h_i}{2} \frac{dy}{dx}) \\ &= (u_{i+1} - u_i) - \frac{1}{2}(h_{i+1} + h_i) \frac{dy}{dx}\end{aligned}\quad (2.81)$$

where  $h_i$  and  $h_{i+1}$  are the depths of the  $i^{\text{th}}$  and  $(i+1)^{\text{th}}$  layers, respectively.

Substituting Eq. (2.81) into Eq. (2.80) gives the energy due to interlayer slip of the connectors as

$$J^c = \frac{1}{2} \sum_{i=1}^{n_L-1} \int_0^L \left( \frac{k_i n_i}{s_i} \right) \left[ (u_{i+1} - u_i) - \frac{1}{2}(h_{i+1} + h_i) \frac{dy}{dx} \right]^2 dx \quad (2.82)$$

The total energy of the beam can then be obtained by summing Eqs. (2.77), (2.78), (2.79) and (2.81) resulting in

$$\begin{aligned}J &= \sum_{i=1}^{n_L} \int_0^L \left\{ \frac{1}{2} E_i I_i \left( \frac{d^2 y}{dx^2} \right)^2 + \frac{1}{2} E_i A_i \left( \frac{du_i}{dx} \right)^2 \right\} dx \\ &+ \sum_{i=1}^{n_L-1} \int_0^L \frac{1}{2} \left( \frac{k_i n_i}{s_i} \right) \left[ (u_{i+1} - u_i) - \frac{1}{2}(h_{i+1} + h_i) \frac{dy}{dx} \right]^2 dx \\ &- \int_0^L q y dx\end{aligned}\quad (2.83)$$



According to the principal of virtual work, the potential energy of the beam system must have a stationary value at a deflection which is an equilibrium position, that is

$$\delta J = 0$$

where

$$\begin{aligned} \delta J = & \sum_{i=1}^{n_L} \left\{ \int_0^L E_i I_i \left( \frac{d^2 y}{dx^2} \right) \delta \left( \frac{d^2 y}{dx^2} \right) dx + \int_0^L E_i A_i \left( \frac{du_i}{dx} \right) \delta \left( \frac{du_i}{dx} \right) dx \right\} \\ & + \sum_{i=1}^{n_L-1} \left\{ \int_0^L \left( \frac{k_i n_i}{s_i} \right) \left[ (u_{i+1} - u_i) - \frac{1}{2}(h_{i+1} + h_i) \frac{dy}{dx} \right] \delta (u_{i+1} - u_i) dx \right. \\ & - \int_0^L \left( \frac{k_i n_i}{s_i} \right) \left[ (u_{i+1} - u_i) - \frac{1}{2}(h_{i+1} + h_i) \frac{dy}{dx} \right] \frac{1}{2}(h_{i+1} + h_i) \cdot \delta \left( \frac{dy}{dx} \right) dx \left. \right\} \\ & - \int_0^L q \delta y dx \end{aligned} \quad (2.84)$$

The deflection and axial displacements of the layered beam which satisfy Eq. (2.84) can be approximated by the finite element form of the Rayleigh-Ritz procedure.

The deflection,  $y$ , and the axial displacement,  $u_i$ , in the above equations are assumed to be one dimensional and are function of the distance along the beam only. Since the potential energy is of first order in  $u_i$ , the axial displacements of the nodal points can be approximated by a piecewise linear function of the nodal point coordinate,  $x$ . On the other hand, the potential energy is of second order in  $y$ , thus a cubic function of  $x$  is necessary to approximate the deflections of the nodal points to attain the continuity of the deflection,  $y$ , and the slope,  $\frac{dy}{dx}$  of the layered beam. The potential energy for the complete

layered beam can therefore be expressed in terms of the nodal point values of deflection, slope and the axial displacements of each layer.

The total unknowns for each nodal point, consequently, are  $2 + n_L$ .

Let the approximations for  $y$  and  $u_i$  in the  $j^{\text{th}}$  element be given as

$$y = [N_y] \{Y\}_j \quad (2.85)$$

and

$$u_i = [N_u] \{U_i\}_j \quad (2.86)$$

where

$[N_y]$  = shape functions for a fourth order approximation for deflections,

$\{Y\}_j$  = nodal point values for deflection and slope for  $j^{\text{th}}$  element,

$[N_u]$  = shape functions for a linear approximation for axial displacement,

$\{U_i\}_j$  = nodal point values for the axial displacements of  $i^{\text{th}}$  layer in  $j^{\text{th}}$  element.

The derivatives of the functions  $y$  and  $u_i$  are then given by

$$\frac{dy}{dx} = [N_y'] \{Y\}_j \quad (2.87)$$

$$\frac{d^2y}{dx^2} = [N_y''] \{Y\}_j \quad (2.88)$$

$$\frac{du_i}{dx} = [N_u'] \{U_i\}_j \quad (2.89)$$

where the primes indicate the term by term differentiation of the matrices.

The variations of the functions  $y$ ,  $\frac{dy}{dx}$ ,  $\frac{d^2y}{dx^2}$ ,  $u_i$  and  $\frac{du_i}{dx}$  are

$$\delta y = [N_y] \{\delta Y\}_j \quad (2.90)$$

$$\delta \left( \frac{dy}{dx} \right) = [N_y'] \{\delta Y\}_j \quad (2.91)$$

$$\delta \left( \frac{d^2 y}{dx^2} \right) = [N_y''] \{\delta Y\}_j \quad (2.92)$$

$$\delta u_i = [N_u] \{\delta U_i\}_j \quad (2.93)$$

$$\delta \left( \frac{du_i}{dx} \right) = [N_u'] \{\delta U_i\}_j \quad (2.94)$$

The variation of potential energy for any element can now be approximated in terms of the nodal point values for  $y$ ,  $\frac{dy}{dx}$ ,  $\frac{d^2 y}{dx^2}$  and  $u_i$  in matrix form. For example, the variation of pure bending energy for the  $j^{\text{th}}$  element is

$$\begin{aligned} & \sum_{i=1}^{n_L} \int_0^{l_j} E_i I_i \left( \frac{d^2 y}{dx^2} \right) \delta \left( \frac{d^2 y}{dx^2} \right) dx \\ &= \sum_{i=1}^{n_L} \int_0^{l_j} E_i I_i [N_y''] \{\delta Y\}_j^T [N_y''] \{Y\}_j dx \\ &= \{\delta Y\}_j^T \int_0^{l_j} [N_y'']^T EI [N_y''] dx \{Y\}_j \end{aligned} \quad (2.95)$$

where

$$EI = \sum_{i=1}^{n_L} E_i I_i$$

Applying the same procedure on the remaining terms of Eq. (2.90) and summing each of the terms into one matrix expression, the variation of the potential energy of the  $j^{\text{th}}$  element can be written as

$$\delta J_j = \{\delta s\}_j^T [k]_j \{s\}_j - \{\delta s\}_j^T \{f\}_j \quad (2.96)$$

where

- $\{s\}_j$  = matrix combining all the generalized displacement for  $y$ ,  $\frac{dy}{dx}$ ,  $u_i$  of  $j^{\text{th}}$  element,
- $[k]_j$  = Stiffness matrix for  $j^{\text{th}}$  element,
- $\{f\}_j$  = matrix combining all generalized external forces corresponding to  $\{s\}_j$  of the  $j^{\text{th}}$  element,
- $\{\delta s\}_j$  = the variation of  $\{s\}_j$ .

Applying Eq. (2.96) on each element and summing the variations of potential energy of all the elements by proper matrix addition, the total variation of potential energy of the beam system can be obtained. Setting the total variation of potential energy to be zero leads to the general equilibrium equation

$$[K] \{S\} = \{F\} \quad (2.97)$$

where  $[K]$ ,  $\{S\}$  and  $\{F\}$  are the beam system equivalents of  $[k]_j$ ,  $\{s\}_j$  and  $\{f\}_j$ . The nodal point values of  $y$ ,  $\frac{dy}{dx}$  and  $u_i$  can then be obtained by solving Eq. (2.97).

The finite element formulation developed above can be modified easily to account for gaps in the sheathing. Wherever a gap occurs in a given layer, the axial displacement  $u_i$ , in that layer is no longer continuous. Furthermore, the axial force in that layer is zero on both sides of the gap. These conditions can be satisfied by using linear discontinuous functions to approximate axial displacements in sheathing but a third order continuous function for deflections. For flexible gaps (tightly butted or glued gaps) it can be handled by inserting an imaginary element with zero length at the point where the gap is located. The MOE of the imaginary element is assigned to be some reasonable small number for a flexible gap to account for a partial

transmission of axial force through the gap. The placing of an imaginary element actually puts two nodal points with the same coordinate at the gap. The generalized displacements and forces associated with the higher numbered nodal points at each gap are treated as dummy quantities with the exception of the axial displacement and force in the gapped layer. For this layer, there are two independent axial displacements which create the desired discontinuity in the function. The corresponding generalized force terms on the right-hand side of Eq. (2.97) are always as zero.

To analyze the floor behavior under loads, the above finite element formulation can be applied for each set of cross beams of the physical floor model. First, the external loads are assumed to act totally on T-beams. The deflections of the T-beams under the external loads are computed. The T-beams deflections are then imposed on the set of sheathing beams on the corresponding nodal points. Forces required to hold down the sheathing beams to the deflected positions are in turn to be evaluated. Then, the loads acted on the set of T-beams are reduced to be the difference of the total external loads and the reactions of the forces on the set of sheathing beams. Deflections of the T-beams under the new loads are computed and imposed on the set of sheathing beams to calculate the forces required to hold down the set of sheathing beams to the new deflected positions.

The above procedure can be repeated by an interactive algorithm. The algorithm is stopped by an accuracy control when the result of two successive cycles shows negligible changes. A direct solution form of the finite element method was also developed using Gaussian elimination method of solving simultaneous equations to avoid the iteration requirement.

## 2.4 Implication and Limiting Cases for Floor Model

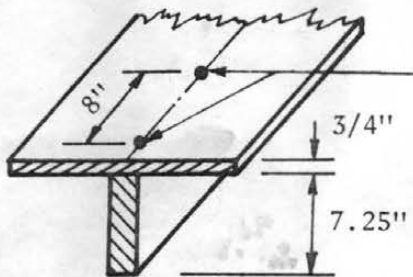
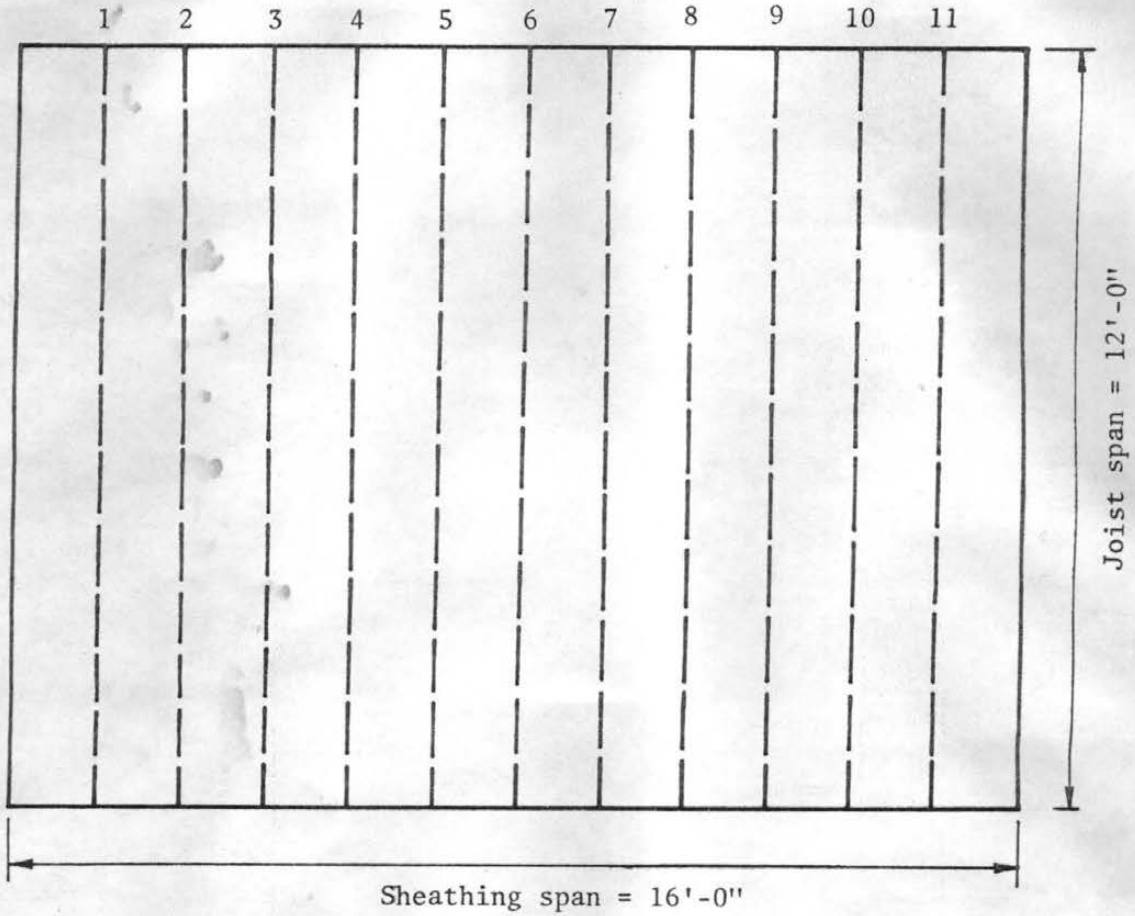
The mathematical floor model can be used for the theoretical study of several extreme cases of the floor system. A better understanding of the interaction of floor components is developed through the examination of limiting cases for the floor system. The merit of the new analysis procedure developed in this study over the traditional methods will also be more evident through the studying of the limiting cases and variation in parameters.

To illustrate the effect of the limiting cases, the deflections of the example floor shown in Fig. 2.13 were computed using the mathematical floor model for the case of uniform load. The floor contains eleven 2x8 nominal size joists and 3/4 inch thick Douglas-fir plywood sheathing. No gaps are assumed. The floor dimensions are 12 ft span and 16 ft width. The face grain of the sheathing is assumed to be perpendicular to the joist span and the nail spacing of 8d nails is eight inches with one nail per row. Simple supports are assumed at all edges of the floor. The results of calculating several limiting cases along with assumed material properties, are shown in Fig. 2.14 and are discussed as follows:

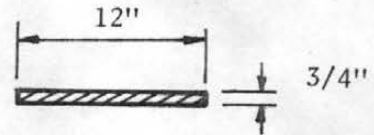
1. No sheathing, joists only

The traditional design practice for wood joist floor systems is based on the generally conservative assumption that the effectiveness of sheathing is negligible and the external loads are resisted by the joists alone. This was done by assigning essentially a zero value for the MOE of the sheathing in both the parallel and the perpendicular to face grain directions such that the sheathing material had no stiffness requiring the joists to

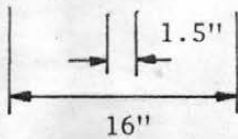
Joist number



8-d common nails



Sheathing strip cross-section



T-beam cross-section

Figure 2.13 Example Floor for Parameter Studies

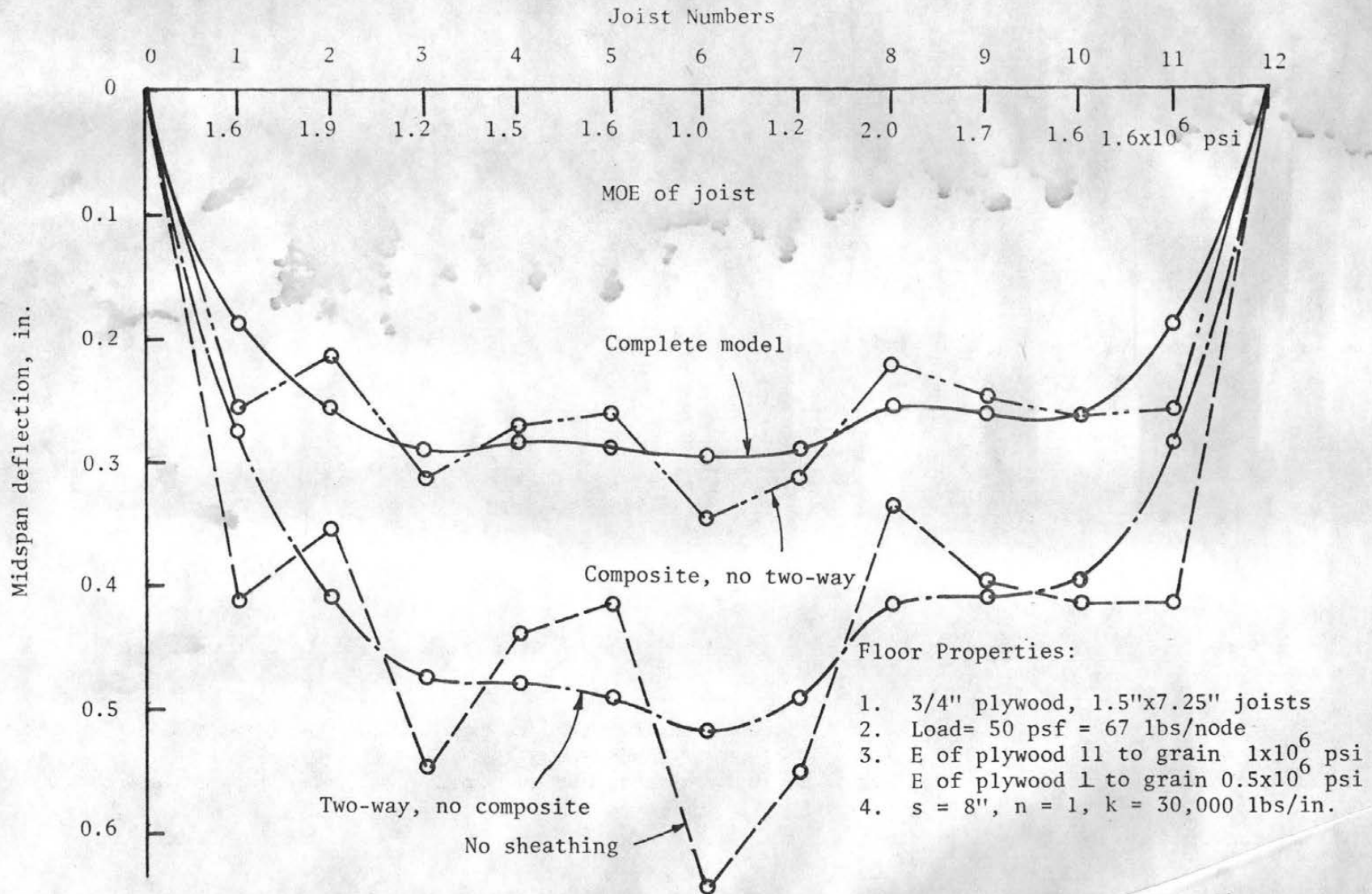


Figure 2.14 Deflection Curves of Limiting Cases for an Example Floor

act independently in resisting loads. The MOE data for the joists are listed under the joist numbers at the top of Fig. 2.14. Large deflections of the joist were obtained as expected when the joist acted individually. The midspan deflections of the joists, connected by straight lines, are presented in Fig. 2.14.

## 2. Two-way actions, no composite behavior

The effect of the loose overlap of the sheathing on the joists is studied next. This is done through the mathematical floor model by assuming a near zero value of the slip modulus of the connectors between the sheathing and the joists. The composite action of the T-beams were thus eliminated by using a slip modulus equal to zero whereas the two-way action of the sheathing was considered by input of usual MOE data for the plywood as given in Fig. 2.14. The effect of the two-way, no T-beam action is seen from the midspan joist deflection curve as shown in Fig. 2.14.

The stiffer joists help the neighboring less-stiff joists in resisting loads through the two-way action of the sheathing material and smooth out the deflection curve as opposed to the result obtained for a set of independently acting joists.

## 3. Composite behavior, no two-way action

The third case to be examined is the effect of considering the floor as a set of unconnected T-beams. This was achieved by using a near zero value for the MOE of the sheathing material in the direction perpendicular to the joist span and a normal MOE in the direction parallel to the joist span. The rigidity of the sheathing material was thus eliminated in the direction perpendicular to the joist span and retained in the direction parallel to the joist and the floor was forced to act as a set of T-beams

by the mathematical floor model. The incomplete composite action of the T-beams were included by setting the slip modulus of the connectors to equal 30,000 lb/in. The midspan deflections of the joists are plotted in Fig. 2.14. It is seen that the midspan deflections of the joists reduce considerably due to the incomplete composite action between the sheathing and the joists.

#### 4. Composite and two-way action

Finally, the full effect of the incomplete composite behavior and two-way action is considered for a complete floor model. The floor data given in Fig. 2.14 were used for the computation of the deflections. The midspan deflections of the joists are again plotted as shown in Fig. 2.14. The two-way action of the sheathing material again shows the effect that the stiffer joists help the neighboring less stiff joists in resisting the loads and smooth out the deflection curve of a set of unconnected T-beams. The differences in deflections range up to greater than 100 percent when deflections of joist acting alone are compared with those predicted by the complete mathematical model. This indicates that the traditional design practice generally overestimates the predicted deflections since it neglects the contributions of the composite and two-way action. It also demonstrates that a full recognition of both composite and two-way action should be included for the complete representation of the behavior of floor systems. Experimental studies discussed in Chapter 3 will demonstrate the required verifications of the mathematical model to assure that the utilization of the analytic method can be expected to produce accurate results.

## CHAPTER 3

### EXPERIMENTAL STUDY

#### 3.1 Introduction

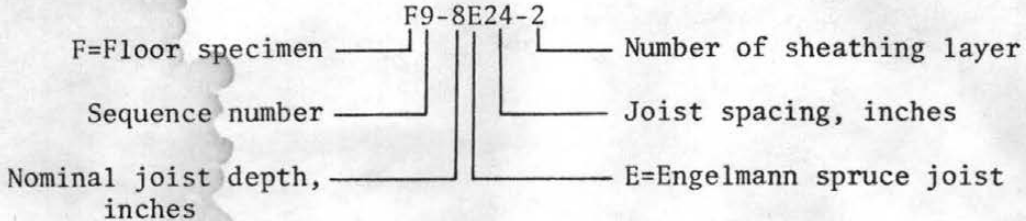
It has been pointed out previously that a vital phase of the floor research project developed at Colorado State University was to conduct load tests on a series of carefully constructed T-beam and floor specimens to verify the validity of the mathematical models for layered beams and for wood joist floor systems. The verification of the mathematical layered beam model has been discussed extensively by Kuo (19).

The results of the verification study of the mathematical floor model are presented in Chapter 4 of this dissertation. The various aspects of the experimental program and the observed test results are discussed in this chapter to provide a better understanding of the experimental aspects of the research effort.

A total of eleven floors were constructed using components with premeasured material properties. Each floor was designed to vary the type of construction. Among the eleven floors built, six were three-layer floors. The three-layer floors were constructed and tested in two stages: first, a layer of plywood sheathing panels was attached to the joists with selected connectors to form a two-layer floor specimen on which load tests in the elastic range were performed; second, an additional layer of particle board sheathing panels were connected to the two-layer floor to form a three-layer floor specimen on which load tests, again, were performed. Therefore, for each three-layer floor there were two floor specimens tested: one was two-layer and the other was three-layer. However, of the eleven

floors constructed the first floor (a two-layer floor) was only a trial floor, built and tested to obtain knowledge of testing techniques and therefore the results of the load tests on it are not included in this report. Consequently, there were a total of sixteen floor specimens available for use in the verification study. A summary of the general data of all the floor specimens constructed and tested is presented in Table 3.1. The detailed data for each floor specimen is listed in Appendix B.

An alphanumeric identifying notation was assigned to each floor specimen to indicate type of joist material and the value of several major parameters. This notation was created to allow easy recognition of the specimen characteristics, and can be illustrated by the following example:



The material used for the construction of floor is described in Sec. 3.2 and Sec. 3.3. The manner in which the floor specimen was constructed is discussed in Sec. 3.4. The testing equipment used in the load tests and the testing procedure are examined in Sec. 3.5 and Sec. 3.6, respectively. In Sec. 3.7, the experimental behavior of the floor specimens due to effects of connectors type, gaps in sheathing layer(s) and number of sheathing layers is examined.

The experimental behavior described in this chapter is observed for specific specimens and is cited as examples of typical behavior. Because each floor was designed to differ from the other floors tested

Table 3.1 General Data of Floor Specimens

Floor Specimen	Joist Material	Number of Unsupported Joists	Joist Spacing (in.)	Sheathing Material	Connectors	Sheathing Joists
F2-8D16-1	2x8 DF	11	16	3/4 DF Plywd	8-d @8" (cement coated)	T & G
F3-8D16-1	2x8 DF	11	16	3/4 DF Plywd	8-d @8"	T & G
F4-8E16-1	2x8 ES	11	16	3/4 ES Plywd	8-d @8"	T & G
F5-8D16-1	2x8 DF	11	16	3/4 DF Plywd	8-d @4"	Glued T & G
F6-8E16-1	2x8 ES	11	16	1/2 ES Plywd	8-d @8"	T&G w/ 1/16" gap
F7-12D24-1	2x12 DF	7	24	1/2 DF Plywd	8-d @4"	Butted w/ 1/16" gap
F8-D19.2-1	2x8 DF	9	19.2	1/2 DF Plywd	8-d @8"	Butted w/ 1/16" gap
F9-8E24-1	2x8 ES	7	24	1/2 ES Plywd	8-d @8"	Butted w/ 1/16" gap
F10-8E24-1	2x8 ES	7	24	1/2 DF Plywd	8-d @4"	Butted w/ 1/16" gap
F11-8D16-1	2x8 DF	11	16	1/2 DF Plywd	Glued	Glued butted joints
F6-8E16-2	2x8 ES	11	16	1/2 DF PB	6-d @8"	Butted w/o gap
				1/2 DF Plywd	8-d @8"	T&G w/ 1/16" gap
F7-12D24-2	2x12 DF	7	24	1/2 DF PB	6-d @4"	Butted w/o gap
				1/2 DF Plywd	8-d @4"	Butted w/ 1/16" gap
F8-8D19.2-2	2x8 DF	9	19.2	1/2 DF PB	6-d @8"	Butted w/o gap
				1/2 DF Plywd	8-d @8"	Butted w/ 1/16" gap

Table 3.1 General Data of Floor Specimen (continued)

Floor Specimen	Joist Material	Number of Unsupported Joists	Joist Spacing (in.)	Sheathing Material	Connectors	Sheathing Joints
F9-8E24-2	2x8 ES	7	24	1/2 DF PB	6-d @8"	Butted w/o gap
				1/2 ES Plywd	8-d @8"	Butted w/ 1/16" gap
F10-8E24-2	2x8 ES	7	24	1/2 DF PB	8-d @4"	Butted w/o gap
				1/2 DF Plywd	6-d @4"	Butted w/ 1/16" gap
F11-8D16-2	2x8 DF	11	16	1/2 DF PB	6-d @8"	Butted w/ 1/16" gap
				1/2 DF plywd	Glued	Glued butted joints

Note: For all floor specimen, floor span = 144 in., floor length = 192 in.  
The nails used are common nails unless otherwise stated.

DF = Douglas-fir,  
ES = Engelmann spruce,  
Plywd = Plywood,  
PB = Particle board

in several respects and the effects of various parameters are often strongly interrelated, only trends rather than precise quantitative information on how the several variables affect floor response can be presented by the analysis of experimental behavior. Parameter studies using the verified mathematical model can better isolate the effect of specific variables. Effects of the sheathing thickness, the joist depth, the MOE of plywood, the MOE of joists, the slip modulus of connectors and the type of loading on the theoretical behavior of a floor system are developed through the use of the mathematical model and presented in Chapter 5.

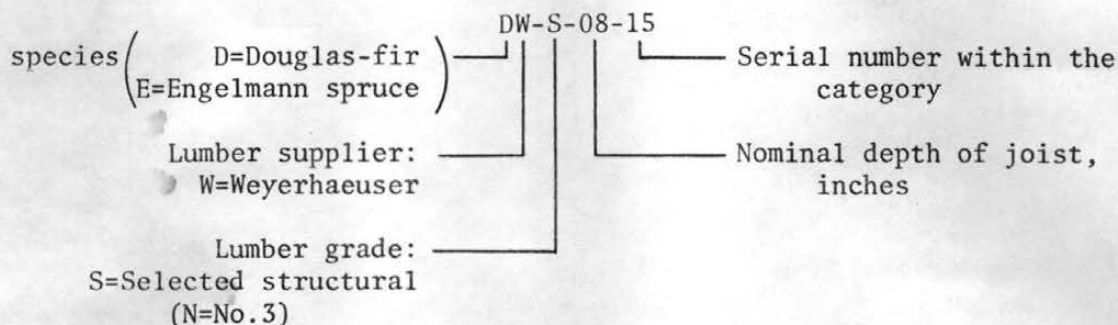
### 3.2 Material Used for Floor Specimens

Of the sixteen floor specimens to be studied, 2x8 inch nominal size joists were used for all but three floor specimens where 2x12 inch nominal joists were used. Douglas-fir joists were used in nine floors and Engelmann spruce joists were used in seven floors. The floor specimens tested had three different joist spacings: 16, 19.2 and 24 inches.

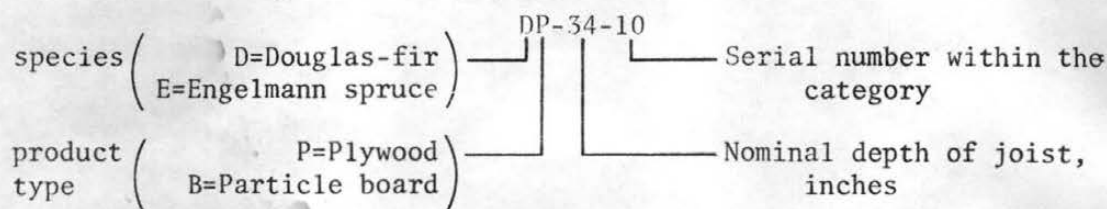
Four floors had only one sheathing layer while six floors were characterized by having two layers of sheathing material. For the three-layer floor specimens, the bottom sheathing layer was plywood and the top sheathing layer was particle board in each case.

Each piece of joist and sheet of plywood or particle board was numbered according to an alphanumeric identifying notation with examples shown below:

## Joist identification



## Plywood and particle board identification



Six and eight-penny common nails at varying spacings, from 4 inches to 8 inches, were used generally as connectors, except in specimen F2-8D16-1 where cement coated nails were used. An elastomeric glue (Franklin Construction Adhesive) was used as the connection between the joists and the plywood sheathing layer of specimen F11-8D16-1.

## 3.3 Material Properties

The behavior of a wood joist floor is affected by three important material properties: the MOE values of joists, the MOE values of each sheathing layer and the slip modulus of the connectors of each inter-layer. The mechanical properties of wood products not only vary from species to species, but also vary from piece to piece within the same species. Furthermore, since wood and wood-based products are neither isotropic nor homogeneous, their mechanical properties vary from section to section along any given piece as well as with the direction of loading. Therefore, measurement of the properties of each joist

and sheathing board rather than properties from samples out of each group of material was considered necessary to adequately describe the material in each floor specimen. This was accomplished by determining the elastic constants of each element of each floor by specimens using nondestructive test procedures.

### 3.3.1 Joist Properties

The MOE values of joists and sheathing boards were determined by nondestructive tests conducted in the Wood Science Laboratory of Colorado State University. Determination of flatwise joist properties was performed using a continuous deflection measurement device. The joist deflection at the center of a 3-ft. span along the moving piece with constant load applied at the center of the span was measured by an LVDT (linear variable differential transformer) and plotted using an X-Y recorder. Each specimen was passed through the machine twice, once with each flatwise face loaded to eliminate the effects due to any warp, twist or thickness variation present in the joist. The recorded deflections were then used to compute the MOE values using the following equation in which deflections attributed from both the bending and shear effects were included:

$$E = \frac{P(L/h)}{4\Delta b} [(L/h)^2 + 19.2] \quad (3.1)$$

where

P = load applied at midspan, lb.,

L = span, in.,

h = board thickness, in.,

b = board width, in.,

$\Delta$  = average deflection, in.

Equation (3.1) was incorporated into a computer program which computed the MOE of specimen from the recorded deflection data. The computed MOE value is an average value over each one foot interval. For more detailed description of the joist flatwise MOE test, reference is made to the work by O'Halloran (24).

In the floor specimen construction, joists were placed edgewise. Because of this configuration, the MOE values of joists obtained in the way described previously can only approximate the MOE of the joists as actually used. Therefore, the edgewise MOE values of joists were determined during the construction of the floor specimen. Deflections were measured for at least three load increments of 100 pounds at mid-span for each of three distinct stages of the joist construction: first, the laterally unsupported edgewise joist sitting on sill plate; second, the joist with guide nails driven in the sill plate and laterally supported by a header plank connected by one nail at mid-depth of each joist; third, two more nails driven to connect each joist and the header plank as shown in Fig. 3.1. The load-deflection curve was plotted to obtain an average load-deflection relationship. A typical plot is shown in Fig. 3.2. The MOE values of joists due to static bending were computed from the deflection equation of simply supported beam including only flexural deformations. The effect of shear deformations were thus included in the calculated MOE values. For further detail of the testing procedure reference is made to work by Kuo (19).

### 3.3.2 Sheathing Properties

Sheathing material including 1/2 and 3/4-in. thick Douglas-fir plywood, 1/2 and 3/4-in. thick Engelmann spruce plywood and 1/2-in.

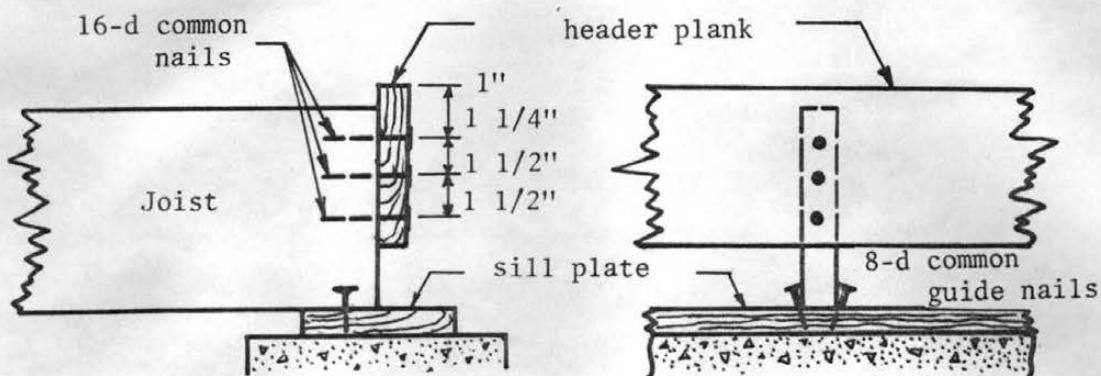


Figure 3.1 Detail of Joist Header Construction

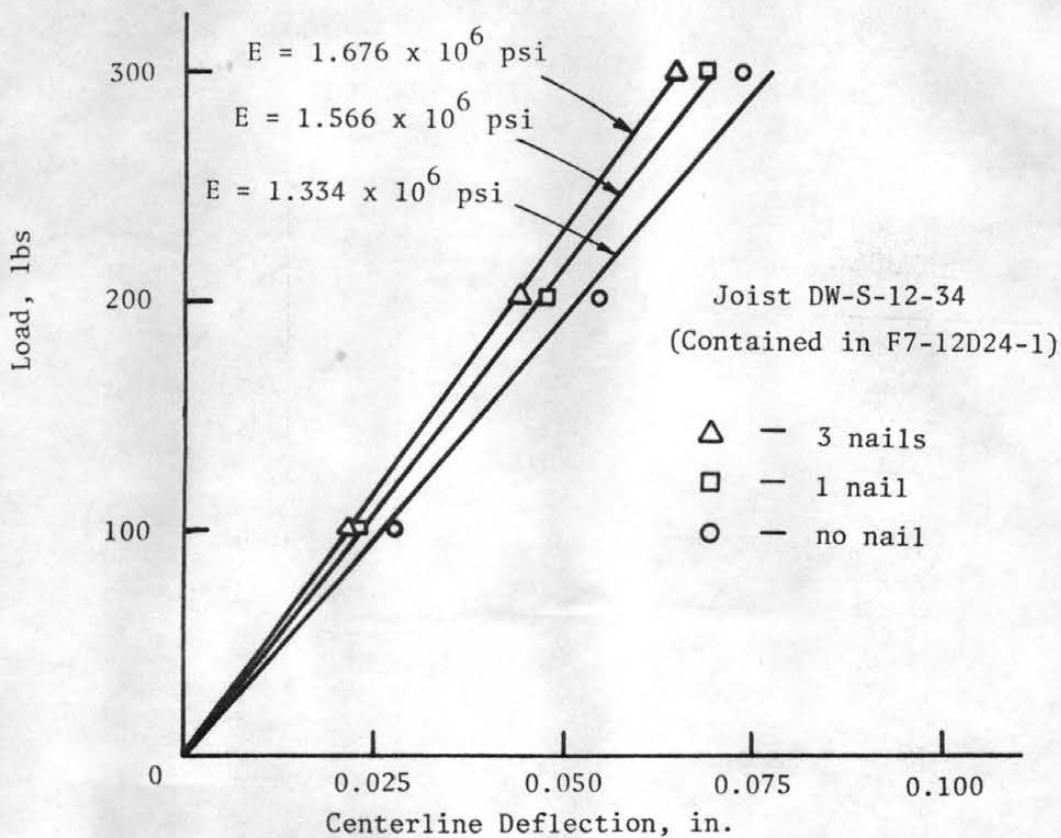


Figure 3.2 Typical Load-Deflection Plot for MOE Test

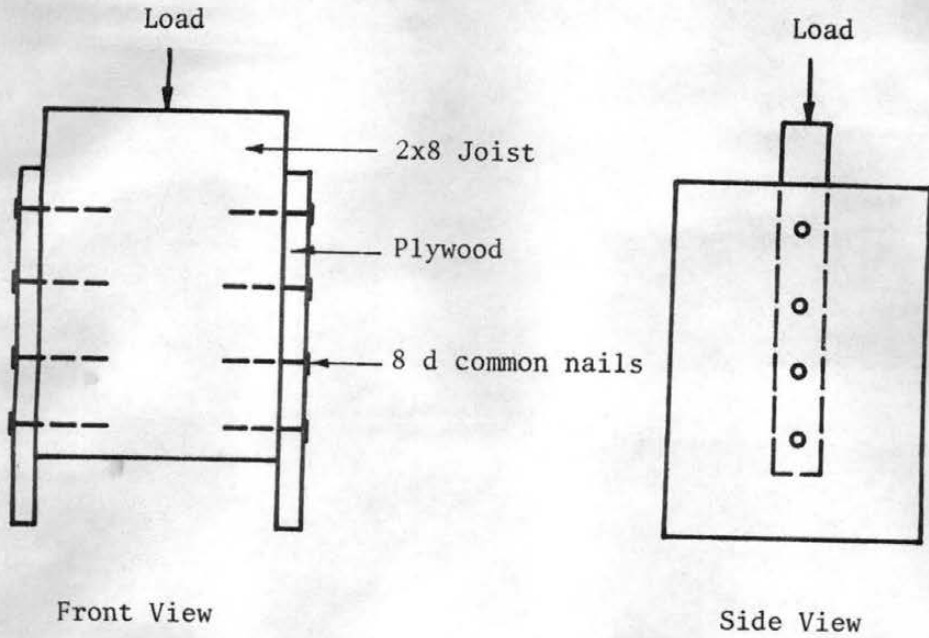
thick Douglas-fir particle board were tested to determine their in-plane elastic parameters. The testing procedure and the theory for the computations of elastic parameters have been discussed extensively by McLain (20).

The MOE values in the directions parallel and perpendicular to face grain of the full-sized panel of plywood and particle board were determined. The testing apparatus (see reference (20)) supported the plywood at one end and at approximately the center. A line load was applied to the free end and deflection of the loaded end was recorded by three LVDT transducers across the width. Four test results were obtained for each direction of the panel by loading each end and with each side of panel upward. These four tested results were averaged and used for the evaluation of the static MOE value. In computing the MOE values, any correction due to Poisson's ratio and shear effect was considered negligible.

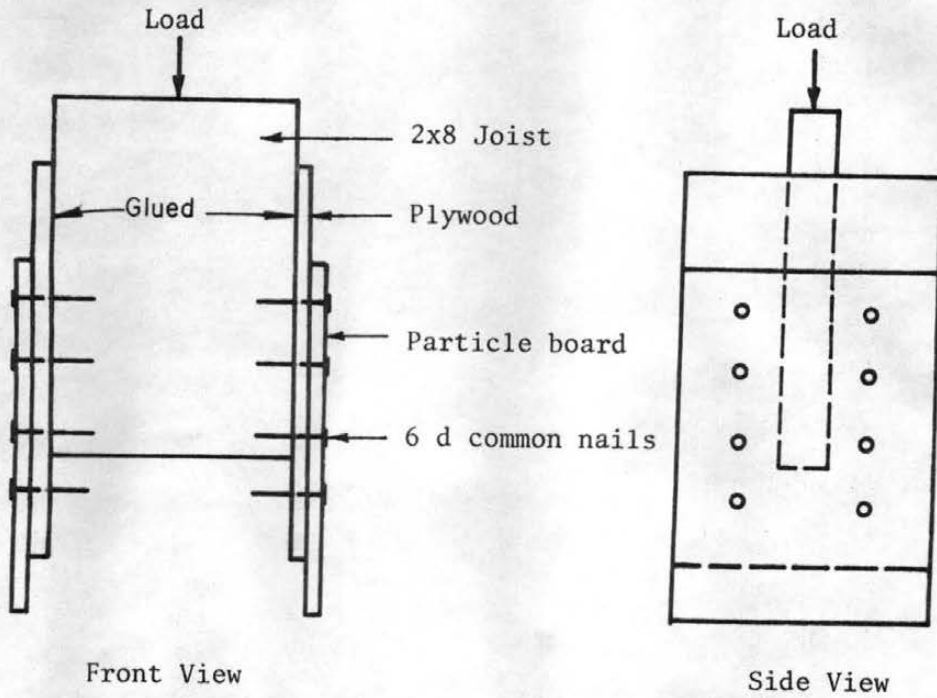
### 3.3.3 Connector Properties

The load-slip characteristics of the connectors in combination with the wood members which they fasten greatly influence the degree of interaction between layers in a floor structure. The slope of the load-slip curve is defined as the slip modulus.

The experimental slip modulus study of the connectors and wood components used in the floor specimens was reported by Patterson (26). Selected 1-ft. long nominal 2x8 inch joist pieces of either Douglas-fir or Engelmann spruce were used as the center member, and the 3/4 or 1/2 in. thick Douglas-fir or Engelmann spruce plywood cut into 8x12 inch boards used as the side members to form a double-shear test configuration as shown in Fig. 3.3(a). A series of tests with



(a) Plywood and joist



(b) Plywood and particle board

Figure 3.3 Nail Slip Modulus Test Specimens

different combinations of lumber and plywood species and connectors were conducted to determine the effect of the number of nails in the load-slip characteristics of the connections. Effects of the plywood face grain parallel and perpendicular to the load direction were also included in the experimental study. Test results expressed in terms of slip modulus based on tangent and secant lines at various load levels are listed in Appendix C. A typical load-slip curve resulting from the tests is shown in Fig. 3.4.

The load-slip characteristics between particle board and plywood with 6-d common nails driven through the particle board and plywood in two rows per face, one on each side of the center member, were also determined for the study of the three-layer floor specimens. For this series of tests, the center member and the plywood were connected by rigid glue. The setup of the test specimens is shown in Fig. 3.4(b) and the test results are shown in Appendix C.

#### 3.4 Construction of Floor Specimens

The floor specimens were built on a reinforced concrete frame on which the load test were performed. A total of sixteen floor specimens were constructed. The details of the construction procedure can be obtained by reference to the work of Penner (27) and Kuo (19).

The joists were selected in two ways. One method was to select the joists from within a predetermined range of average MOE values using data provided by the Wood Science Laboratory. The other method was to select the joists randomly from the lumber supply. Plywood and particle board sheets were selected from the top of the supply pile, in order.

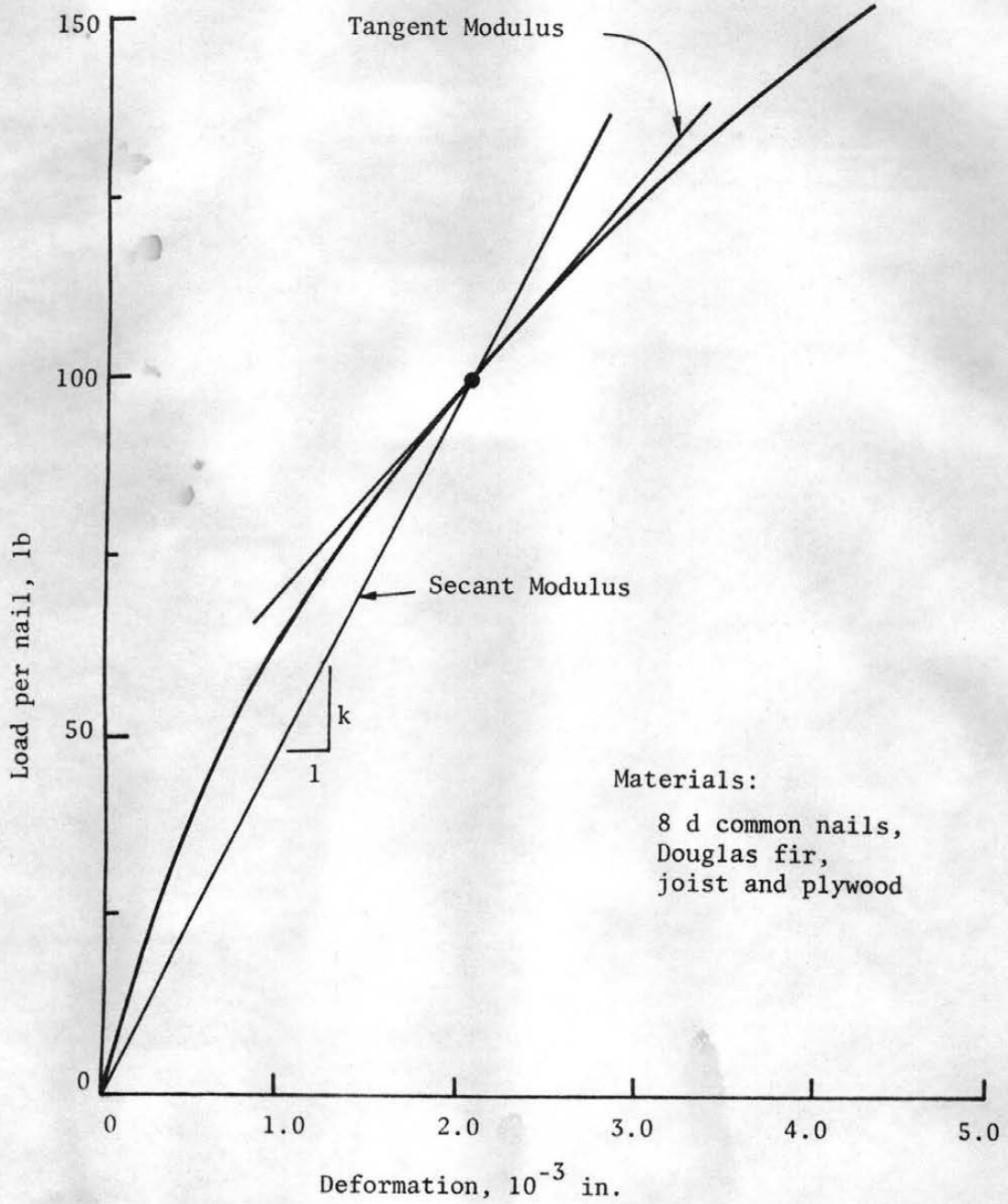


Figure 3.4 Typical Load-Slip Curve

The selected joists were then marked at their center line and placed on the concrete frame resting on the sill plate edgewise according to the normal house construction practice. The crowned edge or an edge with larger knots or defects was placed as the top edge.

The selected plywood sheets were sawed to fit the sheathing configuration of each floor specimen. The plywood was placed on top of joists with face grain perpendicular to the joist span. One row of nails was used per joist except when a gap fell on the joist and parallel to the joist span. In this case, two rows of nails were used with one row on each side of the gap. When glue was used as the connector between the plywood and the joists, the glue was applied in two 1/4-in. wide beads continuously along the upper joist face with a caulking gun. The glue was then spread evenly. After the plywood was placed at the desired position, double-headed common nails were driven into the joists at a spacing of about 8 inches to insure a tight contact between the plywood and joists. The glued specimens were allowed to cure about two weeks. The double-headed nails were pulled out immediately before load testing began.

The sheathing joints were T & G (tongue-and-grove) joints, tightly butted joints, or open joints with a  $\pm$  1/16 inch wide gap. For some specimens, the joints were glued and tightly butted.

One layer of particle board was placed on top of the plywood sheathing in basic floors F6 through F11 to form the three-layer systems. The selected particle board was sawed into the desired sizes according to the top sheathing layer configuration of each three-layer specimen. The particle board sheathing joints were staggered or doubly staggered from the plywood sheathing joints (refer to Appendix B for details).

Six penny common nails were driven through the particle board and the plywood only. Spacings of either four or eight inches were used in making this connection.

### 3.5 Testing Equipment

Facilities used for structural testing for this research project are located in the Structural Engineering Laboratory at the Engineering Research Center. An elevated reinforced concrete frame was constructed to support the test specimen. A 55-kip capacity MTS hydraulic actuator and its associated control equipment were used to apply load on the floor specimens included in this study. In this section a brief summary of the facility and their capabilities are presented. For more detailed descriptions, reference is made to the study by Penner (27).

The MTS closed-loop structural testing system is essentially a self-controlled hydraulic loading system composed of three major components: the power supply, the control console and the actuator. The actuator is mounted on a movable beam with trolleys at ends and supported on a steel frame over the elevated concrete frame such that quick access is available to any point in the floor specimen where the application of load is desired (see Fig. 3.5). A load cell with capacity of either 2.5 or 50 kips was mounted on the actuator, depending on the load level. The control console can operate the actuator in either a load control or stroke control mode. Cyclic loading with various functions can also be generated by a function generator in the console. The load was transmitted to the floor through a one inch diameter ball bearing which was in contact with the ram of the MTS hydraulic loading system and a 4x4 inch steel bearing pad on the floor specimen.

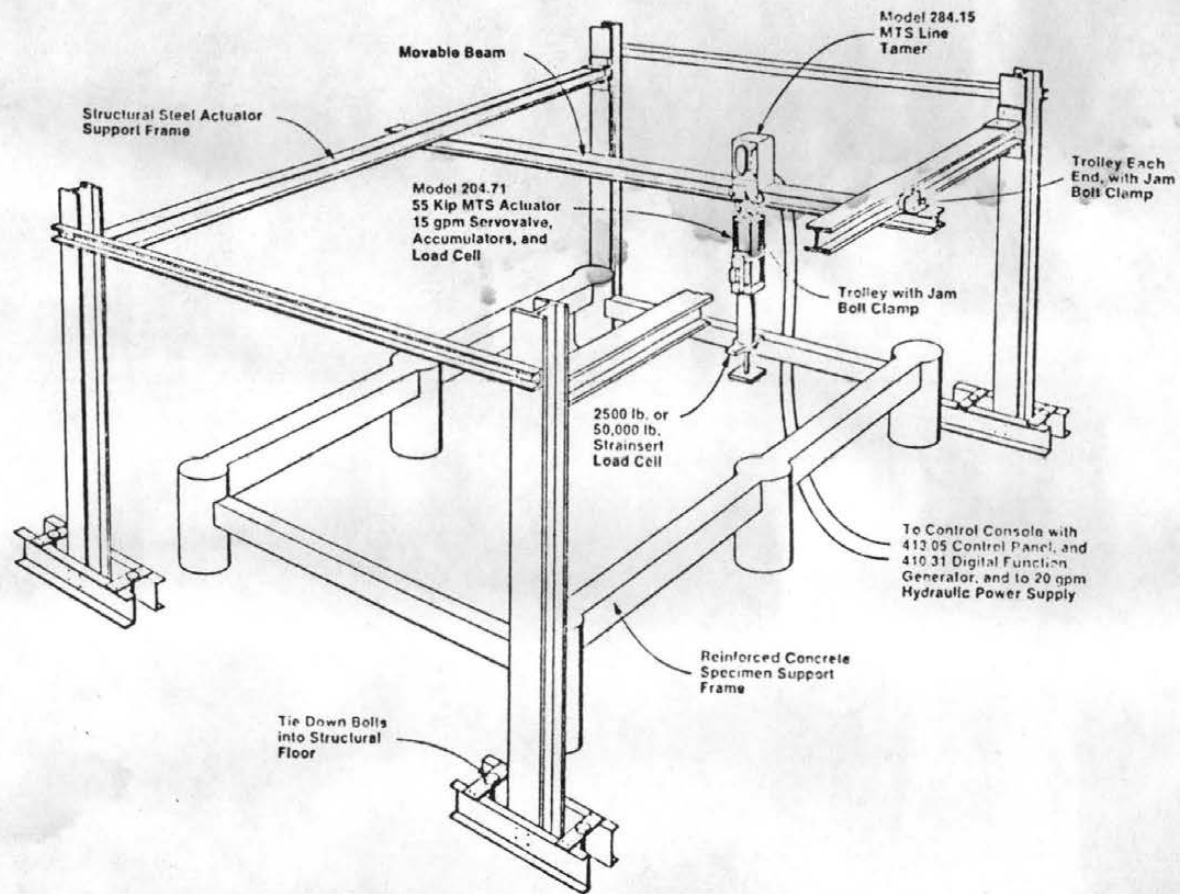


Figure 3.5 55-Kip MTS Loading Actuator and Support Frame

The elevated concrete frame supports the floor specimen over a 12-ft. span and allows a length of 16 ft. Along the top face of each 16-ft. span of the frame, a nominal 2x6 inch Engelmann spruce sill plate was grouted with 1/4-inch thick mortar at its bottom face and fastened to the concrete frame with bolts. The joists of the floor specimens rested upon these sill plates.

Dial gages, a surveying level, and LVDT's (linear variable differential transformers) connected to an X-Y plotter were used to obtain deflection measurements at various load levels. Dial gages with ranges of one and two inches were placed under the joists of floor specimens at selected positions to measure the floor deflections under working load range and readings were taken to the nearest one-thousandths of an inch. The dial gages were fastened to perforated angle irons attached to a supporting bridge across the span of the test area.

During the tests to failure, engineering scales with 50 divisions per inch were attached to the joists at positions where deflection measurements were desired. A Zeiss self-leveling level was used to take the readings of deflection after the application of each load increment.

The LVDT's were used for some tests to obtain a continuous plot of load versus deflection. The LVDT contained within the actuator was used to plot the load deflection curve to failure for most tests.

### 3.6 Testing Procedures

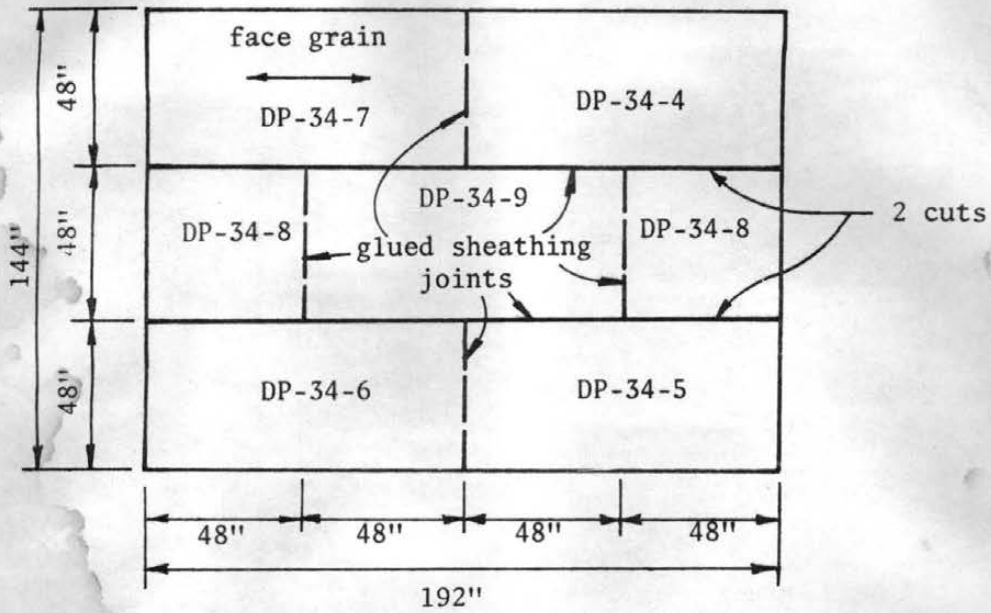
The general testing procedures of the two-layered floor specimens used in this study is essentially the same as those discussed by Penner (27). The differences in a few details of the testing procedure

are included in this section. Also discussed is the difference of the testing procedure used for the three-layer floor specimens.

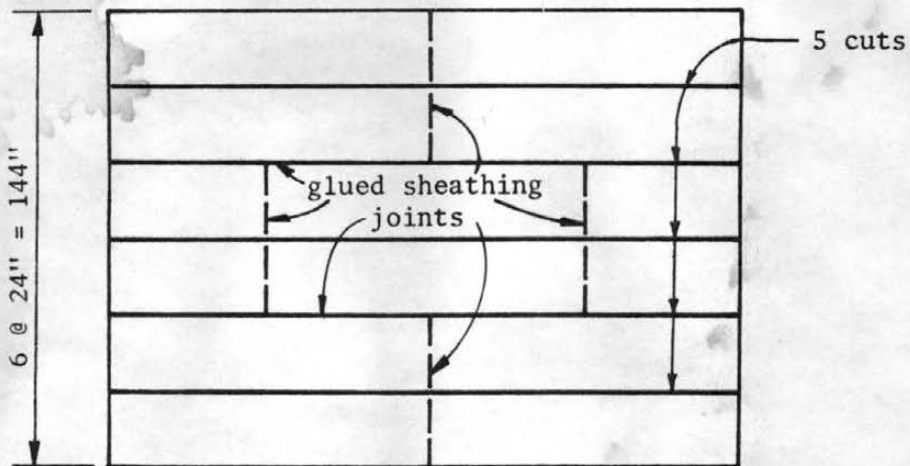
A concentrated load was applied at the desired location directly over one of the joists in the floor specimen tested. Load increments of 50, 100, 200 or 250 pounds were used in the range of service load depending the size of the joists and the arrangement of the components of floor specimens. The service load level was usually taken to be either 800 or 1000 pounds maximum. One exception was specimen F7-12D24-1 which was tested up to 2000 pounds since the maximum deflection of floor at that load did not exceed  $L/360$ , which is 0.4 inches (for the 12-ft span specimen).

The service load tests with the same load increments up to the same level were repeated three times at the same location for specimen F5-8D16-1 to see if the deflections agreed for different tests and to see if the specimen did resume its original position after the applied load was released. In these same tests, the load was sustained for approximately ten minutes at the service load level to examine the effect of creep. Before testing specimen F5-8D16-1 (a glued specimen) to failure, cuts were made through the sheathing. Two cuts and five cuts were introduced in the configuration shown in Fig. 3.6 and load tests were performed to assess the effect of gaps in sheathing on the deflection of the floor specimen. A circular saw adjusted to cut just through the plowood layer was used and the gap width produced was near  $1/8$  inch.

For each of the three-layer floors, load tests were conducted after each layer of sheathing was properly constructed. Only loads in the elastic range were applied to the specimens after the bottom plywood sheathing was attached to the joists according to the construction



(a) Two cuts in sheathing



(b) Five cuts in sheathing

Figure 3.6 The Configuration of Sheathing Gaps for Load Testing of Specimen F5-8D16-1

procedure discussed previously. After the top particle board sheathing was attached for each three-layer specimen, load tests up to service load level were performed in two steps: first, the nails were driven through the bottom layer so that they only reached the top face of joists; second, the nails were driven to their full lengths into the joists (see Fig. 3.7).

Finally, each specimen was tested to failure with the load applied at the center of the floor. The 50-kip capacity load cell was installed and engineering scales were used to replace the dial gages for the measurement of deflections. A concentrated load was applied in 500 pounds increments and deflections obtained with a surveying level were recorded. The LVDT from the actuator was connected to the X-Y plotter to obtain a continuous load-deflection plot.

Observations and sketches of the broken joists and the punch-through of the sheathing were noted after the test to failure for each specimen. After the test to failure was completed, the specimen was dismantled. Some small samples of joists and sheathing panels of the tested specimen were cut, with sizes conforming to the ASTM Specification D 2016-65 (3) and the moisture content was determined by the oven-dry method at the Wood Science Laboratory.

### 3.7 Experimental Behavior of Floor Specimens

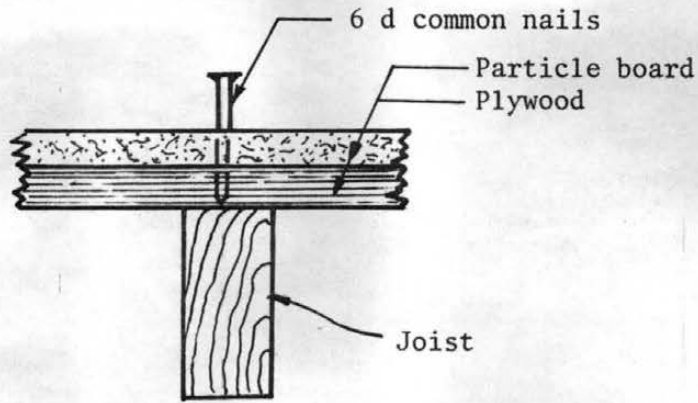
The experimental behavior, in the working load range and in the overload load range, of the first four floor specimens constructed for this research project was discussed by Penner (27). Maxwell's reciprocal theorem and load-sharing among the joists of specimen were examined and load-deflection curves were plotted for each specimen in the elastic loading range. The inelastic behavior of the floor

specimens was explored in three stages: during overloads, near and at the initial joist failure and at final floor failure.

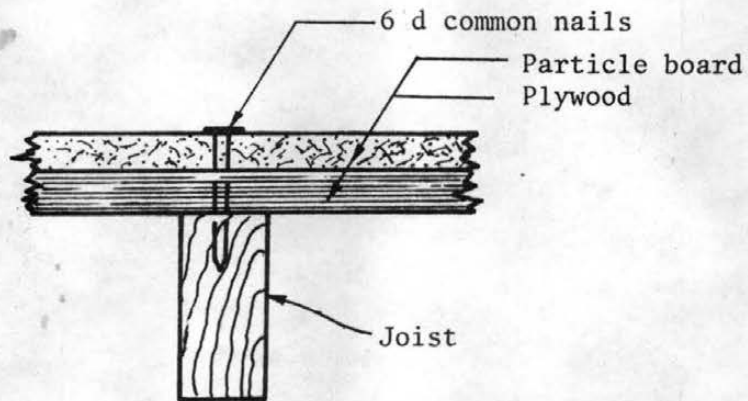
For the remainder of the floor specimens, the experimental behavior which was similar to that discussed by Penner is not repeated here. Instead, in this section, the various factors which affects the behavior of the specimens are discussed. The floor behavior is a function of sheathing thickness and modulus of elasticity both parallel and perpendicular to the face grain, joist size and modulus of elasticity, sheathing joint conditions, number of sheathing layers, as well as the connector properties. The actual floor deflection under load falls somewhere between the following two extremes: (1) the joists and the sheathing layer(s) act as a structurally-independent member and (2) the joists and sheathing layer(s) act as an integral member where the interlayer connection is perfectly rigid. The floor response between these two extremes depends primarily upon the interlayer connector's properties. Joist and sheathing dimensions and properties determine how much the two extreme behaviors differ.

### 3.7.1 Effect of Connectors

The general effect of type of connector on the floor behavior was observed by comparing the floor load-deflection curves of specimens F11-8D16-1, F3-8D16-1 and F5-8D16-1 all constructed with 2x8 inch Douglas-fir joists spaced at 16 inches. Specimen F11-8D16-1 had glued connection (see Sec. 3.4 for the amount of adhesive used and the gluing process) with 1/2-in. Douglas-fir plywood sheathing and glued sheathing joists. Specimens F3-8D16-1 and F5-8D16-1 both were nailed with 8-d common nails spaced at eight and four inches, respectively and with 3/4-in. Douglas-fir plywood sheathing. The sheathing



(a) First stage of nailing



(b) Second stage of nailing

Figure 3.7 Two Stages of Connection During Load Tests for Three-Layered Specimens

joists were tightly butted T & G joints for F3-8D16-1 and glued T & G joints for F5-8D16-1. Thus each floor had somewhat different properties and the effect of connection indicated is only general. The load-deflection curves of the floor center deflections are shown in Fig. 3.8. Although other variables also can affect the floor behavior, however, a general trend seen in Fig. 3.8 shows that the glue-connected specimen has less deflection than the specimen connected by 8-d common nails at 8-inch spacings under the same load.

The spacing of nails along the joists has a significant effect on the overall stiffness of the floor systems. Figure 3.8 also shows that closely spaced nail connectors tend to decrease deflection. Test results of specimen F5-8D16-1, F2-8D16-1 and F3-816-1 shown in Fig. 3.9 show the tendency that the more closely the nails were spaced the less the deflection and therefore the greater is the stiffness.

### 3.7.2 Effect of Gaps in the Sheathing Layer

Gaps in the sheathing layer(s) are unavoidable in the common practice of wood construction. Discontinuities and abrupt reductions in sheathing stiffness are thus introduced at gaps. The presence of gaps in sheathing layer(s) can therefore lower the overall stiffness of floor.

T & G joints and butted joints either glued or tightly butted were generally used in the sheathing construction of the floor specimens in this experimental program. Some specimens were constructed using joints with open gaps of  $\pm 1/16$  inch in the sheathing.

Progressive cutting of gaps in the sheathing layer of specimen F5-8D16-1 allows the study of the effect of gaps on the floor behavior

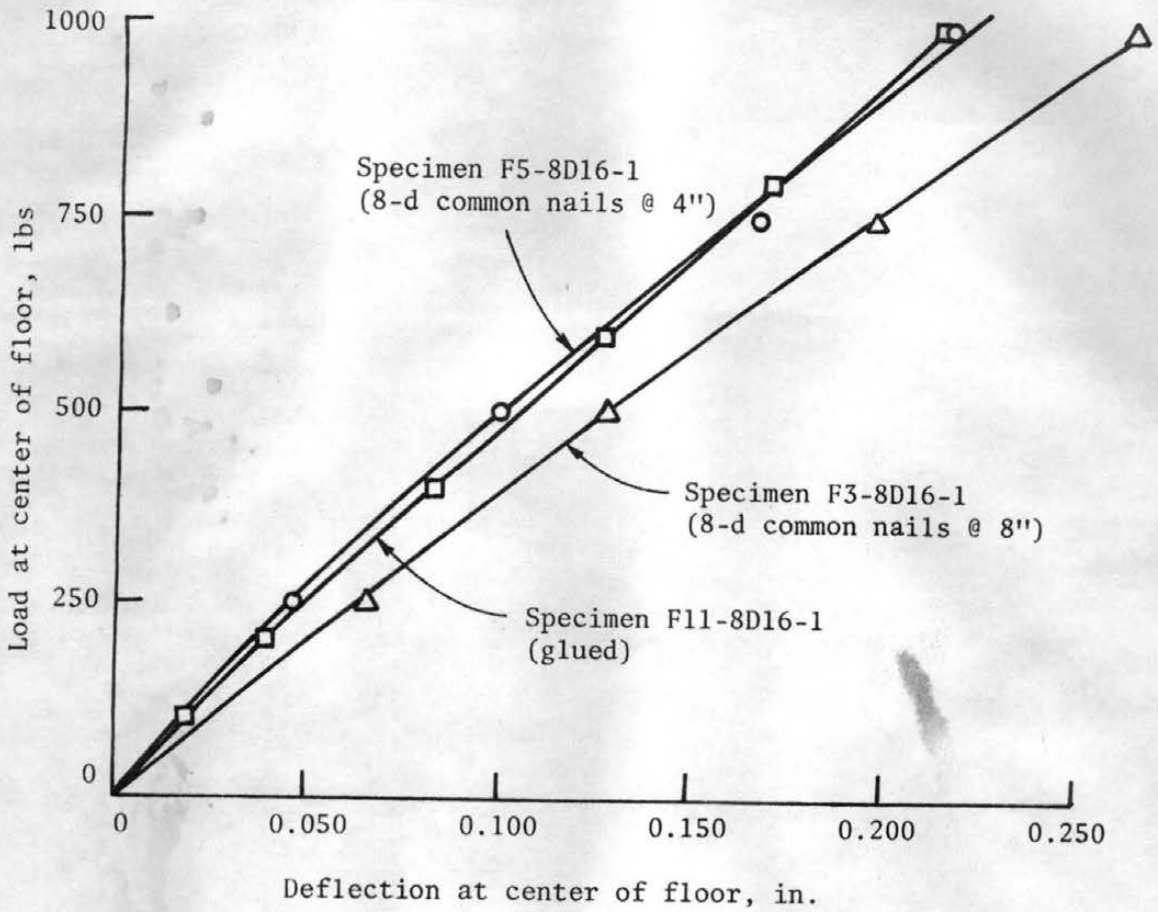


Figure 3.8 Effect of Type of Connector

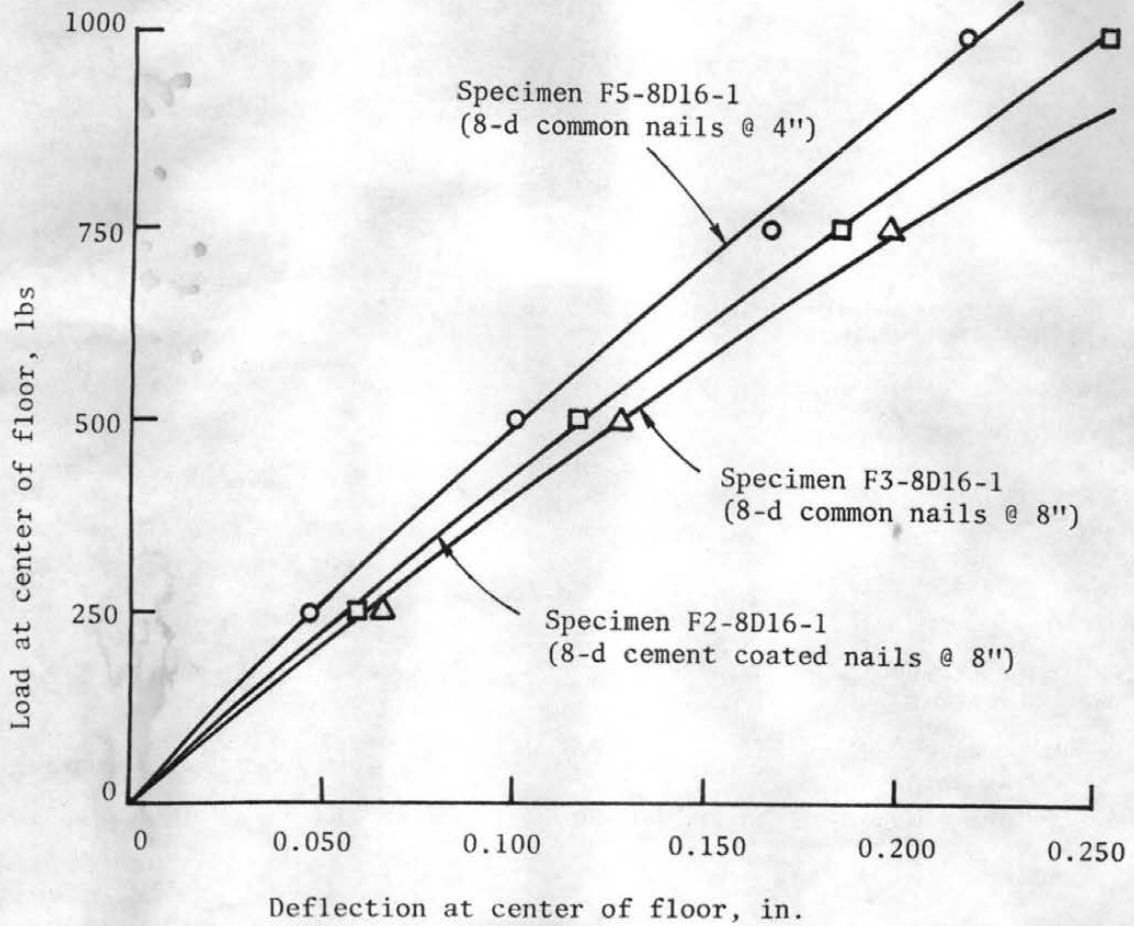


Figure 3.9 Effect of Nail Spacing

by keeping all other variables constant. The sheathing joints of specimen F5-8D16-1 were glued when it was first constructed. Load tests were performed in the service load range. Two cuts, each two feet from the center line of the floor at the glued joints, were then made with a circular saw at a width of approximately 1/8 inch, perpendicular to the joist span. Again, a load test was performed in the service load range. Three more cuts were added in the sheathing to make a total of 5 cuts, each two feet apart. A load test was again conducted. The configuration of the cuts in the sheathing can be seen in Fig. 3.6. The load-deflection curve at each step is shown in Fig. 3.10. It is seen that the gaps in the sheathing reduce the stiffness of the floor. Also shown is the trend that as more cuts were produced in the sheathing, the additional increase of deflection per cut was reduced. The percentage deflection increases due to 2 cuts and 5 cuts in sheathing at 1000 pound load level are about 40 percent and 50 percent, respectively, with respect to the deflection of no gap in sheathing.

### 3.7.3 Effect of Numbers of Sheathing Layers

The modulus of elasticity and thickness of sheathing layer(s) are among the many factors known to affect the behavior of a layered floor. The addition of a second sheathing layer (in this case particle board) can also reduce the floor deflection appreciably. In floors F6 through F11 construction was completed in two stages: first, joists were topped with a layer of plywood sheathing to form two-layer floor specimens; second, a layer of particle board sheathing was added on top of plywood panel to form three-layer floor specimens. Load tests were performed in each stage. Load tests performed on the three-layer specimens were further classified as two types in the service load range:

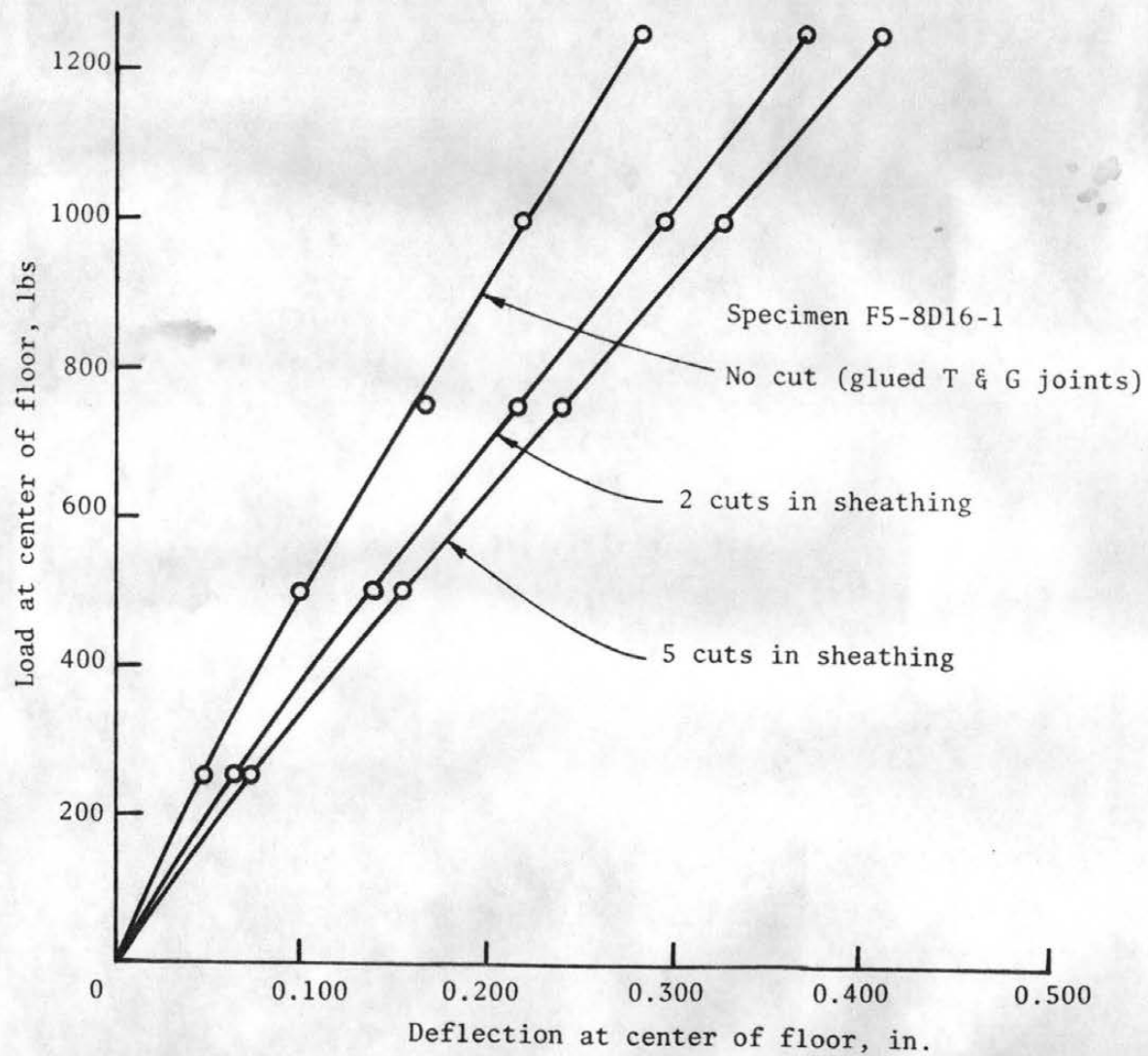


Figure 3.10 Effect of Gaps in the Sheathing

(a) nails were driven through the bottom sheathing layer and barely into the top surface of joists and (b) nails were driven full length down into the bottom sheathing layer and joists.

The load-deflection curves at the center of floor F6 at all stages are shown in Fig. 3.11. The increase of the stiffness of floor or the decrease of deflection at the same level due to the addition of a second sheathing layer is approximately 15 percent for nails driven to the bottom sheathing only. The figure also shows that the stiffness of the floor is increased as expected when the nails attaching the particle board are driven on through the plywood layer to the joist below producing approximately a 30 percent increase. Further increase in stiffness was expected when nails were completely driven in because the additional nails crossing the joist-plywood interface increased the composite action.

#### 3.7.4 Nonlinear Behavior and Mode of Failure

The overload behaviors and the failure modes of the floor specimens tested were essentially the same as those described in the study by Penner (27). Increments of 500 pounds (sustained for approximately one minute to allow the taking of deflection readings) were used when floor specimen was tested to failure.

As the load level increased, the joist directly under the applied load generally failed first. The maximum floor deflection at the first joist failure was greater than  $L/360$  (0.4 inches for 12-ft. span) for the two-layer specimens and generally smaller than  $L/360$  for the three-layer specimens. After the first joist failure, appreciable amounts of additional load could still be applied to the floor specimens before the sheathing was finally punched through by the applied concentrated

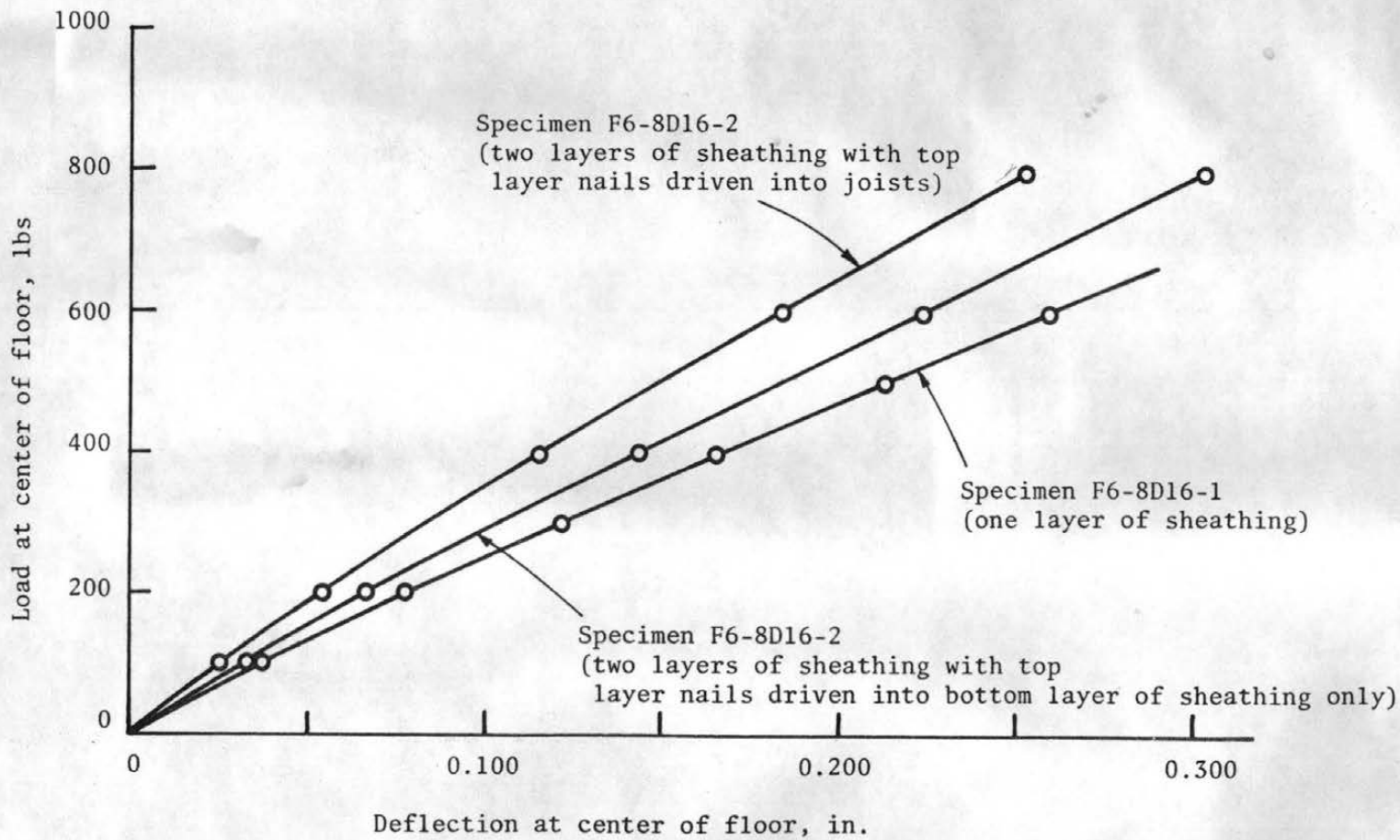


Figure 3.11 Deflection Behavior of a Floor as a Function of Number of Layers

load. For detailed descriptions of the nonlinear behavior and failure mode of the tested specimens, see Penner's report (27).

It should be emphasized that this chapter describes the various aspects of the experimental program and discusses the observed test results qualitatively rather than quantitatively. The main purpose of this study is the verification of the mathematical floor model which is thoroughly discussed in the following chapter.

## CHAPTER 4

### VERIFICATION OF THE MATHEMATICAL FLOOR MODEL

#### 4.1 Introduction

The primary purpose of this study is to examine the verification of the developed mathematical model for wood joist floor systems in the range of working load. The detailed development of the mathematical model has been presented in Chapter 2. In this chapter, the results of the verification studies of the mathematical floor are discussed.

The verification process for the mathematical floor model is to compare the computed floor deflections using the mathematical model with the experimental deflections collected as described in the previous chapter for loads applied within the working load level. In all cases of the verification study, a concentrated load ranging from 600 to 1000 pounds acting at the center of floor specimen was used. Measured deflections at selected positions along the centerline of the floor specimen (midspan) were plotted and compared with the computed results for each floor specimen. The percentage error of the computed deflection at the center of floor with respect to the experimental result was calculated and is presented for each floor specimen. Examples of the verification of the mathematical floor model and the detailed data of each floor specimen tested are presented in this chapter.

#### 4.2 Mathematical Floor Model Used in the Verification Study

Two distinct solution techniques were used to develop the mathematical floor model as presented in Chapter 2. Although the finite difference model can handle the varying dimensions and mechanical

properties of each of the floor components, it is limited in that it can not properly treat the discontinuity problem created by gaps in the sheathing layer(s). The finite element model can, however, incorporate the varying dimensions and mechanical properties of the floor components as well as the gaps between the sheathing panels, thus enabling the analysis of the floor behavior with a closer simulation to the physical condition of the floor system.

Computed deflections for specimen F2-8D16-1, having the configuration and properties shown in Fig. 4.1, using both finite difference and finite element models, along with the measured deflection at selected positions across the midspan profile are plotted in Fig. 4.2. The percentage errors of the computed deflection at the center of floor with respect to the experimental value were +6.51 percent and -6.90 percent for the finite element model and finite difference model, respectively. Although the absolute percentage errors for both mathematical representations of the physical models are very close, the finite difference model does not include the effect of gaps in sheathing and thus predicts slightly less than the actual deflections. Since the mathematical representation using the finite element solution technique can better approximate the actual physical condition of the floor system, it was chosen as the solution technique for use in the verification study.

#### 4.3 Input Data of Floor Specimens

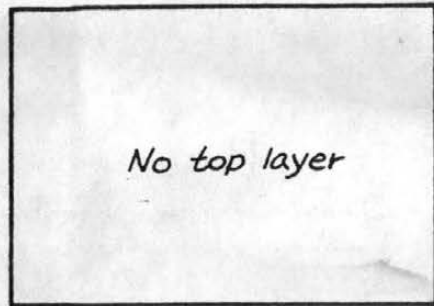
The theoretical analysis of the behavior of each floor specimen requires certain data input to the mathematical model. These data include floor span, floor length, numbers of T-beams and sheathing

strips, dimensions and MOE (modulus of elasticity) values of each T-beam and sheathing strip along its length, the slip modulus for each inter-layer, and the appropriate data for the gaps in sheathing.

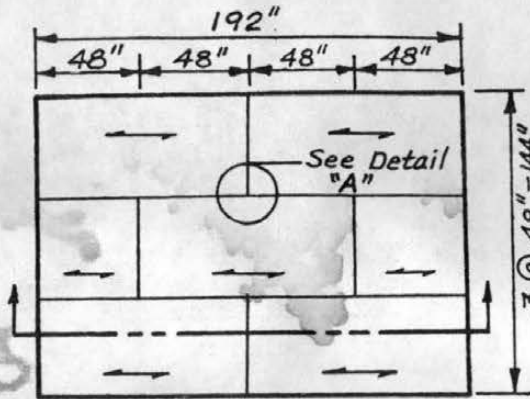
The floor span was 144 inches and the length 192 inches for all the floor specimens. The numbers of joists and sheathing strips chosen for the analysis varied from specimen to specimen and were dependent on the floor arrangement and the locations of the sheathing gaps of each specimen. The selection of the values of slip modulus used in this study is discussed in Sec. 4.4. The MOE values of joists used in the verification study were the average edgewise MOE's obtained from tests when the joist was connected to the header with three 16-d common nails as described in Sec. 3.3.1. The MOE values of plywood and particle board sheathing panels used were the values obtained from the testing of each panel by the Wood Science Laboratory with the testing technique described in Sec. 3.3.2. The MOE values used for gaps in sheathing were 1000 psi for tightly butted and glued gaps and 1 psi for open gaps. The tabularized detailed data showing the arrangement of floor components, dimensions, MOE values of joists and sheathing panels, type of connectors and connector spacing for specimens F2-8D16-1 (a two-layer floor) and F6-8E16-2 (a three-layer floor) are presented in Fig. 4.1 and Fig. 4.3 as examples. The detailed data for the remainder of the floor specimens are listed in Appendix B.

#### 4.4 Selection of the Values of Slip Modulus

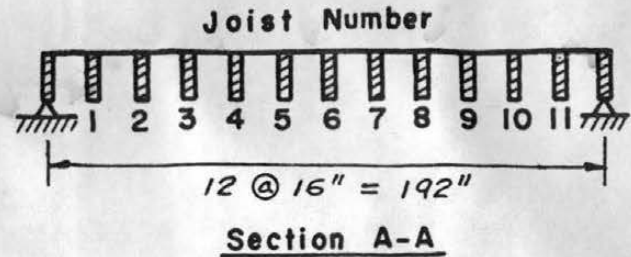
The value of the slip modulus determines the degree of the composite action between layers. Therefore, the choice of the value of slip modulus can significantly affect the theoretical behavior of the floor system. As was pointed out in Sec. 3.3.3, the load-slip



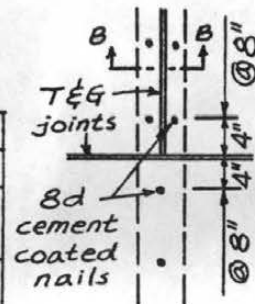
Plan of Top Sheathing Layer



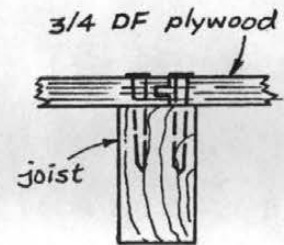
Plan of Bottom Sheathing Layer



Section A-A



Detail "A"



Section B-B

Material	Property	Joist Number										
		1	2	3	4	5	6	7	8	9	10	11
2x8 DF joist	Actual Size, in (width x depth)	1.49 x 7.21	1.49 x 7.19	1.47 x 7.25	1.49 x 7.21	1.50 x 7.30	1.50 x 7.21	1.44 x 7.05	1.47 x 7.17	1.49 x 7.24	1.49 x 7.21	1.49 x 7.22
	Average MOE    Grain, 10 <sup>6</sup> psi	2.19	1.75	2.13	1.73	1.65	1.75	1.45	1.74	2.14	1.59	1.78

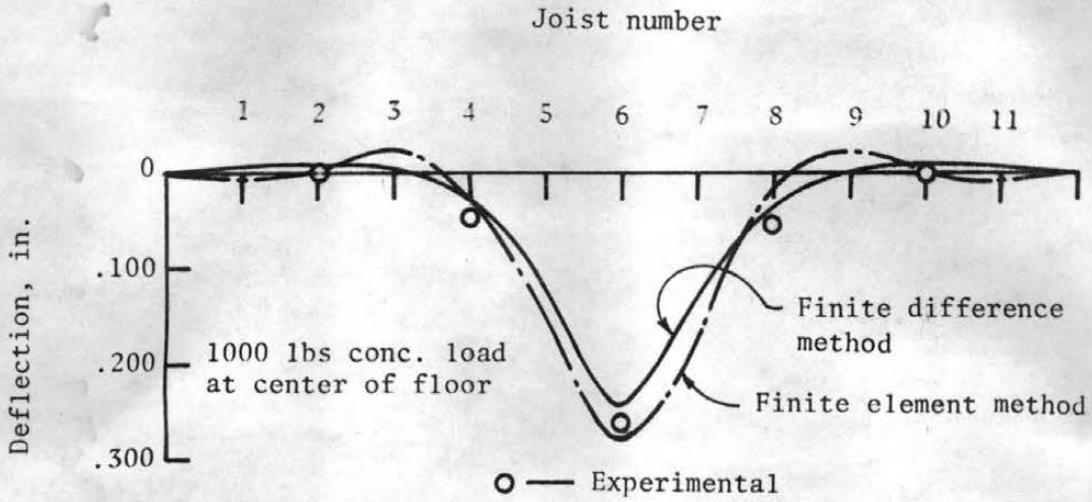
Joist Data

Layer	Material	Thickness in.	Gap	Connector	Average MOE, 10 <sup>6</sup> psi															
					A		B		C		D		E		F		G		H	
						⊥		⊥		⊥		⊥		⊥		⊥		⊥		⊥
Bottom	3/4 DF plywood	3/4	T&G butted tight	8d cement coated nails @ 8"	1.41	0.51	1.41	0.56	1.40	0.53	1.42	0.43	1.40	0.53	1.40	0.55	1.42	0.59	—	—
Top	—	—	—	—	—	—	—	—	—	—	—	—	—	—	—	—	—	—	—	—

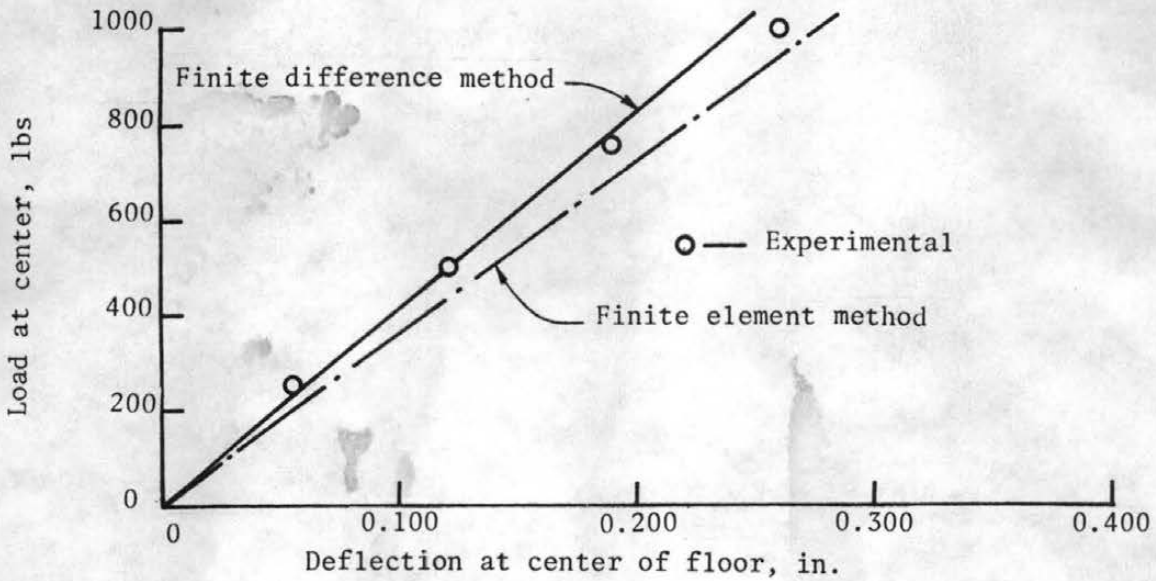
Sheathing Data

Figure 4.1

Layout and Data of Specimen F2-8DI6-1

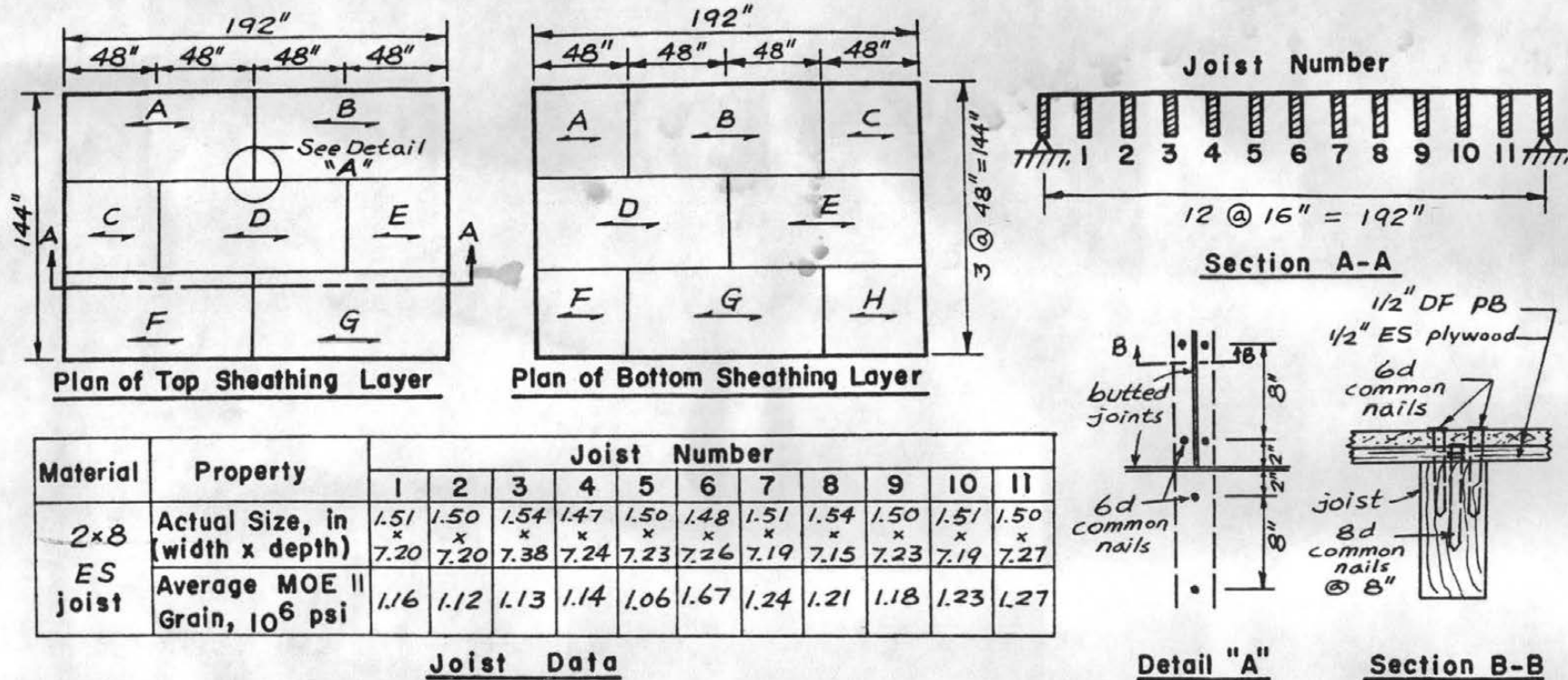


(a) Deflection profile at centerline of joists



(b) Load-deflection behavior

Figure 4.2 Computed vs Measured Results of Floor Specimen F2-8D16-1



Layer	Material	Thickness in.	Gap	Connector	Average MOE, 10 <sup>6</sup> psi															
					A		B		C		D		E		F		G		H	
						⊥		⊥		⊥		⊥		⊥		⊥		⊥		⊥
Bottom	1/2 ES plywood	3/8	1/16" 7x9	8d nails @ 8"	1.36	0.21	1.36	0.20	1.36	0.21	1.41	0.23	1.40	0.23	1.45	0.23	1.43	0.24	1.45	0.23
Top	1/2 DF PB	1/2	butted no gap	6d nails @ 8"	0.42	0.31	0.53	0.41	0.45	0.35	0.46	0.33	0.45	0.35	0.42	0.33	0.51	0.40	-	-

Figure 4.3

Layout and Data of Specimens F6-8E16-1 and F6-8E16-2

relationship for a nailed or glued connection is generally nonlinear (see Fig. 3.4), whereas the mathematical floor model developed in this study requires a constant value for the slip modulus. Therefore, selection of a reasonable value of slip modulus from the load-slip curve of a nailed or glued connection is very important.

In the layered beam system study, portion of the wood floor research project, Kuo (19) conducted an extensive investigation on the verification of the mathematical model of a layered beam system. For consistency, the slip moduli used by Kuo (19) for layered beams were generally adopted for this study of floors. Thus, the values of slip moduli used in the verification study of the mathematical floor model follow closely to those values used by Kuo in verifying T-beam behavior. The slip modulus values recommended by Kuo (19) are presented in Table 4.1. The listed values for nailed connectors are all for 8-inch spacing. The slip modulus for nail connectors with spacing other than 8 inches requires some modification from the values listed in Table 4.1. For the three-layer floor specimens, slip moduli were not the same for the two cases when nails of top layer were driven or not driven into the joists. Adjustment of the slip modulus values for nail spacing other than 8 inches and for the top layer nails driven into joists in three-layer specimens closely follow those used by Kuo (19). The slip moduli used for each floor specimen in this study are summarized in Table 4.2.

#### 4.5 Comparison of Computed and Experimental Results

The data discussed in Sec. 4.3 and Sec. 4.4 were input to the mathematical floor model for each floor specimen. The theoretical floor deflections at the nodal points were obtained for each floor

Table 4.1 Values of Slip Modulus, k

Connector	8-d common nails				Adhesive	6-d common nails	
Joist	Douglas-fir		Engelmann spruce		D.F., E.S.	-----	
Sheathing	D.F.	E.S.	D.F.	E.S.		Particle board	
						D.F.	E.S.
k	1b/in 30,000	1b/in 30,000	1b/in 30,000	1b/in 18,000	1b/in/in <sup>2</sup> 16,000	1b/in 4,000	1b/in 3,000

Note: These values are for 8 inch nail spacing. Adjustment is made in the values for other nail spacing due to the difference in nail loads.

Table 4.2 Slip Moduli, k, Used for Floor Specimens

Floor Specimen	Joists	Sheathing	Connectors	Nails of Top Layer Not into Joist		Nails of Top Layer Driven into Joist	
				k, lbs/in.	k/s lbs/in./in.	k, lbs/in.	k/s, lbs/in./in.
F2-8D16-1	2x8 DF	3/4 DF Plywd	8-d @ 8" (Cement coated)	-	-	30,000	3,750
F3-8D16-1	2x8 DF	3/4 DF Plywd	8-d @ 8" (Common nails)	-	-	30,000	3,750
F4-8E16-1	2x12 ES	3/4 ES Plywd	8-d @ 6" (Common nails)	-	-	23,000	3,833
F5-8D16-1	2x8 DF	3/4 DF Plywd	8-d @ 4" (Common nails)	-	-	45,000	11,250
F6-8E16-1	2x8 ES	1/2 ES Plywd	8-d @ 8" (Common nails)	-	-	18,000	2,250
F7-12D24-1	2x12 DF	1/2 DF Plywd	8-d @ 4" (Common nails)	-	-	45,000	11,250
F8-8D19.2-1	2x8 DF	1/2 DF Plywd	8-d @ 8" (Common nails)	-	-	30,000	3,750
F9-8E24-1	2x8 ES	1/2 ES Plywd	8-d @ 8" (Common nails)	-	-	18,000	2,250
F10-8E24-1	2x8 ES	1/2 DF Plywd	8-d @ 4" (Common nails)	-	-	45,000	11,250
F11-8D16-1	2x8 DF	1/2 DF Plywd	Glued	-	-	24,000	24,000
F6-8E16-2	2x8 ES	1/2 ES Plywd	8-d @ 8" (Common nails)	30,000	3,750	3,000	375
		1/2 ES Plywd	8-d @ 8" (Common nails)	18,000	2,250	35,000	8,750
F7-12D24-2	2x12 DF	1/2 DF DB	6-d @ 4" (Common nails)	4,500	1,125	4,500	1,125
		1/2 DF Plywd	8-d @ 4" (Common nails)	45,000	11,250	50,000	25,000

Table 4.2 Slip Moduli, k, Used for Floor Specimens (continued)

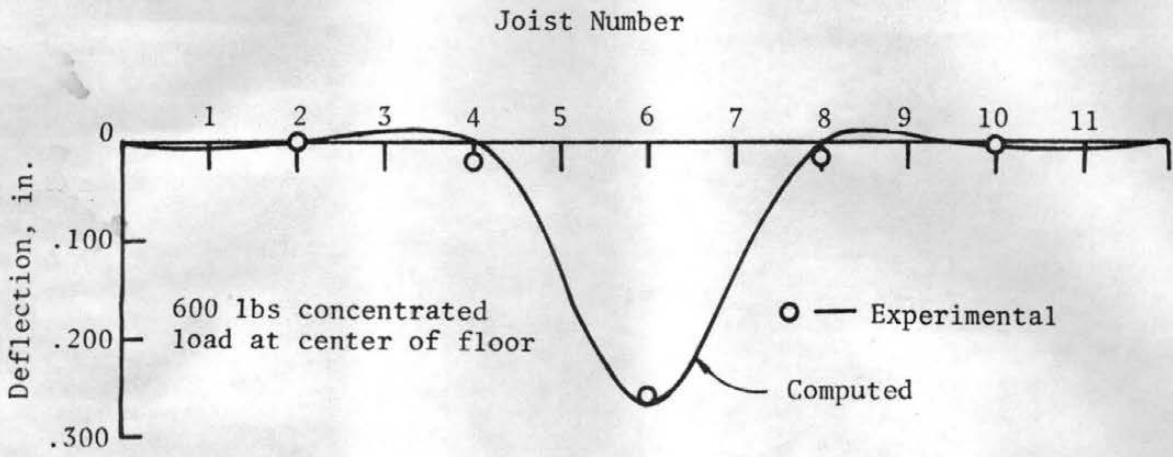
Floor Specimen	Joists	Sheathing	Connectors	Nails of Top Layer Not into Joist		Nails of Top Layer Driven into Joist	
				k, lbs/in.	k/s lbs/in./in.	k, lbs/in.	k/s, lbs/in./in.
F8-8D19.2-2	2x8 DF	1/2 DF PB	6-d @ 8" (Common nails)	4,000	500	4,000	500
		1/2 DF Plywd	8-d @ 8" (Common nails)	3,000	3,750	45,000	11,250
F9-8E24-2	2x8 ES	1/2 DF PB	6-d @ 8" (Common nails)	3,000	375	3,000	375
		1/2 ES Plywd	8-d @ 8" (Common nails)	18,000	2,250	35,000	8,750
F10-8E24-2	2x8 ES	1/2 DF PB	6-d @ 4" (Common nails)	4,500	1,125	4,500	1,125
		1/2 DF Plywd	8-d @ 8" (Common nails)	45,000	5,625	50,000	18,750
F11-8D16-2	2x8 DF	1/2 DF PB	6-d @ 8" (Common nails)	4,000	500	4,000	500
		1/2 DF Plywd	Glued	24,000	24,000	54,000	27,750

Note: DF = Douglas-fir  
 ES = Engelmann spruce  
 Plywd = Plywood  
 PB = Particle board  
 k = Slip modulus  
 s = Nail spacing

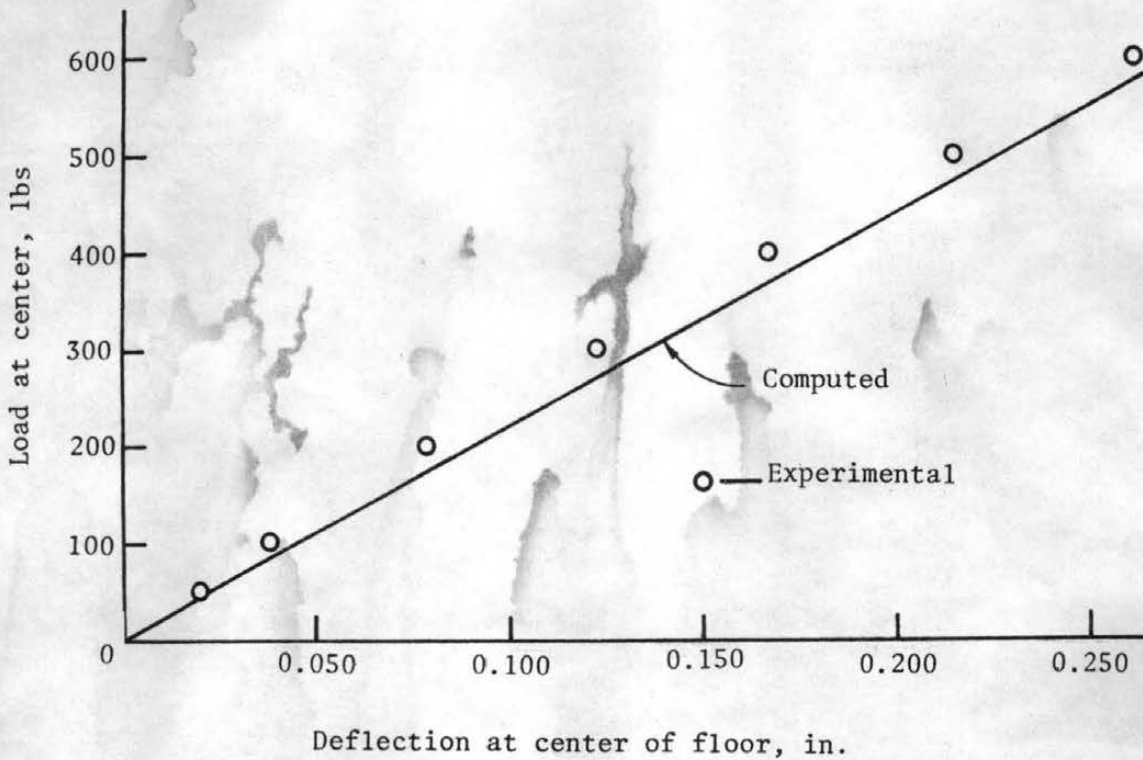
in this study. Each three-layer floor specimen produced two cases for the verification study since the specimen showed different performance with the top layer nails being driven or not driven into the joists. Therefore, the verification study of the mathematical floor model is comprised of 22 testing cases from 16 floor specimens.

The experimental deflections at the midspan of selected joists are plotted against the computed theoretical deflections along the floor centerline (midspan) profile of floor for each of verification cases in this study. Also plotted for each case were the deflections at the center of floor for both the computed and experimental results at several levels of working load. Examples of the computed versus the measured results are shown in Fig. 4.4, through Fig. 4.6 for specimens F6-8E16-1 (a two-layer floor) and F6-8E16-2 (a three-layer floor with top layer nails driven and not driven into joists). The plots of the computed versus the measured results for the rest of the specimens are presented in Appendix D.

Generally, excellent agreement was obtained between the computed and the measured results for each floor specimen as shown in Fig. 4.4 through Fig. 4.6. The calculated upward deflection at approximately the quarter point of the floor length for the computed floor deflection profile across midspan does not generally agree with the measured deflection near that location. This result may be produced by the crossing-beam assumption, since the sheathing strips may be thought as being supported by an elastic foundation (the joists). However, the deflection at the center area of floor (directly under the applied concentrated load) was much greater than anywhere else throughout the floor, therefore interest and attention should be focused in this area.

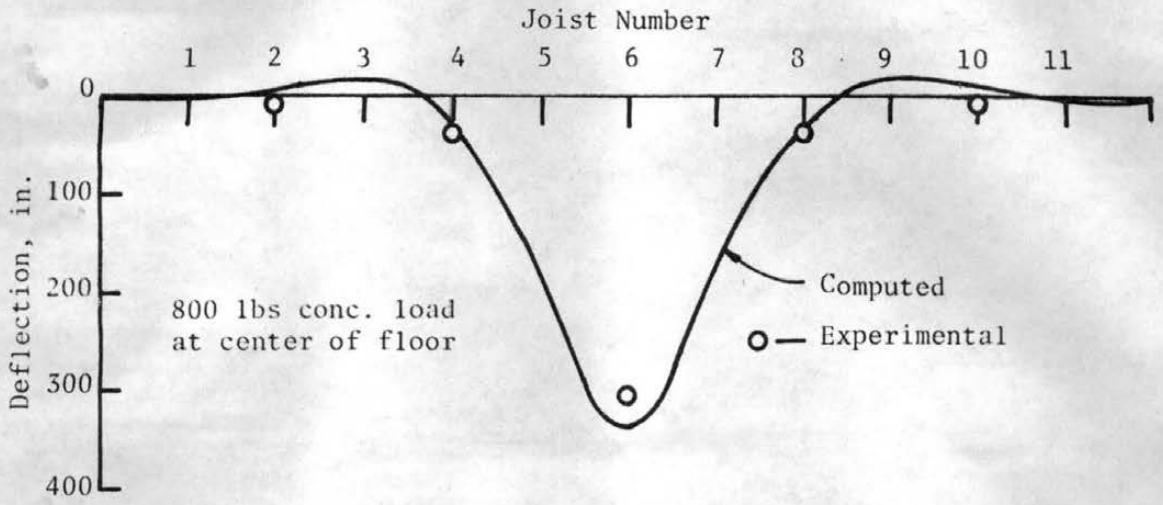


(a) Deflection Profile at Centerline of Joists

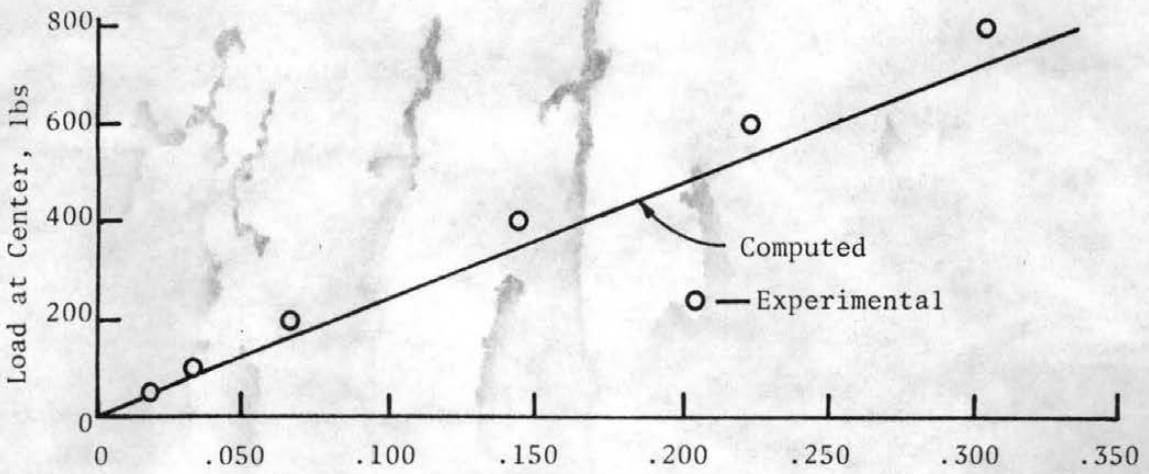


(b) Load-Deflection Behavior

Figure 4.4 Computed vs Measured Results of Floor Specimen F6-8E16-1

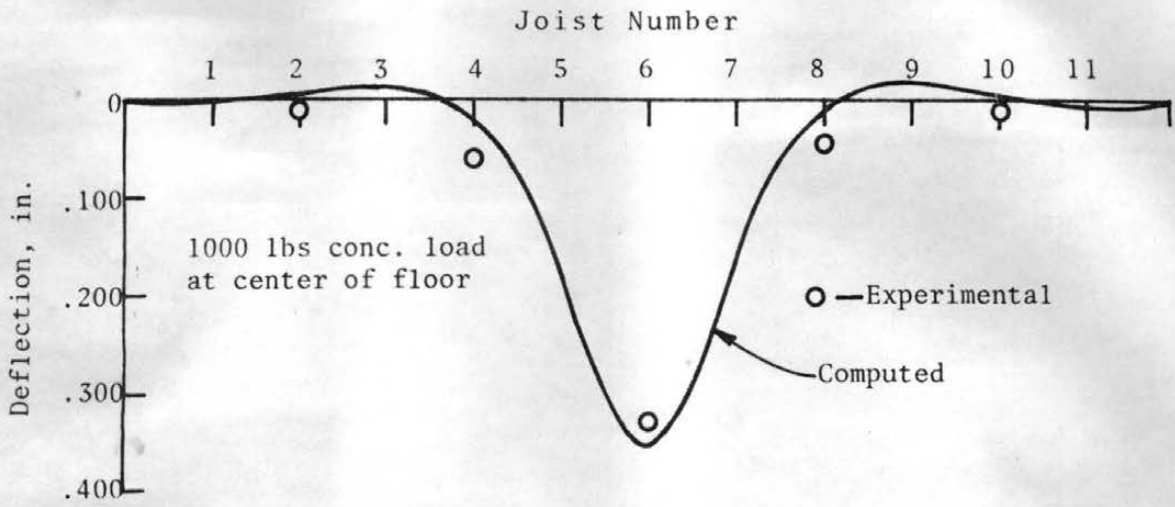


(a) Deflection Profile at Centerline of Joists

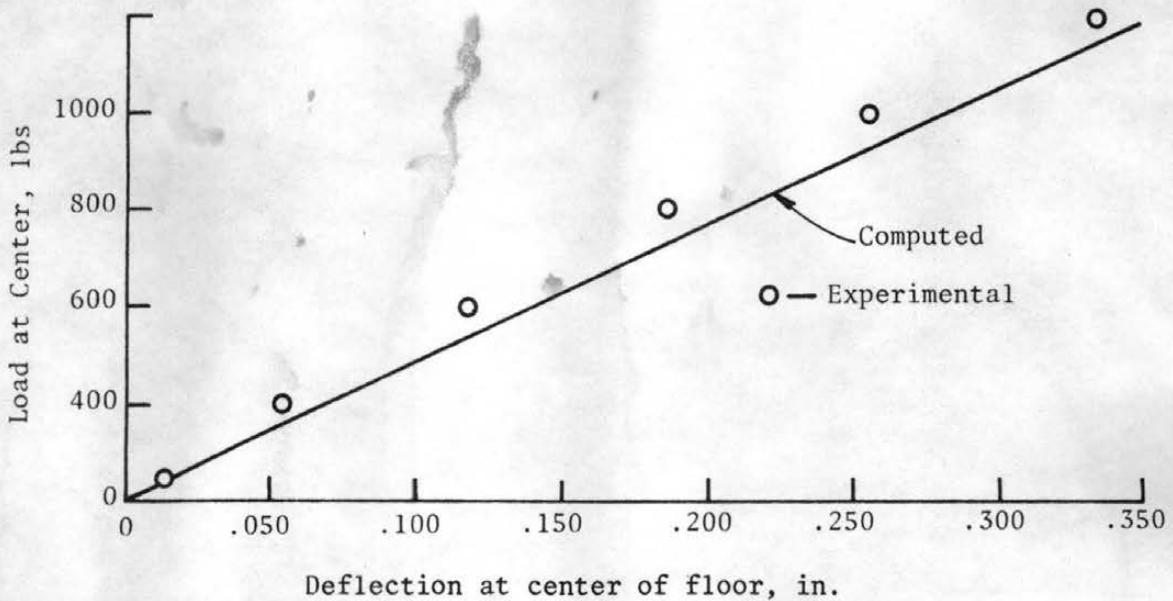


(b) Load-Deflection Behavior

Figure 4.5 Computed vs. Measured Results of Floor Specimen F6-8E16-2. (Nails of Top Layer Not Driven into Joists)



(a) Deflection profile at centerline of joists



(b) Load-deflection behavior

Figure 4.6 Computed vs Measured Results of Floor Specimen F6-8E16-2 (Nails of Top Layer Driven into Joists)

The percentage error of the computed deflection at center of floor with respect to the corresponding measured deflection was calculated for each floor specimen. Table 4.3 summarizes the percentage errors of the verification study of all the floor specimens. Generally, good results were obtained. The percentage errors ranged from less than one percent to a maximum of 12 percent. The computed deflections fluctuated above and below the measured deflections (a positive percentage error means the mathematical model overpredicts the deflections and a negative percentage error means the mathematical model underpredicts the deflection). For the three-layer specimens, a general trend showed that the percentage error was less when the top layer nails were not driven into joists than when the nails were driven into joists. This indicates that the assumed increase in the value of slip modulus due to this effect was generally not enough when the top layer nails were also driven into the joists.

The average absolute error of the computed deflections with respect to the corresponding measured deflections for all the floor specimens is 6.44 percent, whereas the average algebraic error is +3.24 percent. The deflection at the center of floor (directly under the concentrated load) predicted by the mathematical floor model were generally slightly greater than the corresponding measured deflections and are therefore conservative. The assumption made in Sec. 2.3 that the effect due to the torsion action of sheathing can be neglected would aid in producing the computed results for the mathematical floor model to overestimate the deflections slightly.

Overall, the percentage errors of the computed deflections with respect to the measured deflections at center of floor are relatively small, especially when the average percentage error is considered.

Table 4.3 Comparison of Computed and Experimental Results

Floor Specimen	Computed Deflection at Center of Floor, (in.)	Experimental Deflection at Center of Floor, (in.)	Load Level (lbs)	% of Error
F2-8D16-1	0.278	0.261	1,000	+6.51
F3-8D16-1	0.251	0.269	1,000	-6.69
F4-12E16-1	0.112	0.127	1,000	-11.81
F5-8D16-1	0.236	0.217	1,000	+8.76
F6-8E16-1	0.270	0.260	600	+3.85
F7-12D24-1	0.168	0.165	1,000	+1.82
F8-8D19.2-1	0.296	0.337	1,000	-12.17
F9-8E24-1	0.417	0.395	600	+5.57
F10-8E24-1	0.366	0.359	800	+1.95
F11-8D16-1	0.209	0.215	1,000	-2.78
F6-8E16-2 (Nails of top layer not into joists)	0.336	0.303	800	+10.89
F6-8E16-2 (Nails of top layer driven into joists)	0.352	0.326	1,000	7.98
F7-12D24-2 (Nails of top layer not into joists)	0.146	0.141	1,000	+3.55
F7-12D24-2 (Nails of top layer driven into joists)	0.144	0.132	1,000	+9.09
F8-8D19.2-2 (Nails of top layer not into joists)	0.284	0.278	1,000	+2.16

Table 4.3 Comparison of Computed and Experimental Results (continued)

Floor Specimen	Computed Deflection at Center of Floor, (in.)	Experimental Deflection at Center of Floor, (in.)	Load Level (lbs)	% of Error
F8-8D19.2-2 (Nails of top layer driven into joists)	0.274	0.250	1,000	+9.60
F9-8E24-2 (Nails of top layer not into joists)	0.413	0.410	800	+0.73
F9-8E24-2 (Nails of top layer driven into joists)	0.387	0.394	800	-1.78
F10-8E24-2 (Nails of top layer not into joists)	0.367	0.352	1,000	+4.26
F10-8E24-2 (Nails of top layer driven into joists)	0.361	0.321	1,000	+12.46
F11-8E16-2 (Nails of top layer not into joists)	0.206	0.195	1,000	+5.64
F11-8E16-2 (Nails of top layer driven into joists)	0.199	0.183	1,000	+8.74

Average Absolute Error = 6.44%

Average Algebraic Error = +3.24%

Therefore, the mathematical floor model developed in this study is regarded as having a very good accuracy in predicting the behavior of the wood joist floor system.

## CHAPTER 5

### PARAMETER STUDIES AND DEMONSTRATIONS

#### 5.1 Introduction

As discussed in Chapter 3, each floor specimen was designed to be different from the others in several respects and since the effects of various parameters are often strongly interrelated, precise quantitative information on how the several variables affect floor response is difficult to obtain through experimental study. However, parameter studies using the verified mathematical model can better isolate the effect of a specific variable on the floor behavior by fixing the rest of the variables as constants.

The validity of the mathematical model has been proved in the previous chapter. In this chapter, the effect of each of the several parameters of special interest on the floor behavior is investigated and demonstrated through the application of the verified mathematical floor model. Computed quantitative information from parameter studies is presented.

Also to be presented in this chapter are the parameter studies on how the various parameters of a layered beam system can affect the effective flange width of the beam. The mathematical model for effective flange width, developed in Chapter 2, is used in the parameter study.

#### 5.2 Example Floor Specimen Used in Parameter Study

A two-layer floor specimen with dimensions shown in Fig. 2.3 was selected as the basic floor for the parameter studies on the floor behavior. Fixed data included 144-inch floor span, 192-inch

floor length, 2x8 inch nominal joist sizes and 16-inch joist spacings, 8-inch nail spacings and one row of nails per joist. Basic data included a 3/4 inch sheathing thickness, a sheathing MOE of 2,000,000 psi parallel to grain and of 1,000,000 psi perpendicular to grain, a joist MOE values of 2,000,000 psi and a slip modulus of 30,000 pounds per inch.

The face grain of the sheathing was oriented to be perpendicular to the joist span in all cases. The floor was assumed to have no gaps in the sheathing and was idealized as containing 11 T-beams and 11 sheathing strips crossing each other at right angles. Simple supports were assumed at all edges of the floor.

Two example loading patterns were considered. The first was a single concentrated load of 1100 pounds applied at the center of floor; the second was a uniform load of 120 psf throughout the floor which is equivalent to a concentrated load of 160 pounds at each nodal point. These load magnitudes were chosen such that if no two-way or composite action occurred, the deflections of the center joist would be nearly the same for each loading.

### 5.3 Effects of Parameters on Floor Behavior

In this section, the isolated effects of connector slip modulus, MOE value of joists, and effective flange width on the floor behavior are examined using the verified mathematical floor model. Several different values of the parameters which effect floor behavior are studied. The effects of the other variables are held constant by inputting the fixed and basic data of these variables into the mathematical model.

### 5.3.1 Effect of Slip Modulus

The effect of slip modulus on the composite action is shown in Fig. 5.1 for the concentrated loading case. The midspan deflections of joists is plotted versus the slip modulus values. For slip modulus values less than about 1,000 pounds per inch, the sheathing does not act as a T-beam flange. Rather, the sheathing and the joist carry all of the load in the joist direction through nearly independent action. This represents the region of insignificant composite action. While little composite action is present for low values of slip modulus, two-way action exists as seen by the resulting deflections of the adjacent joists as shown in Fig. 5.1. For slip modulus values greater than  $10^6$  pounds per inch, essentially complete composite action is present and the joist plus effective flange behave nearly as a rigidly-connected beam. Consequently, the deflections are reduced by a substantial amount. Values of slip modulus between  $10^3$  and  $10^6$  pounds per inch represent the region of incomplete composite action. Both significant composite action and interlayer slip occur in this region. The slip moduli of currently used structural connectors, except very rigid glues, fall in this range. Thus, either by the neglect of interlayer slip or the assumption of fully composite behavior for the commonly used connectors can lead to gross error.

Similar behavior is observed for the same floor subjected to uniform load, as is shown in Fig. 5.2. Fairly uniform deflections are noted for the joists. The small differences in deflection of joists are due to the fact that while the same load is applied to each joist, the sheathing carries a portion of the load to the supports at the ends of sheathing strips.

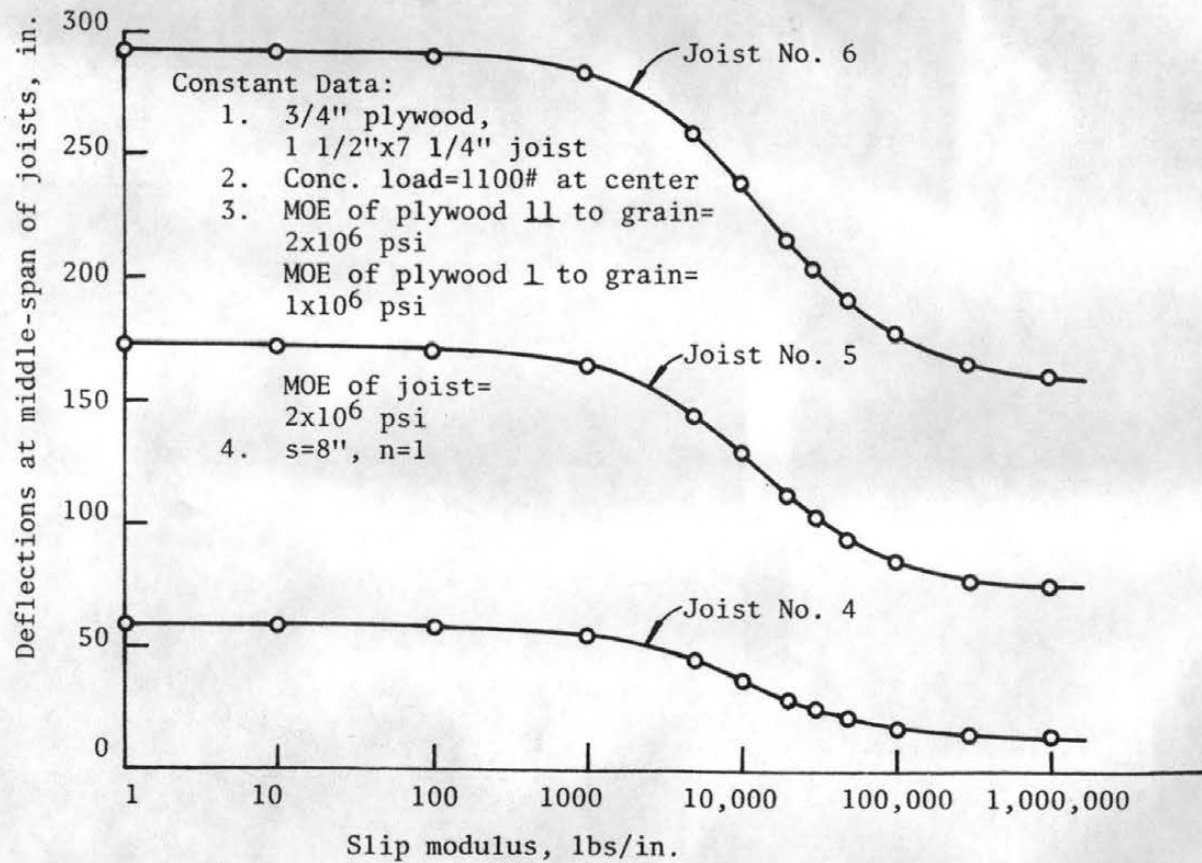


Figure 5.1 Deflections vs Slip Modulus, k, Concentrated Load

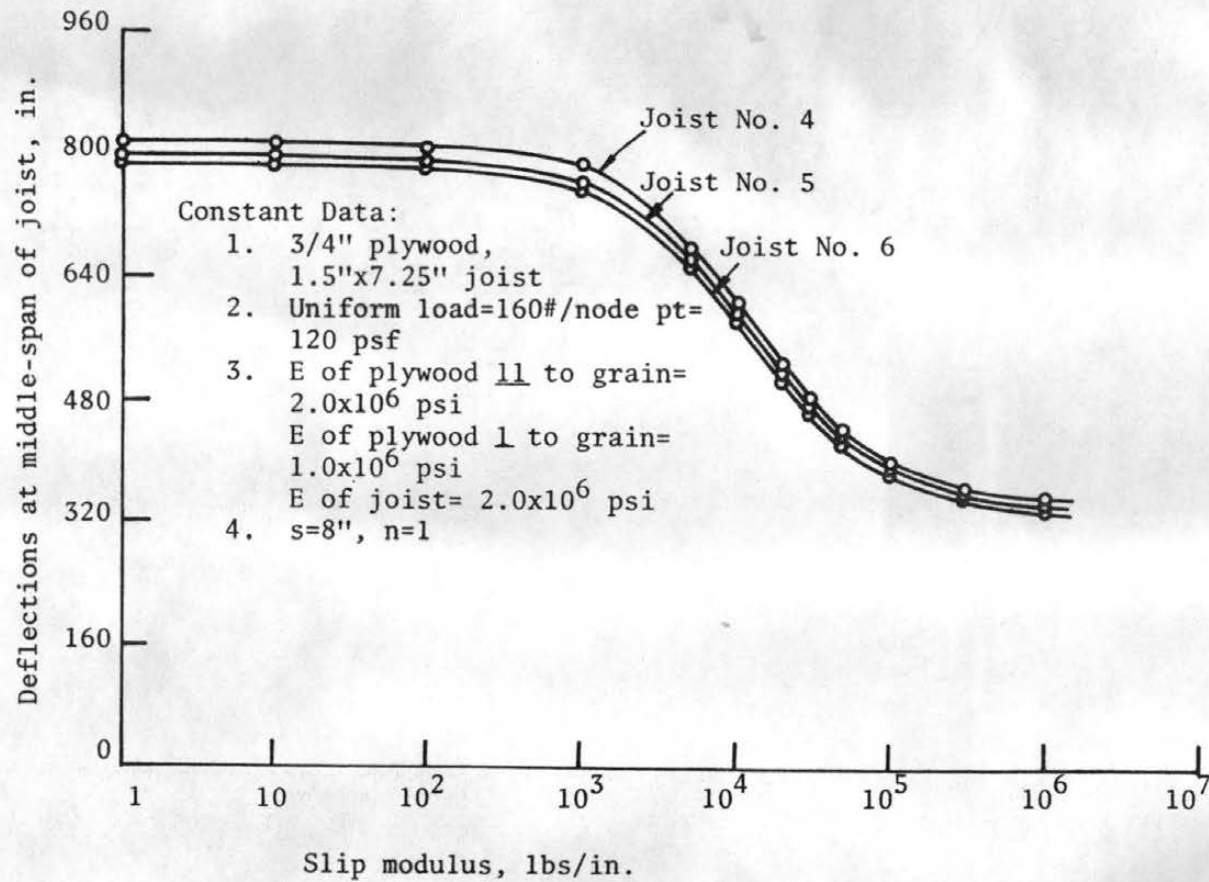


Figure 5.2 Deflections vs Slip Modulus, Uniform Load

### 5.3.2 Effect of Joist MOE

One of the major parameters affecting the floor behavior is the MOE value of joists. Fig. 5.3 shows this effect on the floor deflections for the case of a concentrated load at center of floor. The joist MOE-deflection curves are seen to be very sensitive in the low joist MOE range (less than  $10^6$  psi) and become less sensitive in the high joist MOE range (greater than  $2 \times 10^6$  psi). As the joist MOE increases from  $10^6$  psi to  $2 \times 10^6$  psi with all other parameters being constant, the midspan deflection of the loaded joist decreases by 40 percent. The MOE values of the Douglas-fir and Engelman spruce joists used in the experimental program of this study generally fall between  $10^6$  and  $2 \times 10^6$  psi. The nonlinear deflection versus the joist MOE behavior is due to the two-way interaction of T-beams and sheathing strips. Similar behavior is observed for the same floor subjected to uniform load as seen in Fig. 5.4.

### 5.3.3 Effect of Effective Flange Width

The plot of floor deflections versus the effective flange width for the case of a concentrated load at center of floor is presented in Fig. 5.5. The 16-inch flange width corresponds to the joist spacing. It is seen from Fig. 5.1 that the deflections are relatively insensitive to the effective flange width. For example, reducing the effective flange of the loaded T-beam by 50 percent from 16 to eight inches, which is equivalent to assuming that only 50 percent of the available flange is effective in carrying load, results in only an eight percent increase in deflection of the loaded joist when the other parameters are held constant and even smaller percentage increases are noted for the other joists. Results of the study of effective flange width

## Constant Data:

1. 3/4" plywood, 1.5"x7.25" joist
2. Conc. load=1100# at center
3. E of plywood  $\parallel$  to grain= $2.0 \times 10^6$  psi  
E of plywood  $\perp$  to grain= $1.0 \times 10^6$  psi
4.  $s=8"$ ,  $n=1$ ,  $k=30,000\#/in.$

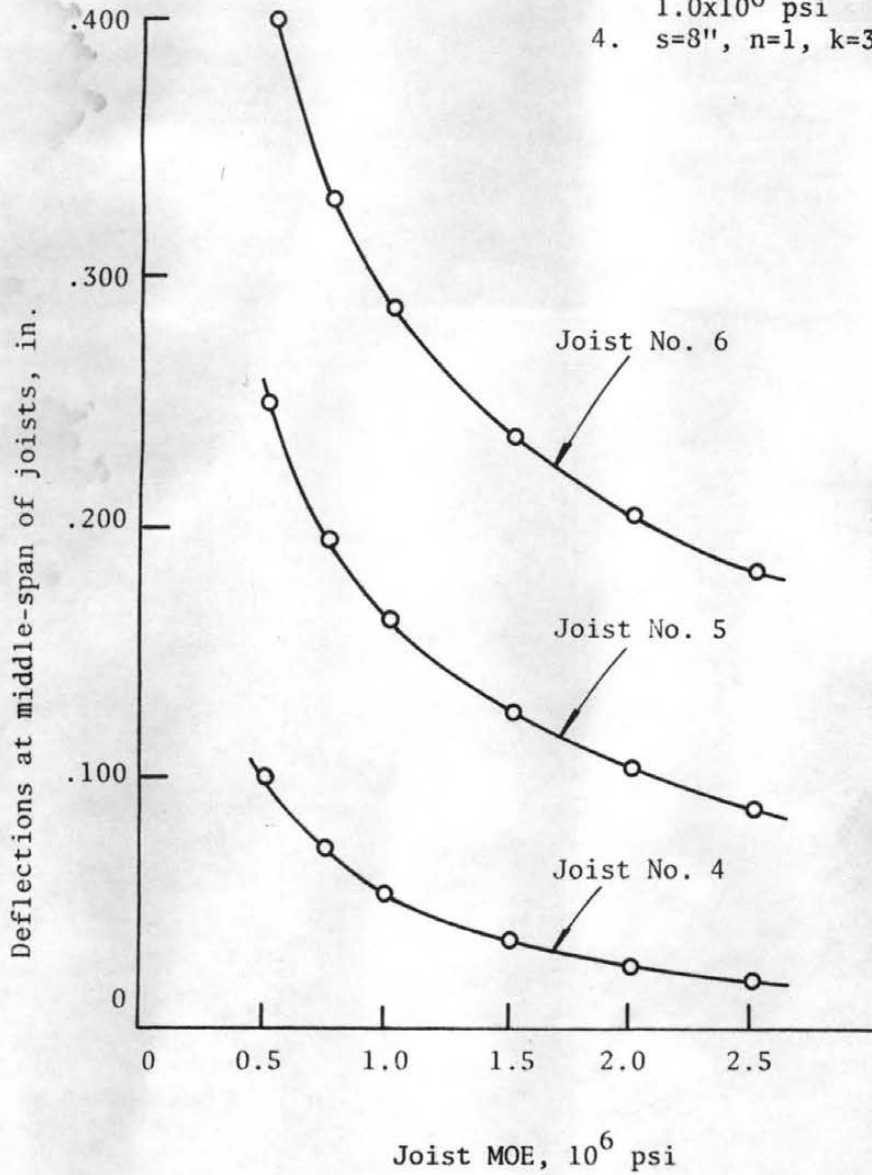


Figure 5.3 Joist MOE vs Deflections

## Constant Data:

1. 3/4" plywood, 1 1/2" by 7 1/4" joist
2. Uniform load=160#/node pt = 120 psf
3. E of plywood  $\perp$  to grain=  $2 \times 10^6$  psi  
E of plywood  $\parallel$  to grain=  $1 \times 10^6$  psi
4.  $s=8"$ ,  $n=1$ ,  $k=30,000\#/in.$
5. No gaps

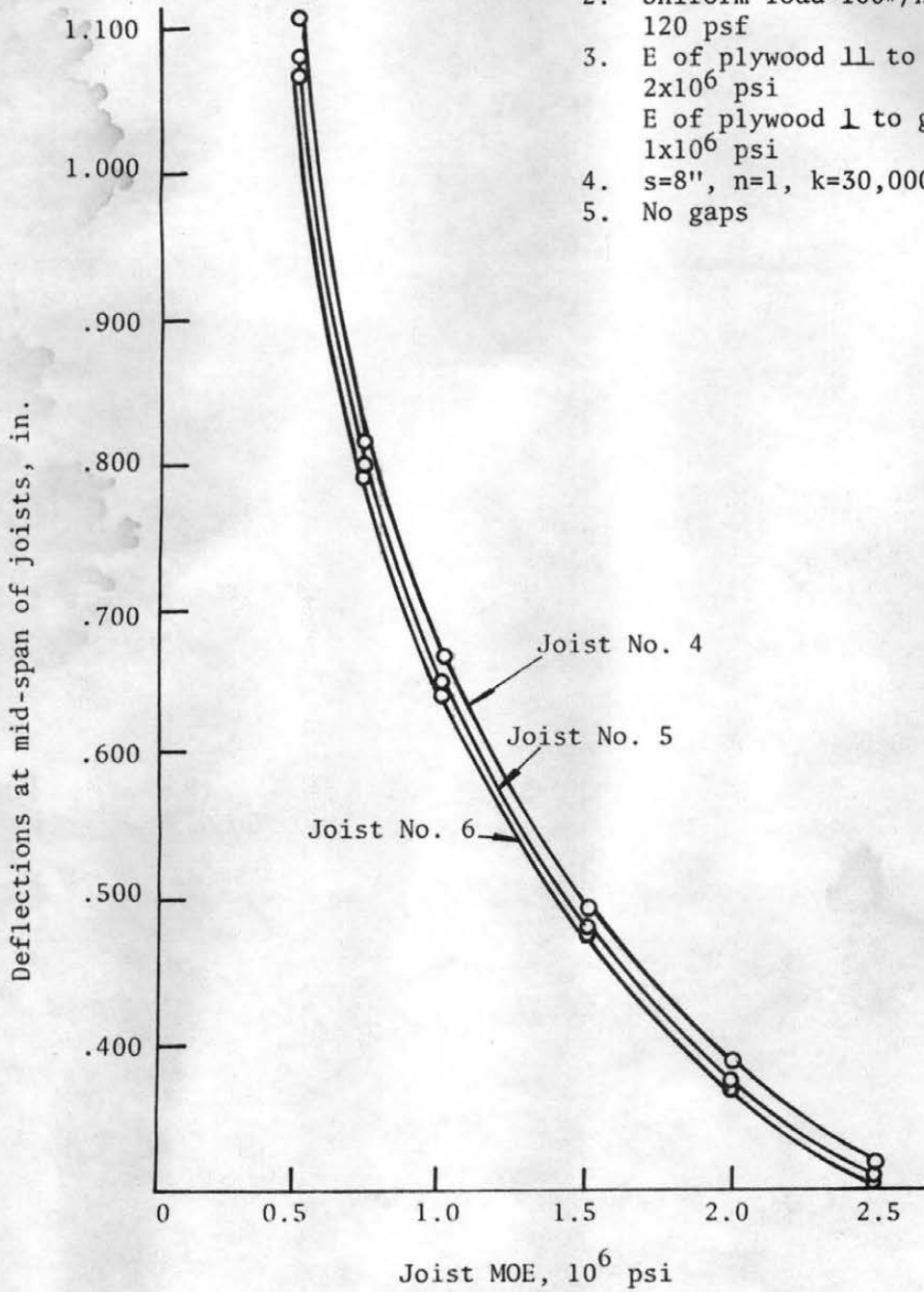


Figure 5.4 Joist MOE vs Deflections, Uniform Load

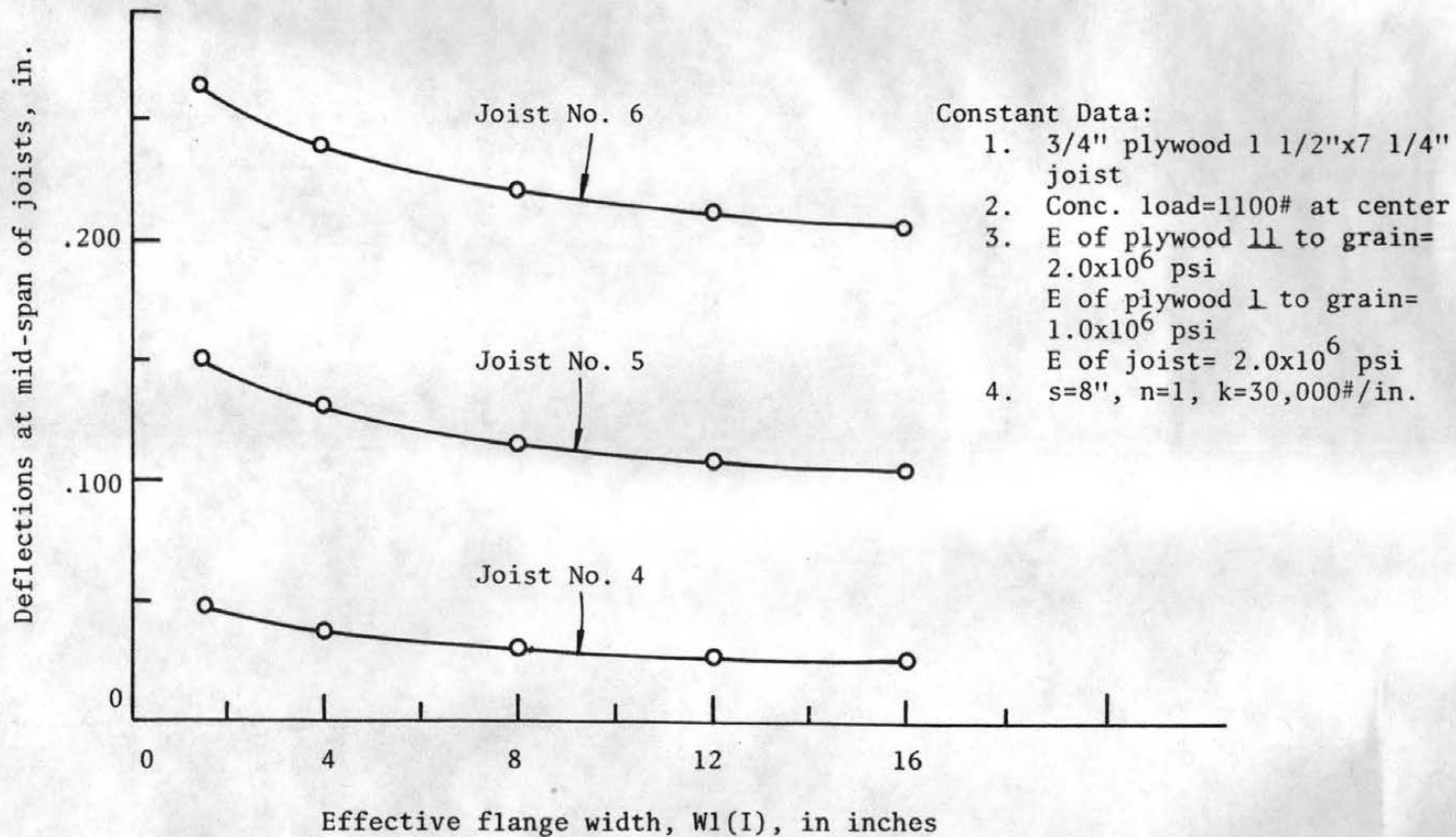


Figure 5.5 Effective Flange Width vs Deflections, Concentrated Load

indicate that for the range of parameters studied, the flange is fully effective at some distance away from the ends and gaps in sheathing, which is consistent with the study by Amana and Booth (2).

A similar trend for the behavior of the effective flange width versus the floor deflections for the uniform load case is illustrated in Fig. 5.6.

#### 5.4 Parameter Studies of Effective Flange Width

The mathematical floor model developed in Chapter 2 simulates a physical wood joist floor with two sets of crossing beams: one set is the T-beams consisting of joists topped by a sheathing flange, the other set is the sheathing strips consisting of sheathing only. Due to the wide flange of the T-beam, shear lag may occur in the flange when subjected to loading. If ordinary beam theory is to be applied to the T-beams, effective flange width must be obtained and used for the analysis. In this section, the effects of several important parameters on the effective flange width of a T-beam are investigated using a computer program developed from the theoretical solution derived in Sec. 2.2.3.

The basic T-beam data used for this parameter study included a 1.5 x 9.25 inch actual joist size, a 3/4-inch thick sheathing with 24-inch available flange, a joist MOE of  $2 \times 10^6$  psi, a sheathing MOE of  $1.2 \times 10^6$  psi parallel to the surface ply grain and of  $5 \times 10^5$  psi perpendicular to grain, a sheathing shear modulus of 80,000 psi, and one row of connectors spaced at 8 inches with a slip modulus of 30,000 pounds per inch. The MOE values and the shear modulus value for the sheathing were chosen from the average values of the data for 3/4-inch Douglas-fir plywood panels obtained by the Wood Science

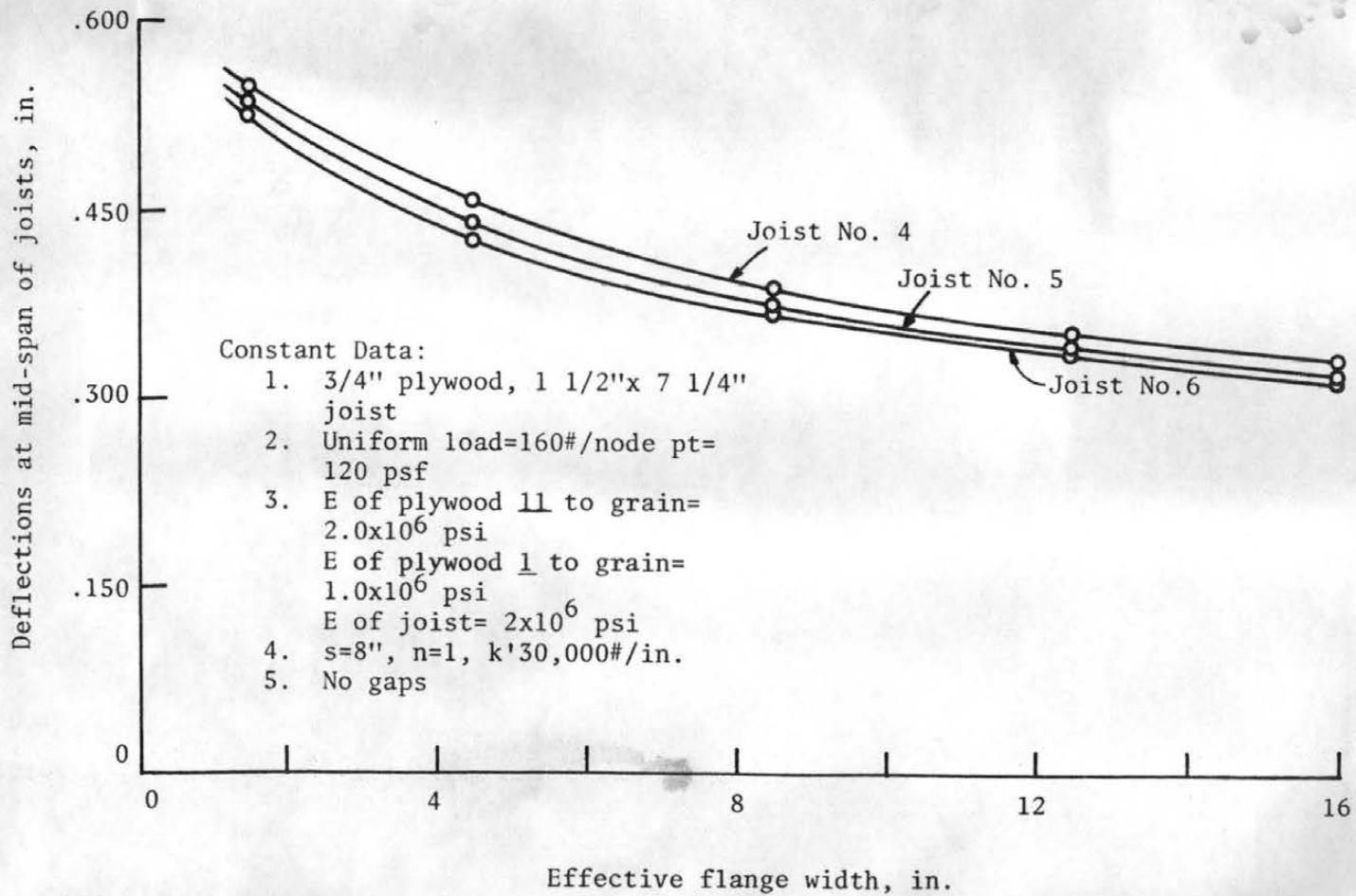


Figure 5.6 Effective Flange Width vs Deflections, Uniform Load

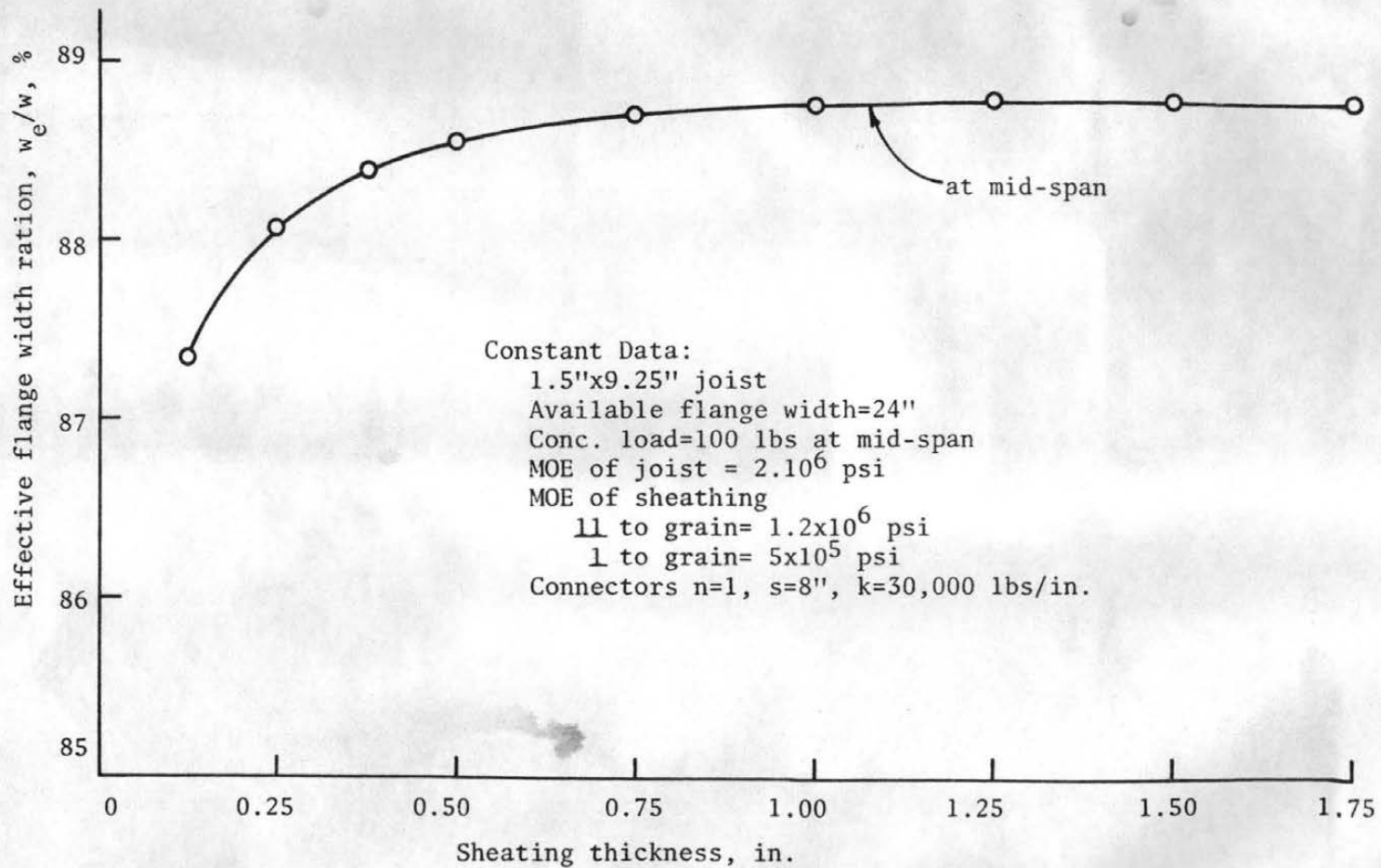


Figure 5.7 Effective Flange Width vs Sheathing Thickness, Concentrated Load

Laboratory. In all cases of the parameter study, a 180-inch span for the simply supported T-beam was used and the face grain of sheathing was oriented perpendicular to the joist span. No gaps were assumed throughout the sheathing. Two types of loading were used for the study, a 100-pound concentrated load applied at midspan and a uniform load of 1 pound per inch distributed along the joist.

The effective flange width of a T-beam varies along the joist length due to varying interlayer shear stress distribution. Generally, the effective flange width is greater toward the ends of beam and smallest at midspan for concentrated load at midspan and vice versa for uniform load. For simplicity the boundary effect at the ends is neglected and only the effective flange width at midspan is reported in this study.

#### 5.4.1 Effect of Sheathing Thickness

The relationship between effective flange width and sheathing thickness with the other parameters held constant is presented in Fig. 5.7 where the percentage of effective flange width with respect to the available flange width is plotted against several different values of sheathing thickness for the concentrated load at midspan. The effective flange width ratio falls between 87 percent and 89 percent for sheathing thickness up to 1.75 inches and approaches 89 percent as an upper limit. For most wood structures, plywood of thickness from  $3/8$  to 1 inch is used with the corresponding effective flange width ratio ranging from 88.38 percent to 88.75 percent, only a 0.37 percent variation. Therefore, the effective flange width can be considered as independent of the sheathing thickness.

Similar behavior is observed for the uniform loading case as shown in Fig. 5.8. The flange effectiveness almost remains constant

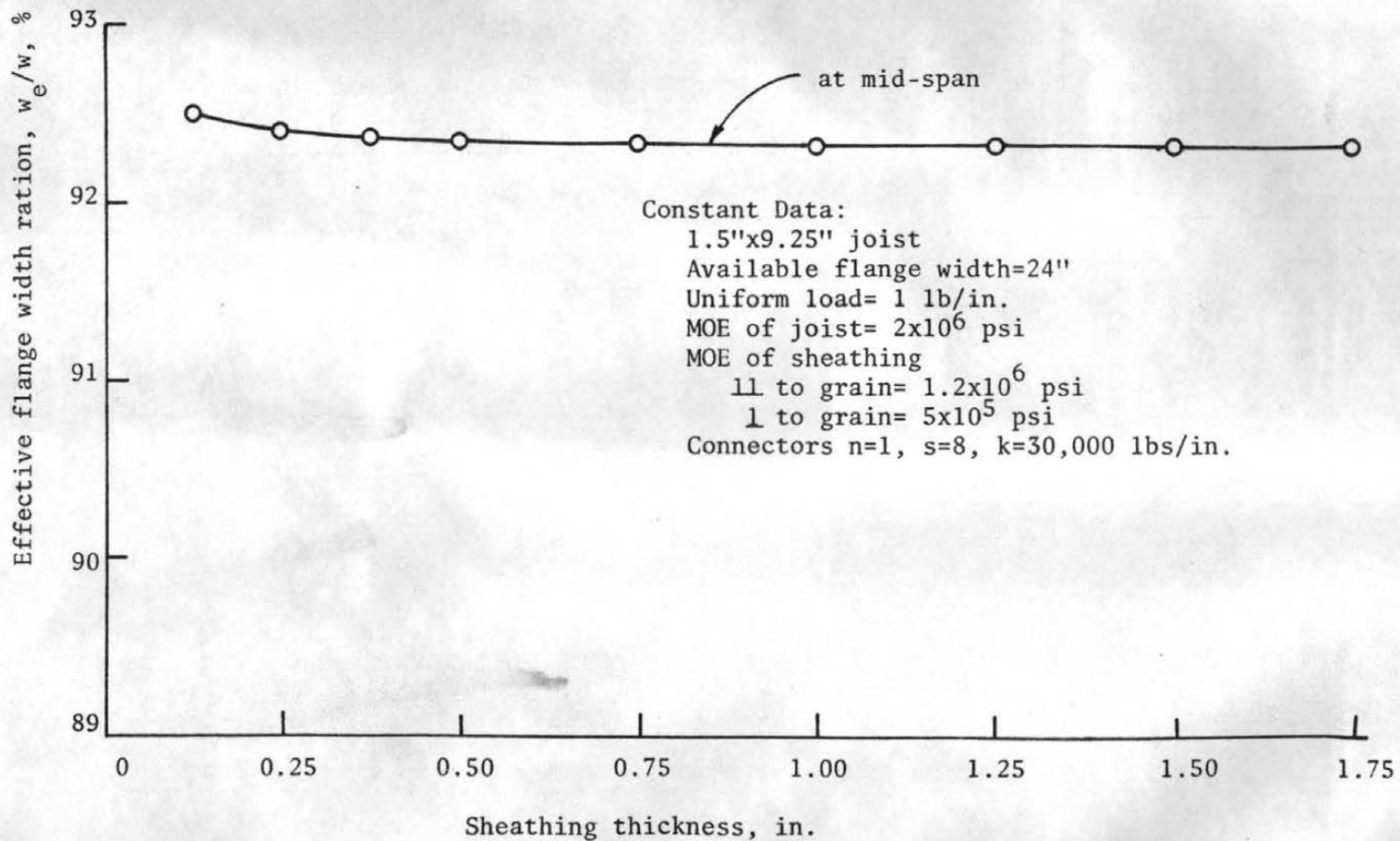


Figure 5.8 Effective Flange Width vs Sheathing Thickness, Uniform Load

except when sheathing thickness is very small where a slight increase of effective flange width ratio occurs. Effective flange width may, therefore, be considered to be independent of sheathing thickness for the uniform loading case as well.

#### 5.4.2 Effect of Joist Depth

A plot of the effective flange width ratio versus joist depth is presented in Fig. 5.9 for a concentrated load at midspan. The effective flange width ratio increases as the joist depth increases. A variation of about 5.7 percent in effective flange width ratio is seen for joist depths ranging from nearly zero to 14 inches. For most floor construction, joist depth varies from 5.5 to 13.25 inches which produces approximately a 1.2 percent variation in the effective flange width ratio. Therefore, joist depth is considered to have small influence on the effective flange width.

For the uniform load case, the effective flange width ratio decreases from 92.9 percent to 92.2 percent when the joist depth increases from nearly zero to 14 inches as shown in Fig. 5.10. For joist depths ranging from 5.5 to 13.25 inches as most commonly used in wood floor construction, a variation of only 0.2 percent is experienced for the flange effectiveness. Consequently, joist depth is considered to have no appreciable effect on the effective flange width for uniform loading.

#### 5.4.3 Effect of Slip Modulus

Figure 5.11 shows the variation in the effective flange width ratio for a T-beam with respect to variation in the slip modulus of connectors for a concentrated load at midspan. The effective flange width ratio remains constant at 90.7 percent when little interaction

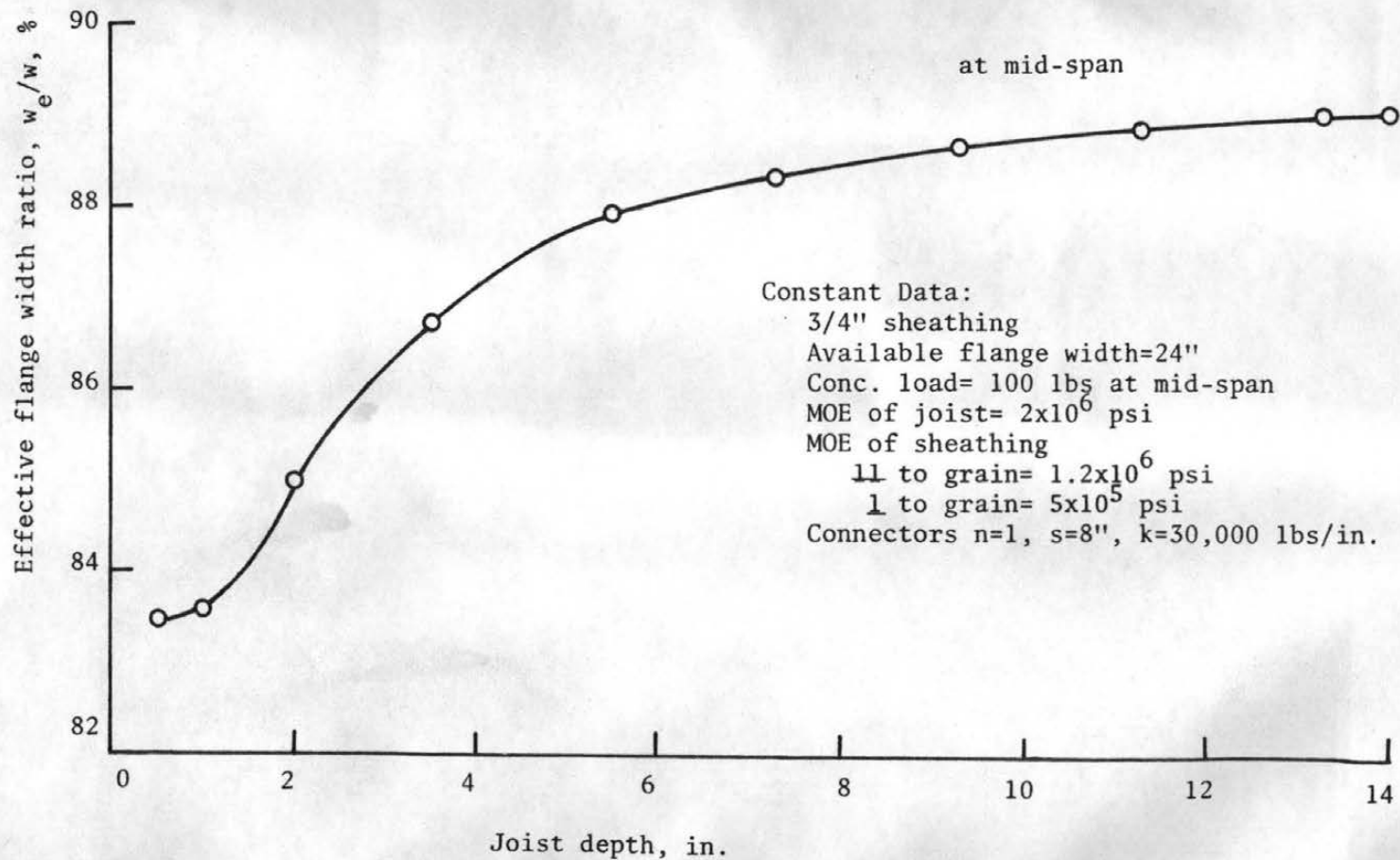


Figure 5.9 Effective Flange Width vs Joist Depth, Concentrated Load

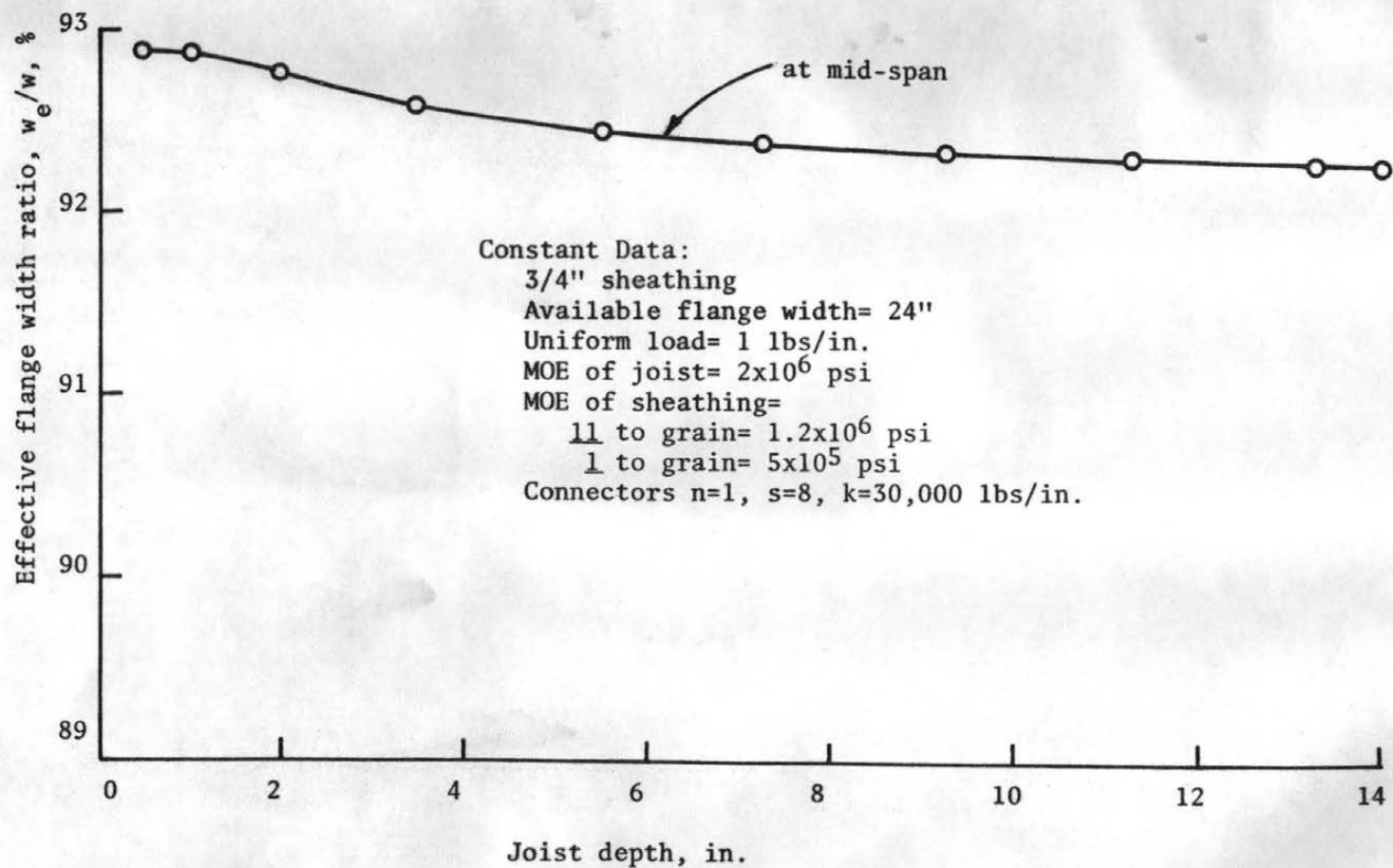


Figure 5.10 Effective Flange Width vs Joist Depth, Uniform Load

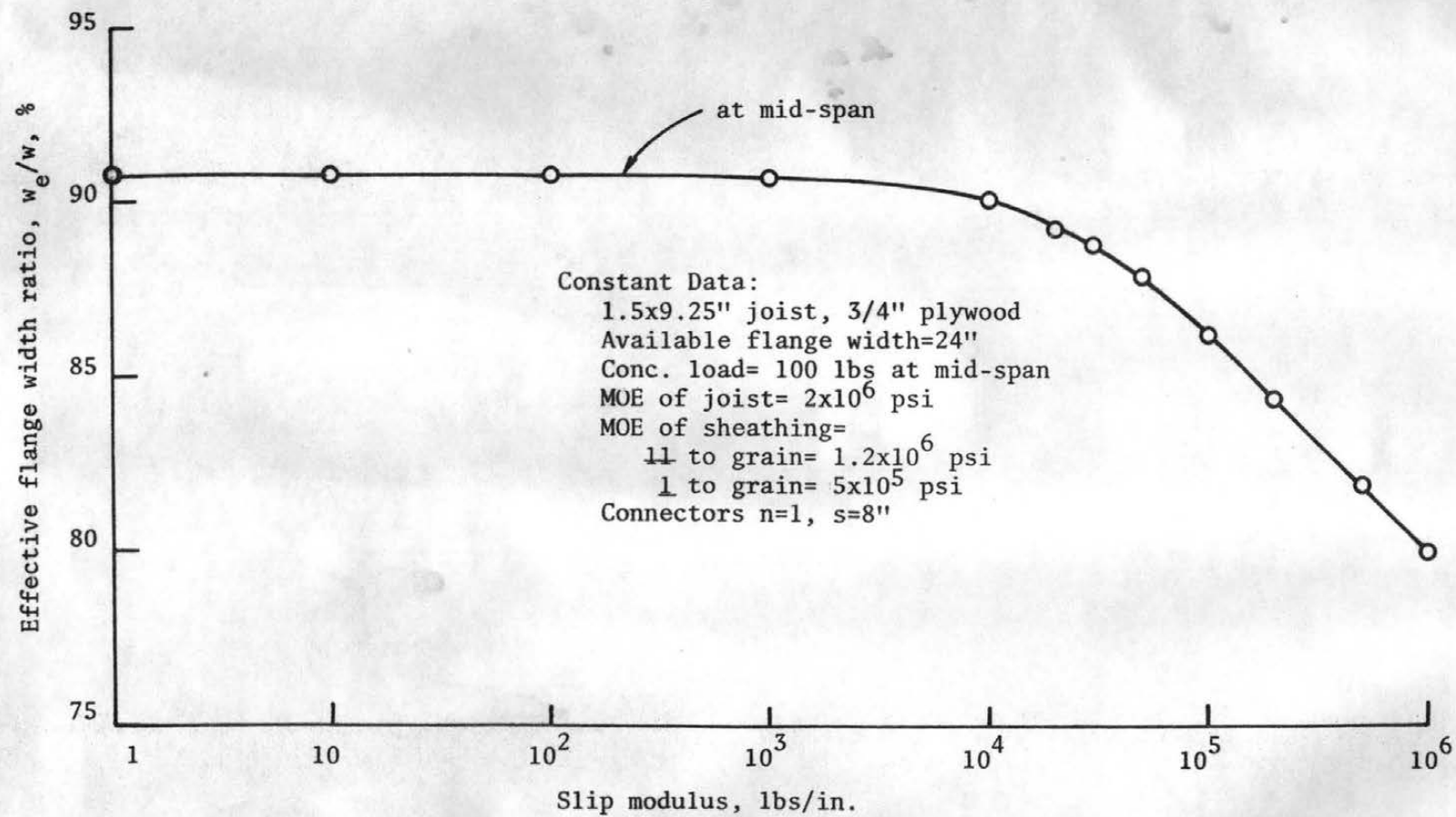


Figure 5.11 Effective Flange Width vs Slip Modulus, Concentrated Load

occurs between the flange and the web as seen in Fig. 5.11 when the slip modulus ranges from one to 1000 pounds per inch. When the degree of interaction between layers increases as the slip modulus exceeds 1000 pounds per inch, the effective flange width ratio decreases slightly. For all structural connectors except very rigid glues, the effective flange width ratio is in the region of from 90 percent to 86.2 percent (corresponding to the slip modulus between  $10^5$  to  $10^6$  pounds per inch), a variation of 3.8 percent. Therefore, the effect of the slip modulus of ordinary connectors on the effective flange width ratio can be regarded as negligible.

For the uniform load case (as shown in Fig. 5.12), the effective flange width ratio remains constant at about 92 percent for a low value of slip modulus ranging from one to 1000 pounds per inch. Less than one percent of change is seen in the effective flange width ratio for the slip modulus varying from one to  $10^6$  pounds per inch. For the ordinary structural connectors, a variation of about 0.8 percent is experienced. Therefore, the slip modulus is considered to have negligible influence on the effective flange width for uniform load.

#### 5.4.4 Effect of Sheathing MOE

The sheathing MOE values, both parallel to grain and perpendicular to grain, and the shear modulus value of plywood are interrelated. A ratio of 15:6.25:1 was assumed for the MOE parallel to grain, MOE perpendicular to grain and the shear modulus for the study of the effect of sheathing MOE on the effectiveness of flange. This ratio was obtained from the average data on 3/4-inch Douglas-fir plywood panels tested by Wood Science Laboratory. Figure 5.13 shows the effect of sheathing MOE on the effective flange width ratio for the

Constant Data:

1.5"x9.25" joist, 3/4" plywood  
Available flange width=24"  
Uniform load= 1 lb/in.  
MOE of joist=  $2.10^6$  psi  
MOE of sheathing=  
    11 to grain=  $1.2 \times 10^6$  psi  
    1 to grain=  $5 \times 10^5$  psi  
Connectors n=1, s=8"

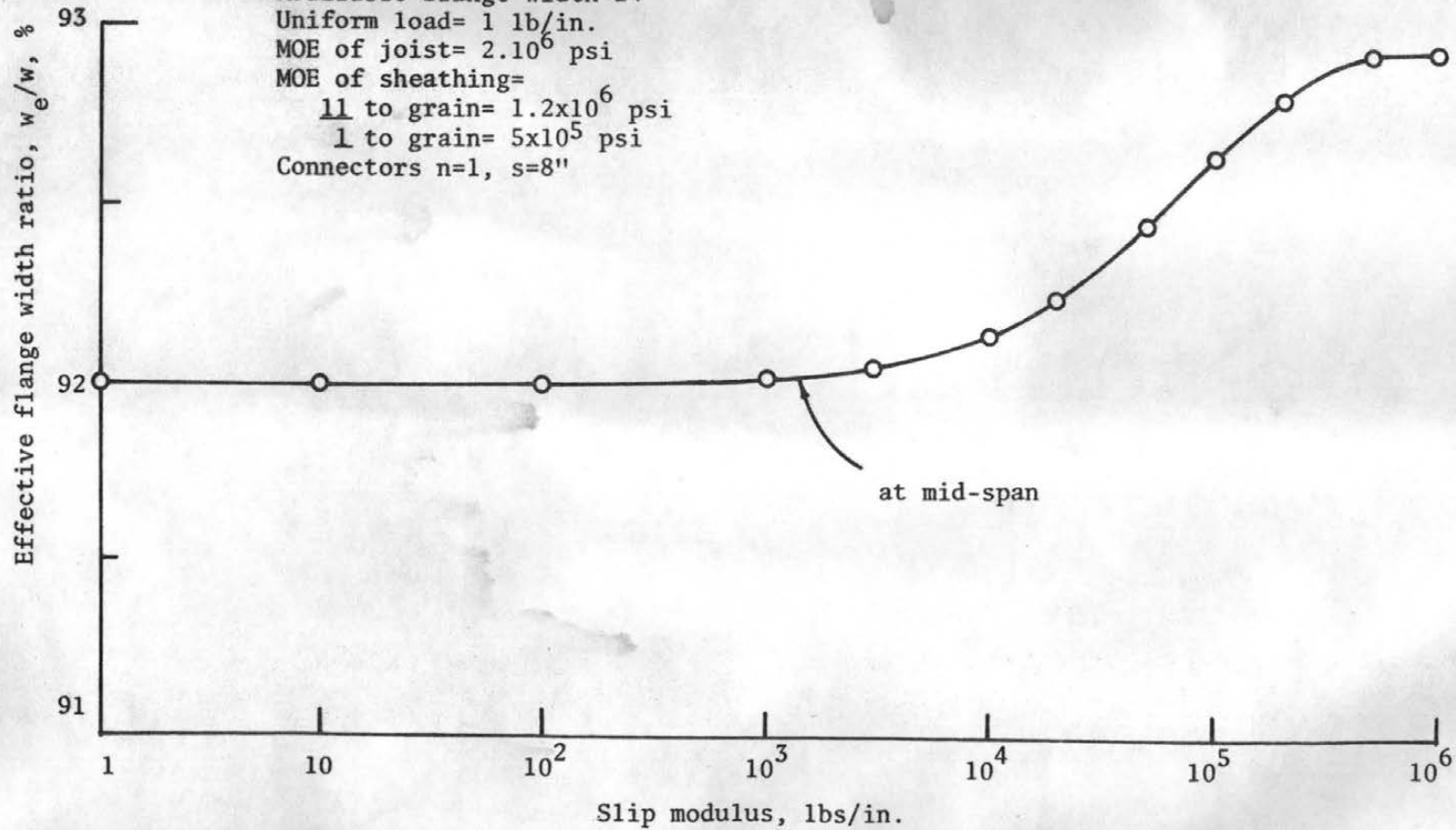


Figure 5.12 Effective Flange Width vs Slip Modulus, Uniform Load

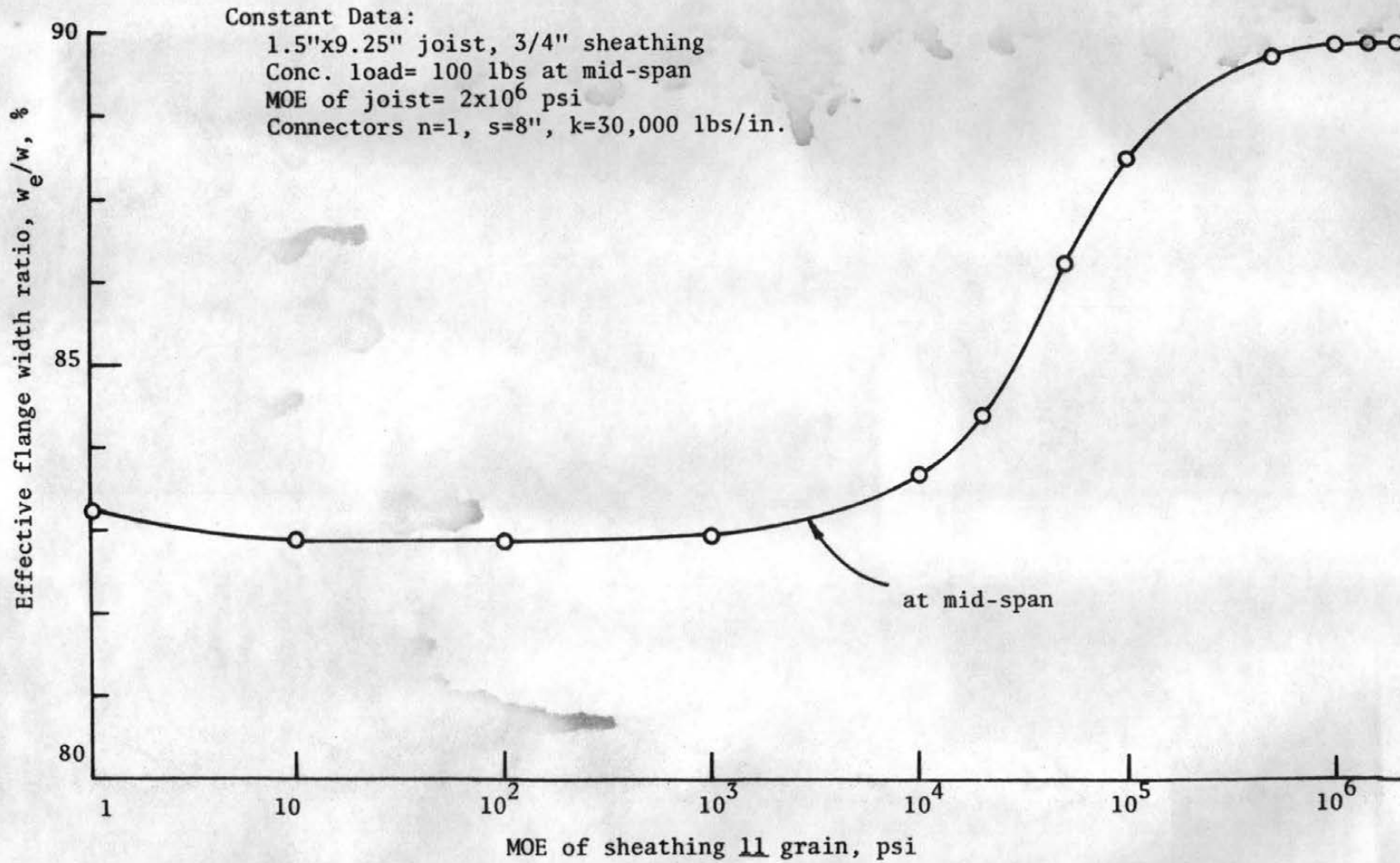


Figure 5.13 Effective Flange Width vs MOE of Sheathing, Concentrated Load

concentrated load at midspan. Approximately constant effective flange width ratio of 83 percent is seen for low MOE values, less than 1000 psi, for sheathing parallel to grain and an increasing effective flange width ratio up to about 89 percent when the MOE of sheathing parallel to grain increases to  $10^6$  psi. For most of the structural plywood a value of only 1.4 percent of change in the effective flange width ratio is seen for the sheathing MOE parallel to grain ranging from  $10^5$  to  $10^6$  psi. No appreciable effect needs, therefore, to be assumed for the sheathing MOE on the effective flange width.

For the uniform load case (as shown in Fig. 5.14), an even smaller variation of the effective flange width ratio is seen with respect to the sheathing MOE. For most of the structural plywood, a range of 0.4 percent of the change in the effective flange width ratio is experienced. Consequently, this effect may be neglected for uniform load as well.

#### 5.4.5 Effect of Available Flange Width

The most important parameter that affects the effective flange width is the available flange width as shown in Fig. 5.15 for the concentrated load case. The effective flange width ratio increases toward 100 percent as the available flange width approaches zero and decreases down to about 53 percent as the available flange width increases to 80 inches. The greater the available flange width is, the less efficient the flange becomes. Approximately the same behavior is observed for the uniform load case as shown in Fig. 5.16.

For simplicity, straight lines can be used to approximate the curves in Fig. 5.15 and Fig. 5.16. The recommended equations for an approximate linear relationship between the effective flange

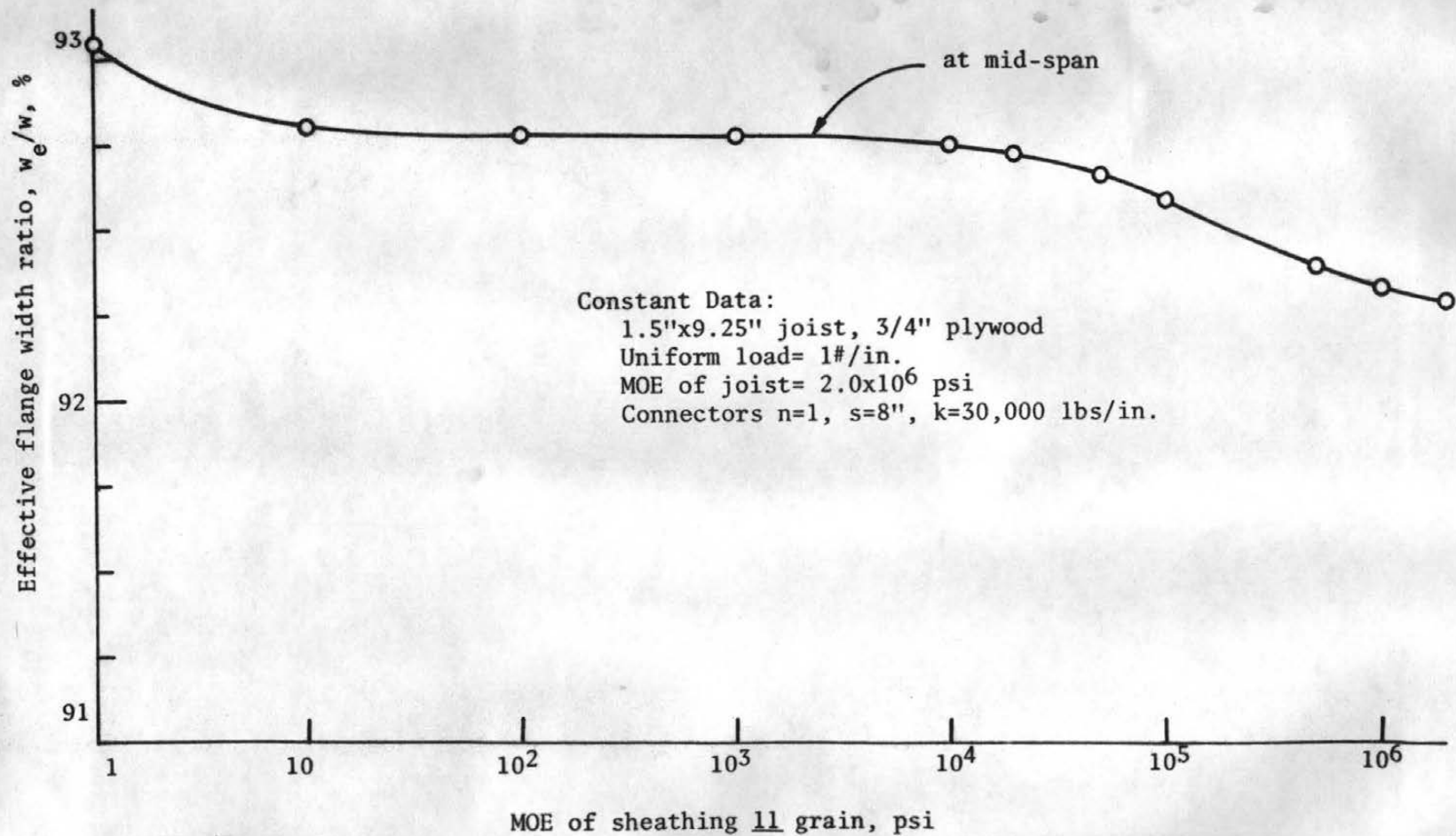


Figure 5.14 Effective Flange Width vs MOE of Sheathing, Uniform Load

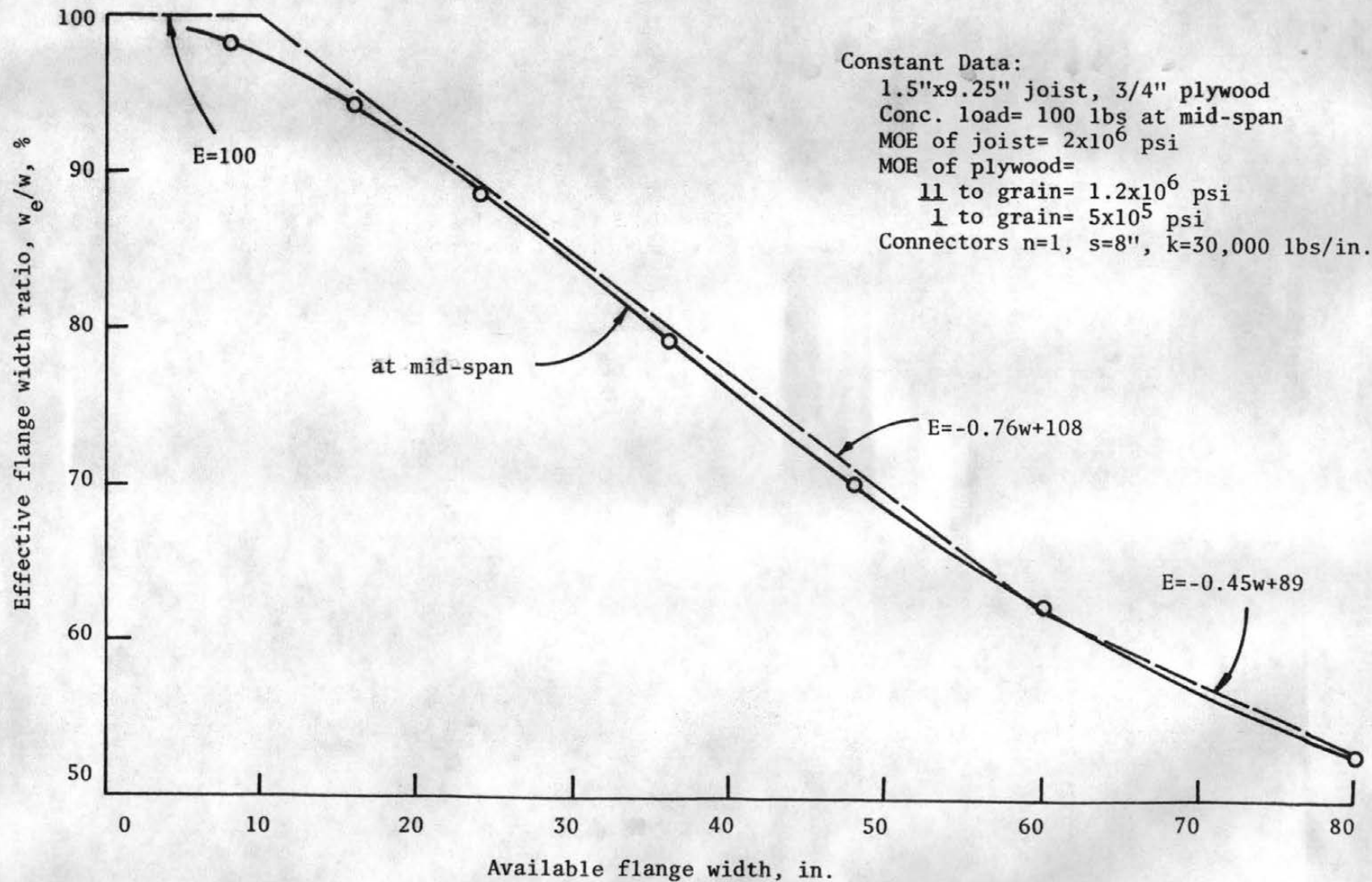


Figure 5.15 Effective Flange Width vs Available Flange Width, Concentrated Load

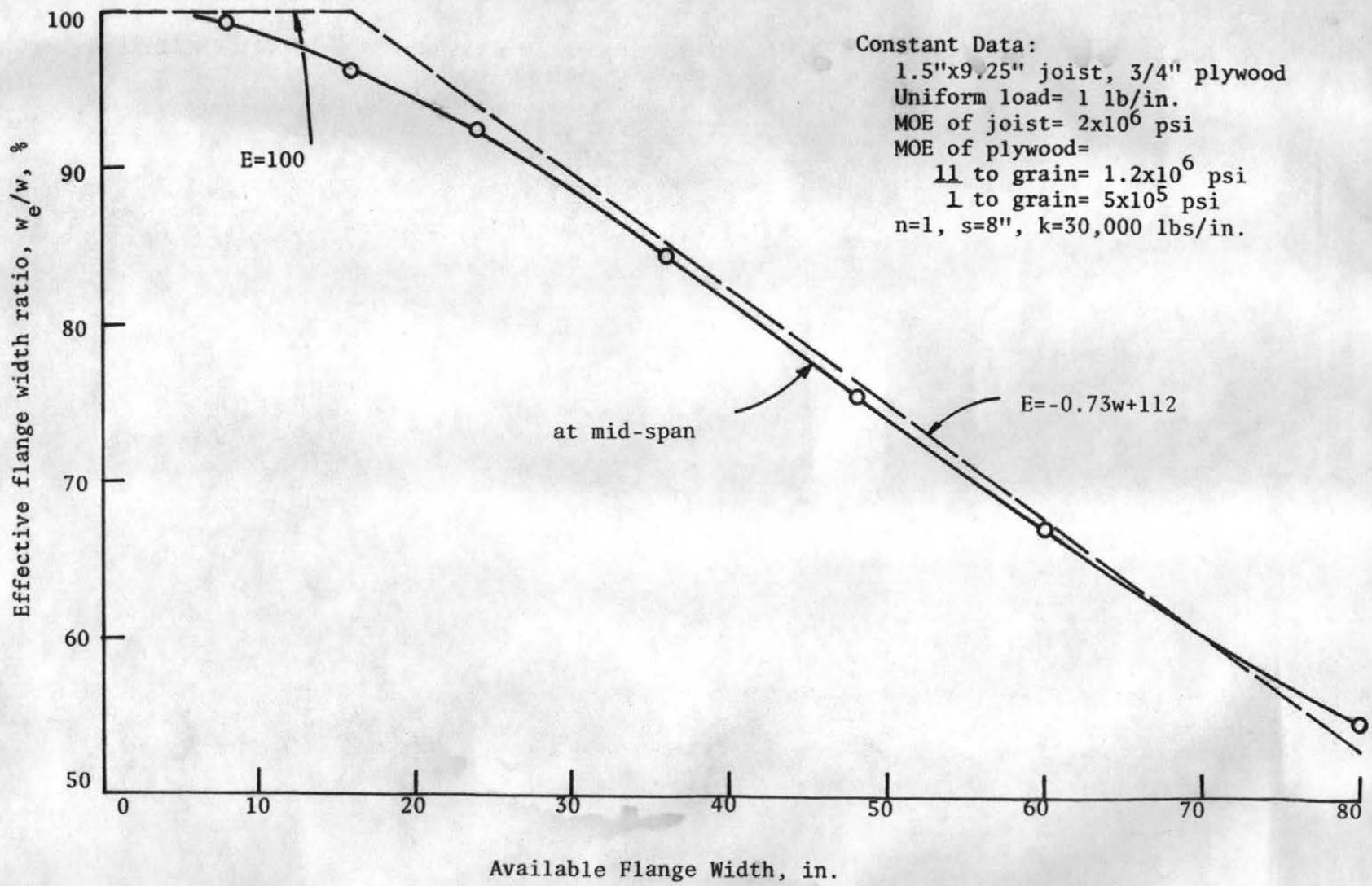


Figure 5.16 Effective Flange Width vs Available Flange Width, Uniform Load

width ratio and the available flange width are presented as follows:

For concentrated load at midspan,

$$E = 100 \quad \text{for } w \leq 10 \text{ in.} \quad (5.1a)$$

$$E = -0.76w + 108 \quad \text{for } 10 < w \leq 60 \text{ in.} \quad (5.1b)$$

$$E = -0.45w + 89 \quad \text{for } 60 < w \leq 80 \text{ in.} \quad (5.1c)$$

For uniformly distributed load,

$$E = 100 \quad \text{for } w \leq 16 \text{ in.} \quad (5.2a)$$

$$E = -0.73w + 112 \quad \text{for } 16 < w \leq 80 \text{ in.} \quad (5.2b)$$

where,

$E$  = effective flange width ratio,  $w_e/w$ , %,

$w_e$  = effective flange width, in.,

$w$  = available flange width, in.

In actual design practice, uniform load is used as the design criteria for most wood joist floors. The effective flange width ratio for the commonly used joist spacings in wood floor construction is recommended in Table 5.1 for the uniform load case using the results of Eq. (5.2).

Table 5.1 Recommended Effective Flange Width for Uniform Load

Joist Spacing, in.	Effective Flange Width Ratio, $w_e/w$ , %
16	100
24	94
36	85
48	77

The effective flange width ratio for the concentrated load has slightly different values from those for the uniform load case and can be evaluated from Eq. (5.1). The resulting effect of effective

flange width on the deflection of a typical floor can be evaluated by reference to Fig. 5.6 in Sec. 5.3.3.

## CHAPTER 6

### SUMMARY AND CONCLUSIONS

The theoretical development of a mathematical model of wood joist floor systems using both finite difference and finite element techniques has been presented in this study. This model simulates the floor system as two sets of crossing beams: one set consists of T-beams made of joists and sheathing with effective flange width and the other set consists of sheathing strips perpendicular to the joists. Torsional effects of the sheathing are assumed to be negligible. The theory developed for layered beam systems with interlayer slip is applied on each T-beam or sheathing strip and compatibility conditions are invoked to compute the floor deflections at the crossing points. While the finite difference technique can not properly handle the discontinuity problem caused by the gaps in the sheathing, the finite element technique is able to incorporate this effect as well as the different size of each beam and varying material properties along the length of each beam, in evaluating the floor behavior.

Due to the shear lag phenomenon in the flange of T-beams used to approximate the floor, effective flange width instead of the actual available flange width must be used for the T-beams to allow the ordinary beam theory to be applied for the T-beams. The theory of effective flange width of a wide flange T-beam with interlayer slip therefore, also has been investigated and evaluated.

Due to the orthogonal orientation of the adjacent veneers of plywood, its mechanical properties are different when subjected to different types of loading. The determination of the transformation

constant, which converts the effective modulus of elasticity in bending of plywood to the effective modulus of elasticity for axial loading has been presented and evaluated.

A total of twenty-two full-scale floor tests were conducted in the experimental phase of this study to supply the experimental demonstration of the validity of the mathematical floor model. Of the twenty-two tests conducted, ten were two-layer floor systems and twelve were three-layer floor systems. Furthermore, of the twelve three-layer floors tested, half of them were with the top sheathing layer nails driven into the joists, the other half were made with the top layer nails driven into the bottom sheathing layer only. The material properties of all the sheathing panels of the tested specimens were premeasured by the Wood Science Laboratory using non-destructive testing techniques. The joist MOE (modulus of elasticity) values were determined during the construction of floor specimens. Most floor specimens were constructed with nails connecting the joists and sheathing layers, while selected floor specimens were connected with elastomeric adhesives. The slip modulus curves for various types of connection were also determined by Wood Science Laboratory.

Verification of the mathematical floor model was achieved since generally excellent agreement between the measured deflections and the computed deflections at the centerline of the floor was obtained for each floor specimen. The average absolute percentage of error of the predicted results by the mathematical model with respect to the measured results was only 6.44 percent while the average algebraic percentage of error was +3.24 percent. The plus sign of the average algebraic percentage error indicates that the predicted deflection at center

of floor by the mathematical model is generally slightly greater than the measured deflection, and thus the floor model is generally conservative. These results are, at least, partly due to the assumption made in neglecting the torsional rigidity of the sheathing.

Floor deflections depend to a considerable degree on the values of the slip modulus. In the working load range the assumption of a linear load-slip relationship predicts the floor behavior with good accuracy as seen in the verification study of the model. Yet, with the load increased to the overload stage, greater discrepancy is introduced by using a constant slip modulus. This difficulty results from the linear floor model being unable to incorporate the nonlinear load-slip relationship of connectors. Modification of the mathematical floor model to include the non-linear load-slip characteristics is recommended as one aspect of a future study and would result in a better depiction of the floor behavior at a load levels beyond the working load range.

The isolated effects of some major parameters on the floor behavior were investigated using the verified mathematical floor model. The effect of the slip modulus value was seen to be very important in the practical range of incomplete composite action. The effect of the joist MOE was very critical on the floor behavior. Effective flange width appears to have a limited effect on the floor behavior. A reduction of 50 percent of the effective flange width induced only an eight percent increase in deflection of the loaded joist.

Parameters studies on effective flange were accomplished by examining the effect of several major parameters on the determination of the proper flange width of T-beams. Sheathing thickness, joist

depth, slip modulus of connectors and sheathing MOE in the normal range were all observed to have small effect on the effective flange. The only parameter which had a substantial effect was the available flange width. For the uniform distributed load case a 16-inch or less available flange width may be considered fully effective and a 24-inch available flange width was recommended to have an effective flange width of 22.5 inches. Approximate linear equations were recommended for computing the effective flange width as a function of available flange width for both concentrated load and uniform load.

In conclusion, the verification studies of the linear mathematical floor model showed that the model can predict closely the load-deflection behavior of two and three-layer wood joist floors in the working load range. The study of the limiting cases using the floor model showed that traditional design practice overestimated the predicted deflections of the floor model and that both the composite and two-way action should be included for a correct representation of the behavior of floor systems. The parameter studies using mathematical models give an improved understanding of how each parameter affects the floor behavior and the effective flange width of a T-beam. The verified mathematical floor model and the other aspects developed in this study can lead the way to a rational design procedure for wood joist floor systems and will, therefore, allow more economical design and more efficient use of material in the wood joist floor construction.

## REFERENCES

1. Amana, E. J. and L. G. Booth, "Theoretical and Experimental Studies on Nailed and Glued Plywood Stressed-skin Components: Part I. Theoretical Study," Journal of the Institute of Wood Science, Vol. 4, No. 19, September 1967.
2. Amana, E. J. and L. G. Booth, "Theoretical and Experimental Studies on Nailed and Glued Plywood Stressed-skin Components: Part II. Experimental Study," Journal of the Institute of Wood Science, Vol. 4, No. 20, April 1967.
3. American Society for Testing and Materials, 1972 Annual Book of ASTM Standards, part 16, "Structural Sandwich Construction; Wood," ASTM, Philadelphia, Pa., 1972.
4. Atherton, G. and S. E. Corder, "Strength of Floors with Douglas-fir Utility-grade Joists," Forest Research Laboratory, Oregon State University Preliminary Report, Corvallis, Oregon, 1965.
5. Angleton, H. D., J. Colville and D. Snodgrass, "The Effect of Framing and Subfloor Attachment of the Stiffness of Residential Floors," NAHB, Residential Institute Laboratory Research Report LR-4, Rockville, Maryland, 1961.
6. Chwalla, E., "Über das Problem der voll mittragenden Breite von Gurtund Rippenplatten," Alfons-Leon-Gedenkschrift (Vienna), 1952.
7. Colville, J., H. D. Angleton, D. Snodgrass, et al., "Bridging in Residential Construction," NAHB, Residential Institute Laboratory Research Report LR-6, Rockville, Maryland, 1961.
8. Girkmann, K., "Spannungsverteilung in geschweissten Blechträgern," Der Stahlbau, No. 12/13, 1933.
9. Goodman, J. R., "Layered Wood Systems with Interlayer Slip," Ph.D. Dissertation, University of California, Berkely, 1967.
10. Goodman, J. R., and E. P. Popov, "Layered Beam Systems with Interlayer Slip," Journal of the Structural Division, ASCE Vol. 94, No. ST11, Proc. Paper 6214, pp. 2535-2547, 1968.
11. Goodman, J. R., "Layered Wood Systems with Interlayer Slip," Wood Science, 1, (3): pp. 148-158, 1969.
12. Goodman, J. R., M. D. Vanderbilt, M. E. Criswell, and J. Bodig, "Composite and Two-way Action in Wood Joist Floor Systems," Wood Science, 7, (1): pp. 25-33, 1974.

13. Granholm, H., "Om Sammansatta Balkar Och Pelare Med Sarkilo Hansyn Till Spikade Trakonstruktioner," ("On Composite Beams and Columns with Particular Regard to Nailed Timber Structures"), Chalmers Tekniska Hogskoas Handlingar, No. 88, 1949.
14. Henghold, W. M., "Layered Beam Vibrations Including Slip," Ph.D. Dissertation, Colorado State University, Fort Collins, Colorado, March 1969.
15. Henghold, W. M. and J. R. Goodman, "Static and Dynamic Behavior of Layered Beams Including Slip," Presented and Published, Sixth St. Louis Symposium on Composite Materials in Engineering Design, May 1972.
16. Kloot, N. H. and K. B. Schuster, "Load Distribution in Wood Floors Subjected to Concentrated Loads," Division of Forest Products Technical Paper No. 29, Commonwealth Scientific and Industrial Research Organization, Melbourne, Australia, 1963.
17. Ko, M. F., "Layered Beam Systems with Interlayer Slip," M.S. Thesis, Colorado State University, Fort Collins, Colorado, December 1972.
18. Kuenzi, E. W. and T. L. Wilkinson, "Composite Beams - Effect of Adhesive on Fastener Rigidity," USDA Forest Service Research Paper FPL 152, 1971.
19. Kuo, M. L., "Verification of a Mathematical Model for Layered T-beams," M.S. Thesis, Colorado State University, Fort Collins, Colorado, March 1974.
20. McLain, T. E., "Nondestructive Evaluation of Full Size Wood Composite Panels," M.S. Thesis, Colorado State University, Fort Collins, Colorado, May 1973.
21. Metzger, W., "Die mittragende Breite," Luftfahrtforschung, 1929.
22. National Association of Home Builder, "Performance of Glued Single-layer Plywood-to-Wood Joist Floor Systems."
23. Newmark, N. M., C. P. Siess and I. M. Viest, "Tests and Analysis of Composite Beams with Incomplete Interaction," Proceedings, Society for Experimental Stress Analysis, Vol. 19, No. 1, 1951.
24. O'Halloran, M. R., "Nondestructive Tests for Lodgepole Pine," M.S. Thesis, Colorado State University, Fort Collins, Colorado, December 1969.

25. Onysko, D. M., "Performance of Wood-Joist Floor Systems, A Literature Review," Information Report OP-X-24, Forest Products Laboratory, Canadian Forestry Service Department of Fisheries and Forestry, January 1970.
26. Patterson, D. W., "Nailed Wood Joints Under Lateral Loads," M.S. Thesis, Colorado State University, Fort Collins, Colorado, April 1973.
27. Penner, B. G., "Experimental Behavior of Wood Flooring Systems," M.S. Thesis, Colorado State University, Fort Collins, Colorado, December 1972.
28. Pietzker, F., "Festigkeit der Schiffe," Berlin, 1914.
29. Pleshkov, P. F., "Teoriia Rashceta Depeviannykh," ("Theoretical Studies of Composite Wood Structures,") Moscow, 1952.
30. Polensek, A., "Static and Dynamic Properties of Glued Wood-Joist Floors," Paper No. 732, Forest Research Laboratory, Corvallis, Oregon, March 1971.
31. Polensek, A., "Frequency Analysis of Timber-Joist Floors," M.S. Thesis, Oregon State University, June 1969.
32. Polensek, A., G. H. Atherton, S. E. Corder and J. L. Jenkins, "Response of Nailed Wood-Joist Floors to Static Loads," Forest Product Journal, Vol. 22, No. 9, September 1972.
33. Polensek, A., "Static Dynamic Analysis of Wood-Joist Floors by the Finite Element Method," Ph.D. dissertation, Oregon State University, Corvallis, Oregon, June 1972.
34. Reissner, E., "Beitrag zur Theorie der Plattenbalken," Det Kongelige Norske Videnskabers Selskab Forhandling (Trondheim), V. 8, No. 4.
35. Rose, J. D., "Field-Glued Plywood Floor Test," Laboratory Report 118, American Plywood Association, May 1970.
36. Thompson, E. G., "Analysis of Layered Wood Systems with Gaps at Joints," To be published.
37. Vanderbilt, M. D., "Matrix Structural Analysis," Quantum Publishers, Inc., New York, 1973.
38. Vanderbilt, M. D., J. R. Goodman, M. E. Criswell and J. Bodig, "Service and Overload Behavior of Wood Joist Floor Systems," Journal of Structural Division, ASCE, Vol. 100, No. ST1, Proc. Paper 10274, pp., 11-29, 1974.
39. von Kármán, T., "Die mittragen de Breite," August-Föppler-Festschrift, 1924.

APPENDIX A

TABLE OF MOE TRANSFORMATION CONSTANT FOR PLYWOOD

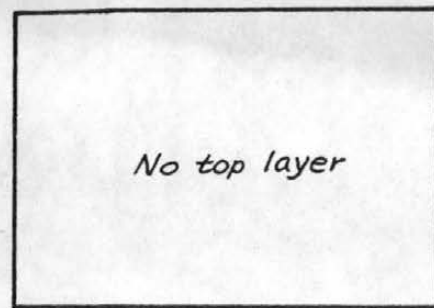
Table A.1 Values of MOE Transformation Constant of Plywood

Plywood Species	Thickness in.	Surface ply	$A_t$ in <sup>2</sup> /ft	$A_{gr}$ in <sup>2</sup> /ft	$I_t$ in <sup>4</sup> /ft	$I_{gr}$ in <sup>4</sup> /ft	$K^* = \frac{A_t \cdot I_{gr}}{A_{gr} \cdot I_t}$
Douglas-Fir	1/2	11	3.060	6.0	0.1072	0.125	0.5947
		1	3.060	6.0	0.0183	0.125	3.4836
	3/4	11	4.435	9.0	0.2682	0.422	0.7753
		1	4.563	9.0	0.1301	0.422	1.6445
Englemann spruce	1/2	11	2.641	6.0	0.0781	0.125	0.7045
		1	2.641	6.0	0.0120	0.125	4.5850
	3/4	11	3.998	9.0	0.2105	0.422	0.8905
		1	2.728	9.0	0.0794	0.422	1.6110

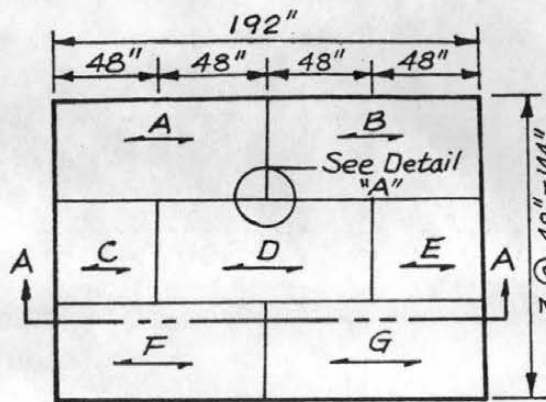
Note: (MOE)<sub>axial force</sub> =  $K^* \cdot$  (MOE)<sub>bending</sub>

APPENDIX B

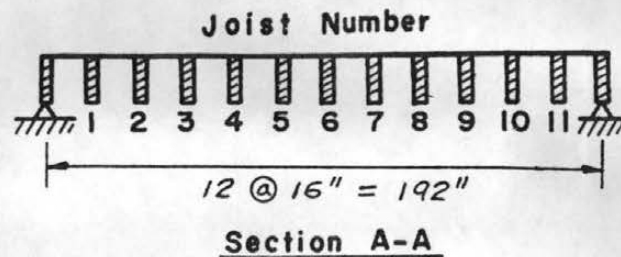
DETAILED DATA OF FLOOR SPECIMENS



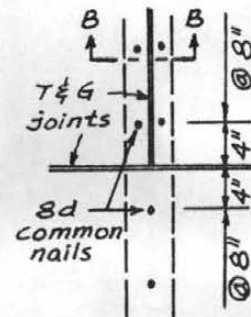
Plan of Top Sheathing Layer



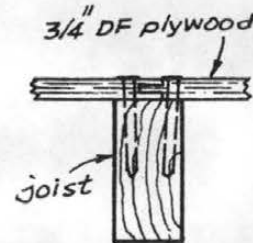
Plan of Bottom Sheathing Layer



Section A-A



Detail "A"



Section B-B

Material	Property	Joist Number										
		1	2	3	4	5	6	7	8	9	10	11
2x8 DF joist	Actual Size, in (width x depth)	1.49 x 7.24	1.48 x 7.14	1.47 x 7.21	1.49 x 7.22	1.48 x 7.17	1.48 x 7.20	1.44 x 7.05	1.47 x 7.24	1.46 x 7.17	1.48 x 7.21	1.51 x 7.26
	Average MOE    Grain, 10 <sup>6</sup> psi	2.41	2.56	2.42	2.54	2.46	1.70	1.38	1.76	1.63	1.85	1.87

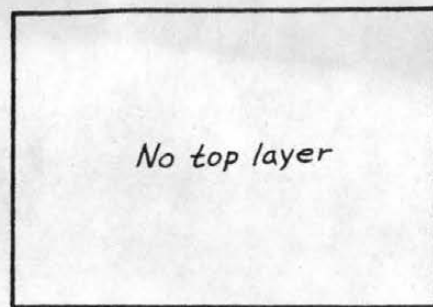
Joist Data

Layer	Material	Thickness in.	Gap	Connector	Average MOE, 10 <sup>6</sup> psi															
					A		B		C		D		E		F		G		H	
						⊥		⊥		⊥		⊥		⊥		⊥		⊥		⊥
Bottom	3/4 DF plywood	3/4	T & G	8d nails @ 8"	1.38	0.51	1.46	0.56	1.40	0.53	1.31	0.42	1.40	0.53	1.40	0.55	1.42	0.59	—	—
Top	—	—	—	—	—	—	—	—	—	—	—	—	—	—	—	—	—	—	—	—

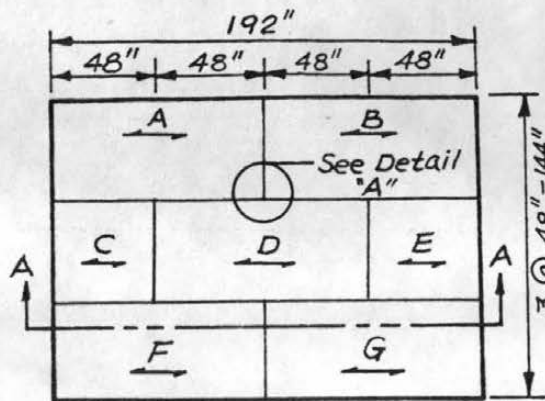
Sheathing Data

Figure B.1

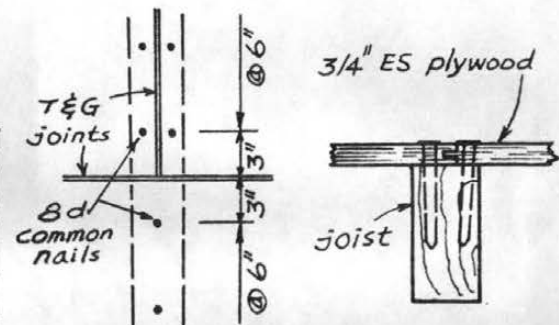
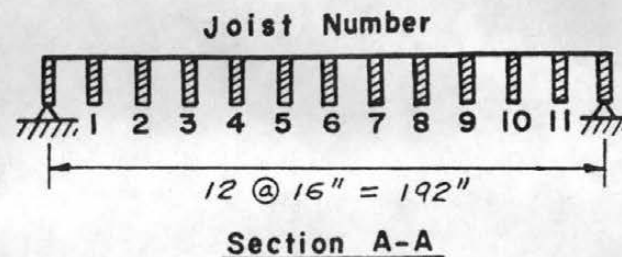
Layout and Data of Specimen F3-8DI6-1



Plan of Top Sheathing Layer



Plan of Bottom Sheathing Layer



Detail "A"

Section B-B

Material	Property	Joist Number										
		1	2	3	4	5	6	7	8	9	10	11
2 x 12 ES joist	Actual Size, in (width x depth)	1.52 x 11.21	1.52 x 11.20	1.52 x 11.13	1.51 x 11.51	1.50 x 11.23	1.52 x 11.14	1.50 x 11.18	1.51 x 11.20	1.50 x 11.08	1.50 x 11.27	1.53 x 11.18
	Average MOE    Grain, 10 <sup>6</sup> psi	1.31	0.92	0.87	1.35	1.28	1.39	1.15	0.97	1.09	0.98	1.06

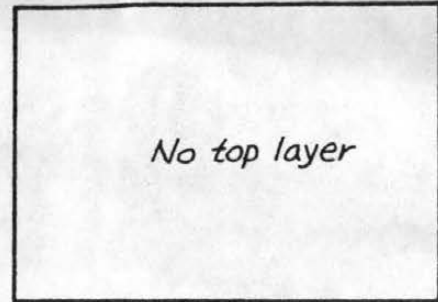
Joist Data

Layer	Material	Thickness in.	Gap	Connector	Average MOE, 10 <sup>6</sup> psi															
					A		B		C		D		E		F		G		H	
						⊥		⊥		⊥		⊥		⊥		⊥		⊥		⊥
Bottom	3/4 ES plywood	5/8	T&G	8d nails @ 6"	1.29	0.42	1.39	0.40	1.37	0.39	1.49	0.40	1.37	0.39	1.48	0.46	1.29	0.44	—	—
Top	—	—	—	—	—	—	—	—	—	—	—	—	—	—	—	—	—	—	—	—

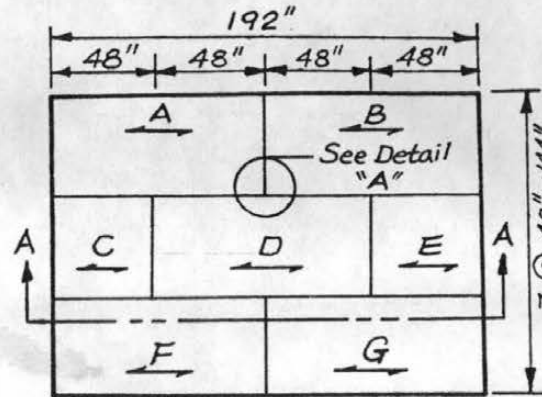
Sheathing Data

Figure B.2

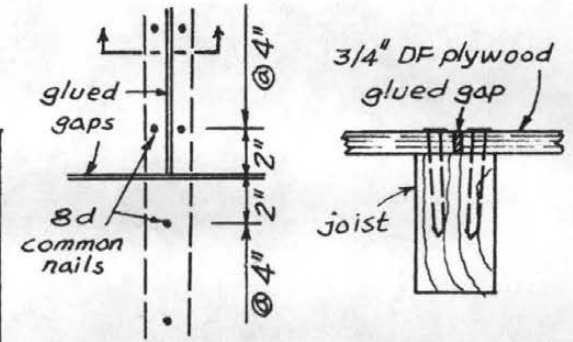
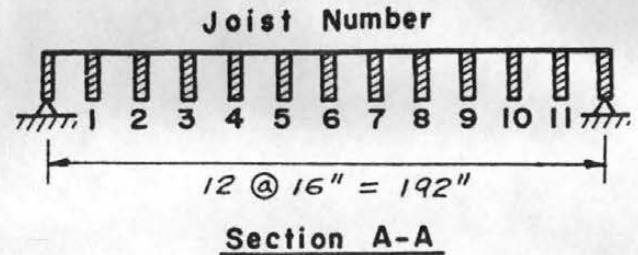
Layout and Data of Specimen F4-12E16-1



Plan of Top Sheathing Layer



Plan of Bottom Sheathing Layer



Detail "A"

Section B-B

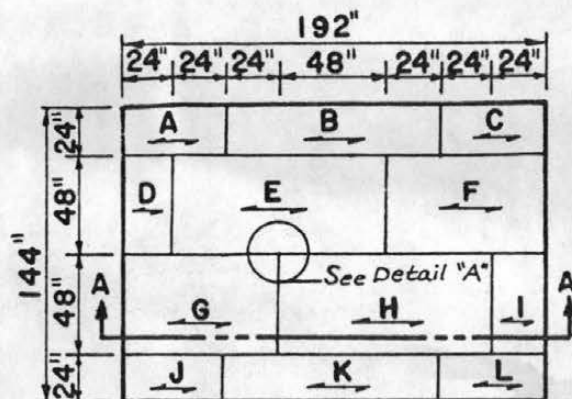
Material	Property	Joist Number											
		1	2	3	4	5	6	7	8	9	10	11	
2x8 DF joist	Actual Size, in (width x depth)	1.47 x 7.21	1.47 x 7.21	1.50 x 7.29	1.44 x 7.22	1.45 x 7.06	1.51 x 7.29	1.49 x 7.23	1.50 x 7.27	1.51 x 7.28	1.48 x 7.04	1.48 x 7.26	
	Average MOE    Grain, 10 <sup>6</sup> psi	1.29	1.24	1.22	1.45	1.56	1.21	1.44	1.08	1.53	1.42	1.01	

Joist Data

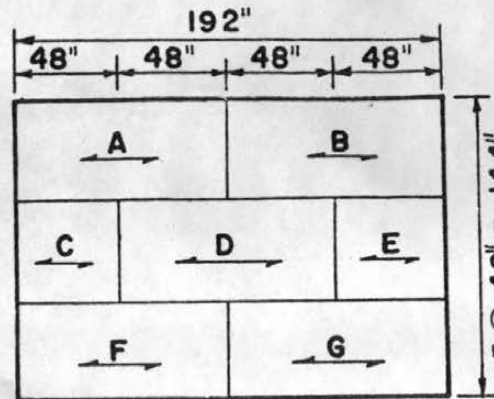
Layer	Material	Thickness in.	Gap	Connector	Average MOE, 10 <sup>6</sup> psi															
					A		B		C		D		E		F		G		H	
						⊥		⊥		⊥		⊥		⊥		⊥		⊥		⊥
Bottom	3/4 DF plywood	3/4	glued	8d nails @ 4"	1.31	0.52	1.29	0.56	1.25	0.53	1.56	0.55	1.25	0.53	1.33	0.58	1.21	0.61	—	—
Top	—	—	—	—	—	—	—	—	—	—	—	—	—	—	—	—	—	—	—	—

Sheathing Data

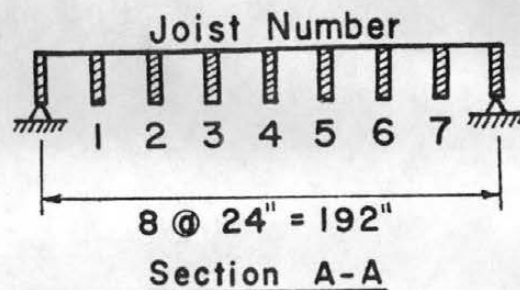
Figure B.3 Layout and Data of Specimen F5-8DI6-1



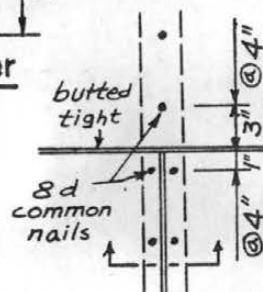
Plan of Top Sheathing Layer



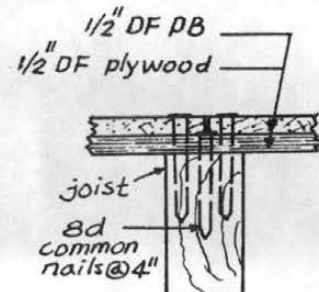
Plan of Bottom Sheathing Layer



Section A-A



Detail "A"



Section B-B

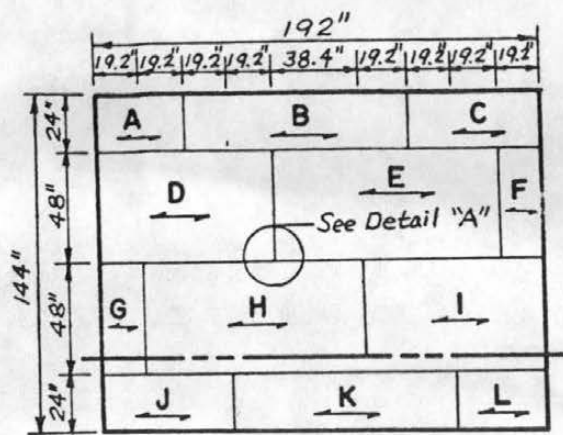
Material	Property	Joist Number						
		1	2	3	4	5	6	7
2x12 DF joist	Actual Size, in. (width x depth)	1.50 x 11.10	1.49 x 11.07	1.49 x 11.01	1.48 x 11.12	1.51 x 11.12	1.51 x 11.16	1.51 x 11.25
	Average MOE // Grain, 10 <sup>6</sup> psi	1.47	1.58	2.39	1.39	1.68	1.37	1.31

Joist Data

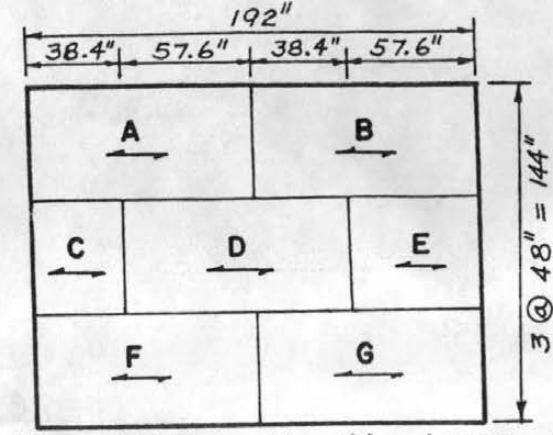
Layer	Material	Thickness in.	Gap	Connector	Average MOE, 10 <sup>6</sup> psi																							
					A		B		C		D		E		F		G		H		I		J		K		L	
						⊥		⊥		⊥		⊥		⊥		⊥		⊥		⊥		⊥		⊥		⊥		⊥
Bottom	1/2 DF plywood	1/2	butted 1/16" gap	8d nails @ 4"	1.83	0.23	1.62	0.24	1.64	0.25	1.79	0.22	1.64	0.25	1.61	0.24	1.66	0.24	-	-	-	-	-	-	-	-		
Top	1/2 DF PB	1/2	butted no gap	6d nails @ 4"	0.60	0.48	0.60	0.48	0.60	0.48	0.45	0.34	0.46	0.35	0.62	0.51	0.45	0.34	0.45	0.35	0.62	0.51	0.45	0.35	0.45	0.35	0.45	0.35

Sheathing Data

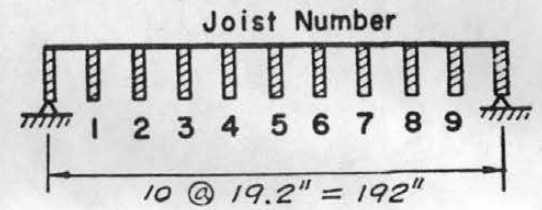
Figure B. 4 Layout and Data of Specimens F7-I2D24-1 and F7-I2D24-2



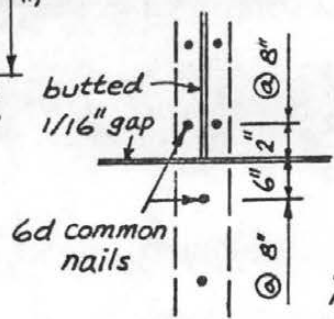
Plan of Top Sheathing Layer



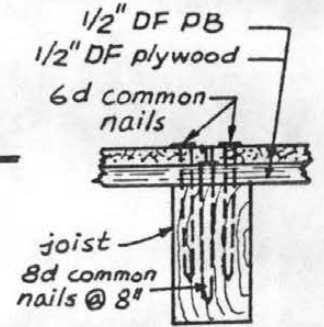
Plan of Bottom Sheathing Layer



Section A-A



Detail "A"



Section B-B

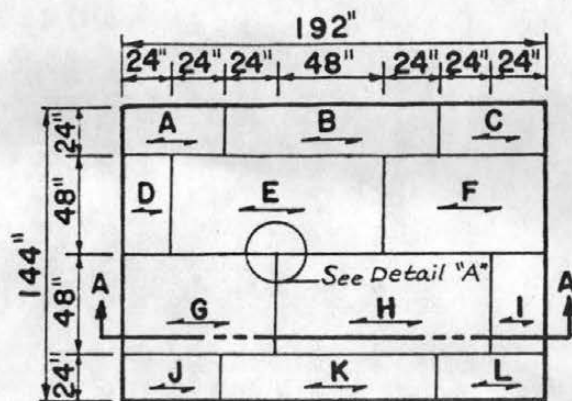
Material	Property	Joist Number								
		1	2	3	4	5	6	7	8	9
2 x 8 DF joist	Actual Size, in. (width x depth)	1.58 x 7.21	1.50 x 7.20	1.50 x 7.14	1.49 x 7.25	1.48 x 7.30	1.48 x 7.19	1.48 x 7.29	1.51 x 7.24	1.50 x 7.30
	Average MOE Grain, 10 <sup>6</sup> psi	1.83	2.41	2.31	2.15	2.07	2.58	2.08	2.27	1.94

Joist Data

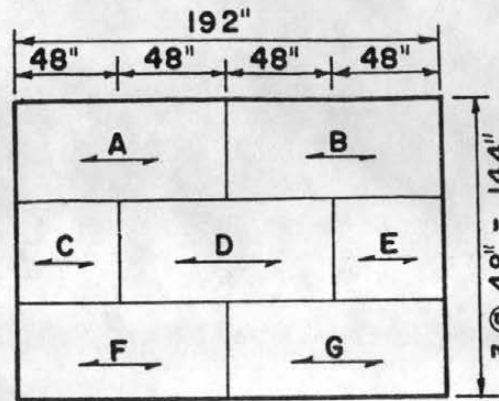
Layer	Material	Thickness in.	Gap	Connector	Average MOE, 10 <sup>6</sup> psi																							
					A		B		C		D		E		F		G		H		I		J		K		L	
						⊥		⊥		⊥		⊥		⊥		⊥		⊥		⊥		⊥		⊥		⊥		⊥
Bottom	1/2 DF plywood	1/2	butted 1/16" gap	8d nails @ 8"	1.58	0.25	1.47	0.26	1.25	0.27	1.90	0.24	1.25	0.27	1.66	0.24	1.50	0.21	-	-	-	-	-	-	-	-		
Top	1/2 DF PB	1/2	butted tight	6d nails @ 8"	0.62	0.50	0.62	0.50	0.62	0.50	0.65	0.51	0.58	0.47	0.65	0.51	0.62	0.51	0.47	0.35	0.62	0.51	0.62	0.50	0.62	0.50	0.62	0.50

Sheathing Data

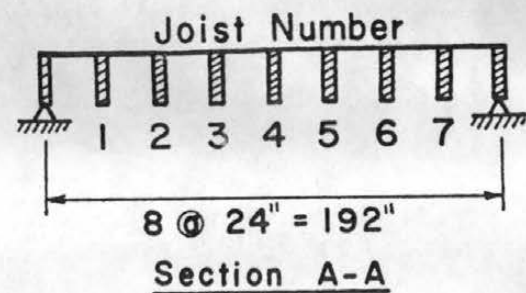
Figure B.5 Layout and Data of Specimens F8-8DI9.2-1 and F8-8DI9.2-2



Plan of Top Sheathing Layer



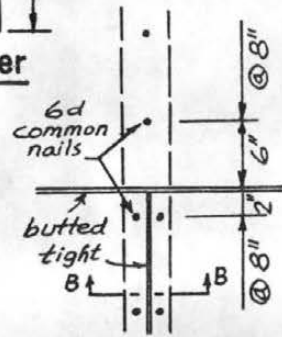
Plan of Bottom Sheathing Layer



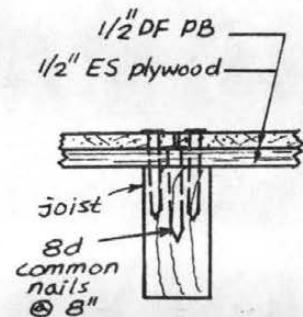
Section A-A

Material	Property	Joist Number						
		1	2	3	4	5	6	7
2x8 ES joist	Actual Size, in. (width x depth)	1.48 x 7.13	1.51 x 7.16	1.51 x 7.19	1.48 x 7.17	1.51 x 7.21	1.50 x 7.24	1.50 x 7.18
	Average MOE    Grain, 10 <sup>6</sup> psi	1.16	1.48	1.41	1.25	1.69	1.44	1.64

Joist Data



Detail "A"

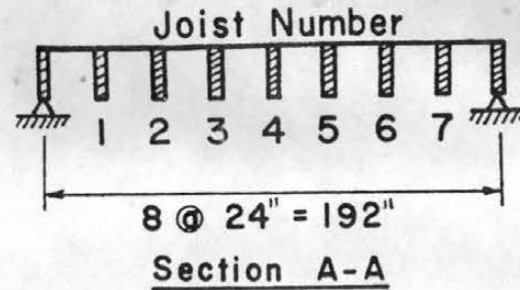
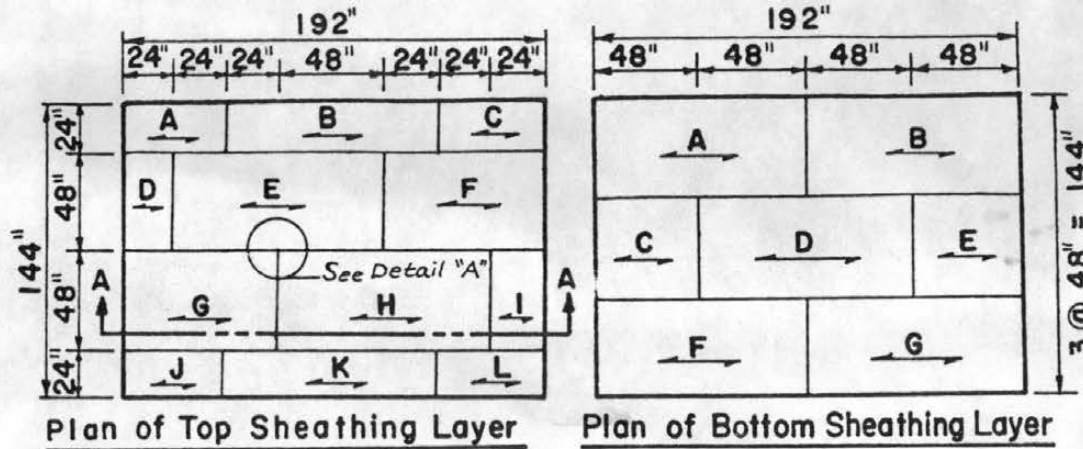


Section B-B

Layer	Material	Thickness in.	Gap	Connector	Average MOE, 10 <sup>6</sup> psi																							
					A		B		C		D		E		F		G		H		I		J		K		L	
						⊥		⊥		⊥		⊥		⊥		⊥		⊥		⊥		⊥		⊥		⊥		⊥
Bottom	1/2 ES plywood	3/8	butted 1/16 gap	8d nails @ 8"	1.45	0.21	1.56	0.23	1.47	0.21	1.53	0.23	1.47	0.21	1.42	0.22	1.59	0.22	-	-	-	-	-	-	-	-	-	
Top	1/2 DF PB	1/2	butted tight	6-d nails @ 8"	0.42	0.32	0.57	0.47	0.42	0.32	0.44	0.34	0.58	0.47	0.44	0.32	0.44	0.34	0.45	0.34	0.44	0.32	0.42	0.32	0.57	0.47	0.42	0.32

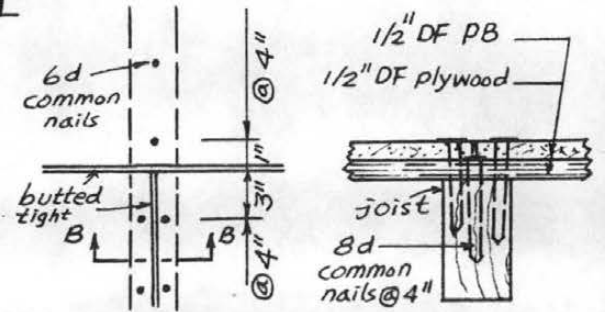
Sheathing Data

Figure B. 6 Layout and Data of Specimens F9-8E24-1 and F9-8E24-2



Material	Property	Joist Number						
		1	2	3	4	5	6	7
2x8 ES joist	Actual Size, in. (width x depth)	1.50 x 7.15	1.51 x 7.24	1.52 x 7.22	1.52 x 7.22	1.52 x 7.25	1.52 x 7.24	1.50 x 7.20
	Average MOE // Grain, 10 <sup>6</sup> psi	1.66	1.62	1.20	1.49	1.39	1.25	1.49

Joist Data



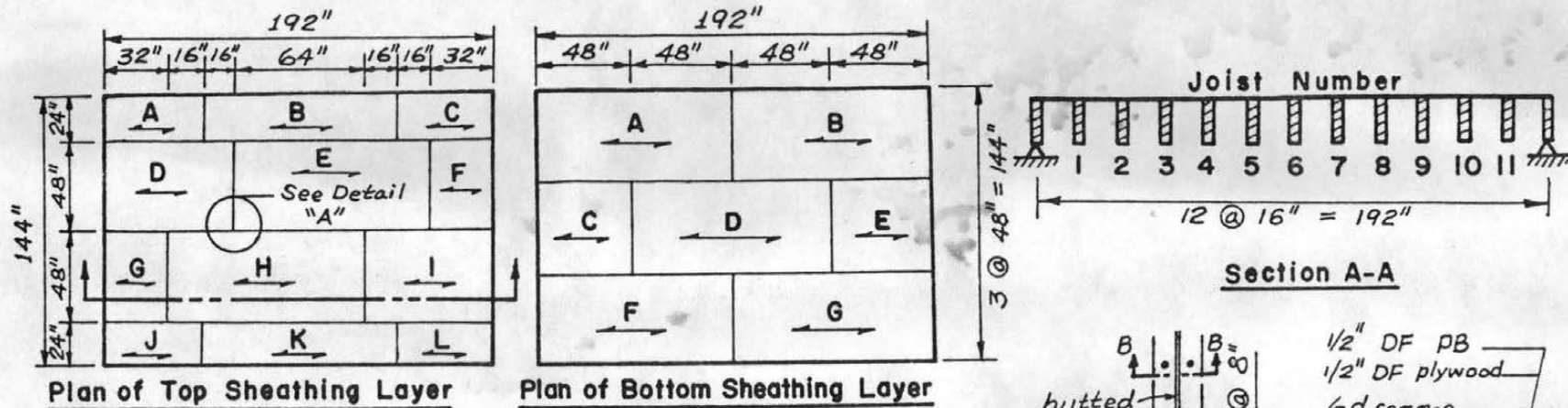
Detail "A"

Section B-B

Layer	Material	Thickness in.	Gap	Connector	Average MOE, 10 <sup>6</sup> psi																							
					A		B		C		D		E		F		G		H		I		J		K		L	
						⊥		⊥		⊥		⊥		⊥		⊥		⊥		⊥		⊥		⊥		⊥		⊥
Bottom	1/2 DF plywood	1/2	butted 1/16" gap	8d nails @ 4"	1.54	0.26	1.39	0.26	1.83	0.23	1.61	0.23	1.83	0.23	1.76	0.25	1.50	0.25	—	—	—	—	—	—	—	—		
Top	1/2 DF PB	1/2	butted tight	6d nails @ 4"	0.42	0.32	0.57	0.47	0.58	0.47	0.58	0.47	0.61	0.51	0.44	0.32	0.44	0.34	0.63	0.51	0.44	0.34	0.42	0.32	0.57	0.47	0.42	0.32

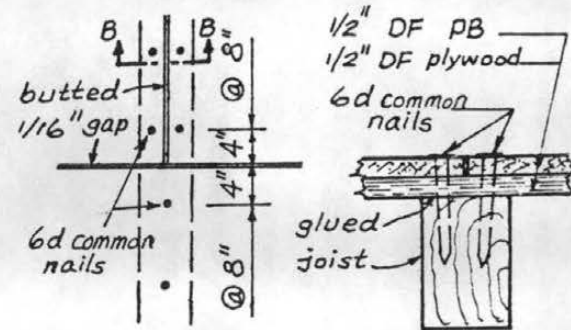
Sheathing Data

Figure B.7 Layout and Data of Specimens FIO-8E24-1 and FIO-8E24-2



Material	Property	Joist Number											
		1	2	3	4	5	6	7	8	9	10	11	12
2 x 8 DF Joist	Actual Size, in. (width x depth)	1.50 x 7.23	1.51 x 7.10	1.49 x 7.13	1.46 x 7.25	1.50 x 7.22	1.50 x 7.21	1.50 x 7.24	1.50 x 7.27	1.49 x 7.20	1.48 x 7.13	1.48 x 7.10	
	Average MOE // Grain, 10 <sup>6</sup> psi	1.64	2.20	2.40	1.54	2.15	2.57	2.12	1.53	2.89	2.31	2.12	

Joist Data



Detail "A"

Section B-B

Layer	Material	Thickness in.	Gap	Connector	Average MOE, 10 <sup>6</sup> psi																							
					A		B		C		D		E		F		G		H		I		J		K		L	
						⊥		⊥		⊥		⊥		⊥		⊥		⊥		⊥		⊥		⊥		⊥		⊥
Bottom	1/2 DF plywood	1/2	glued	glue	1.26	0.22	1.63	0.26	1.48	0.26	1.67	0.24	1.48	0.26	1.49	0.24	1.50	0.26	-	-	-	-	-	-	-	-		
Top	1/2 DF PB	1/2	butted 1/16" gap	6d nails @ 8"	0.58	0.47	0.62	0.50	0.44	0.34	0.47	0.35	0.46	0.34	0.58	0.47	0.58	0.47	0.42	0.35	0.45	0.34	0.62	0.50	0.62	0.50		

Sheathing Data

Figure B.8 Layout and Data of Specimens FII-8DI6-1 and FII-8DI6-2

APPENDIX C

AVERAGE CONNECTOR SLIP MODULI VALUES

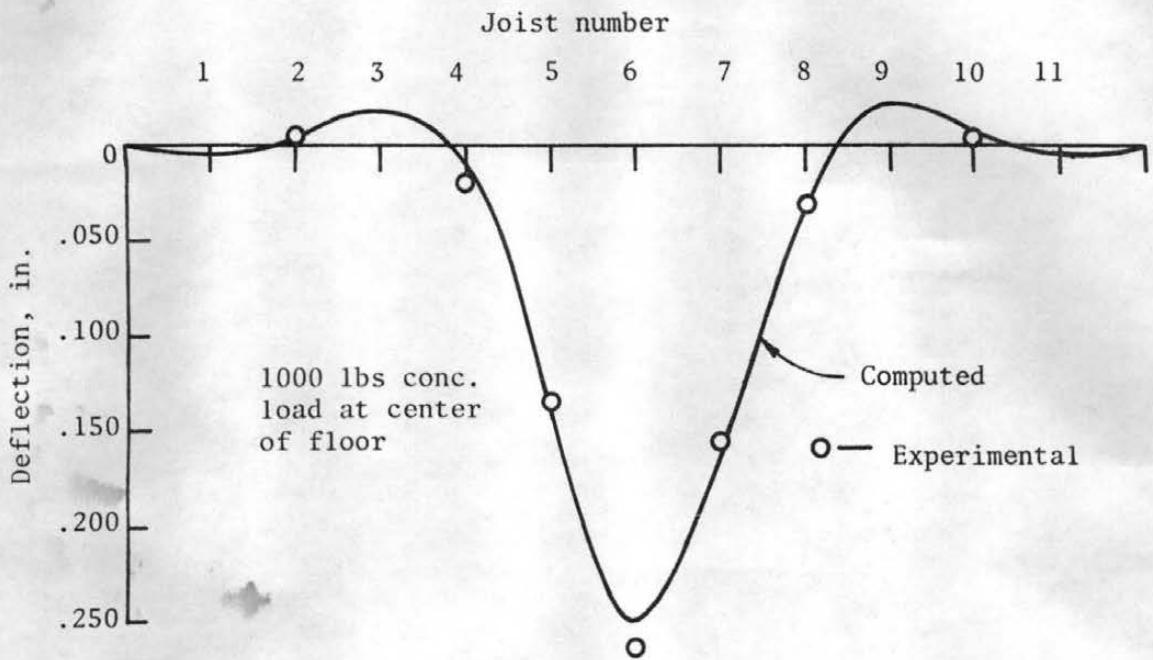
Table C.1 Average Connector Slip Moduli Values

Load Level lb.	Douglas fir Joist		DF Joist	DF Joist	ES Joist	ES Joist	Joist	Joist	1/2" DF Particle board		DF Joist
	Douglas fir Plywood		3/4" DF Plywood	3/4" ES Plywood	3/4" ES Plywood	3/4" DF Plywood	1/2" DF Plywood	1/2" ES Plywood	1/2" DF Plywood	1/2" ES Plywood	DF Plywood
	Parallel to veneer	Perpendicular to veneer									
	8d cement-coated				8d common				6d common		Glue
	lb/in.				lb/in.				lb/in.		lb/in./in. <sup>2</sup>
	Average tangent moduli										
KT 25	93,200	3,280	69,800	59,400	36,300	48,000	29,025	32,900	3,920	3,900	46,800
KT 50	58,900	3,540	56,400	33,700	32,500	25,500	15,070	13,800	3,870	3,930	36,700
KT 100	16,200	3,570	27,300	10,500	10,300	14,200	3,300	3,620	3,370	2,340	7,810
KT 150	6,080	2,890	20,000	4,160	3,700	4,900	1,217	2,300	2,460	1,010	2,750
	Average secant moduli										
KS 25	---	---	75,900	56,800	52,700	63,100	29,475	31,120	4,000	3,780	39,400
KS 50	83,400	3,260	73,500	53,700	39,000	45,200	23,900	21,360	3,900	3,810	37,300
KS 100	41,900	3,420	49,200	25,300	23,000	30,100	9,583	8,922	3,780	3,450	24,000
KS 150	---	---	31,200	12,200	11,300	12,800	3,958	4,502	3,480	2,560	8,440

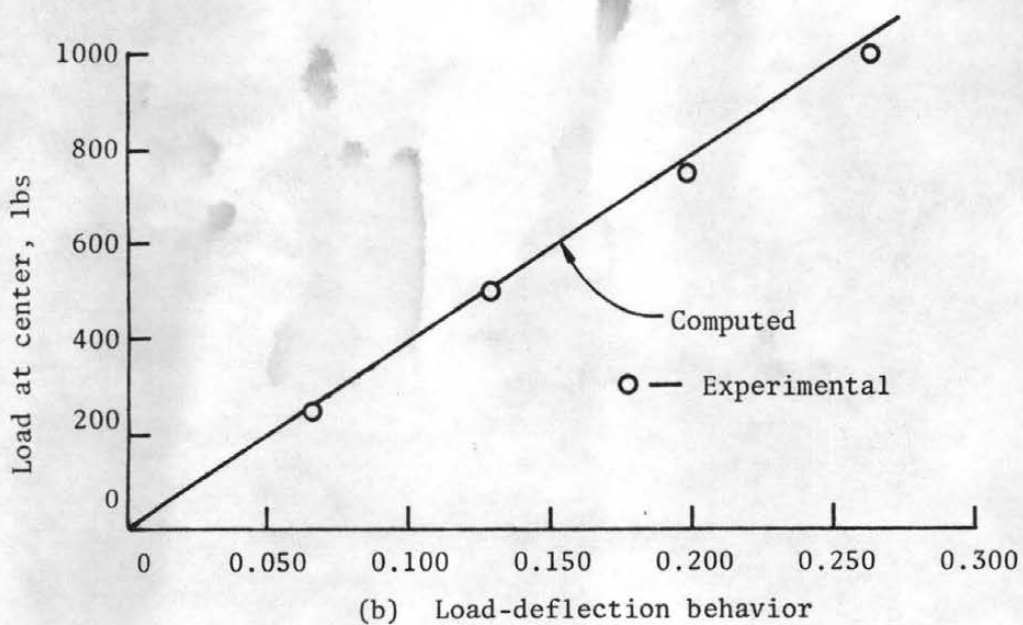
Note: All values from tests conducted by the Wood Science Laboratory, see Section 3.3.3. The slip modulus is divided by the nail spacing to obtain the effective slip modulus per linear inch of joist length. For glued connections the values given is multiplied by joist width to obtain the slip modulus per linear inch of joist length.

APPENDIX D

COMPUTED VERSUS MEASURED DEFLECTIONS  
OF FLOOR SPECIMENS

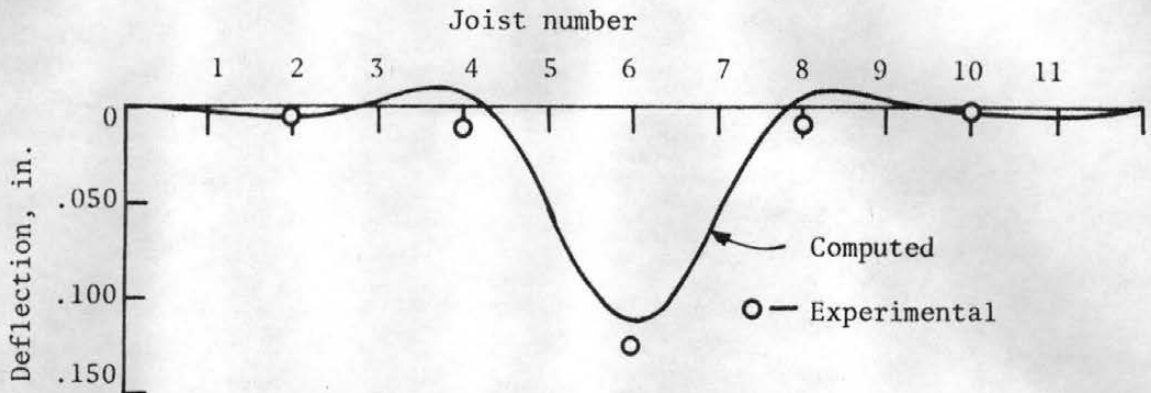


(a) Deflection profile at centerline of joists

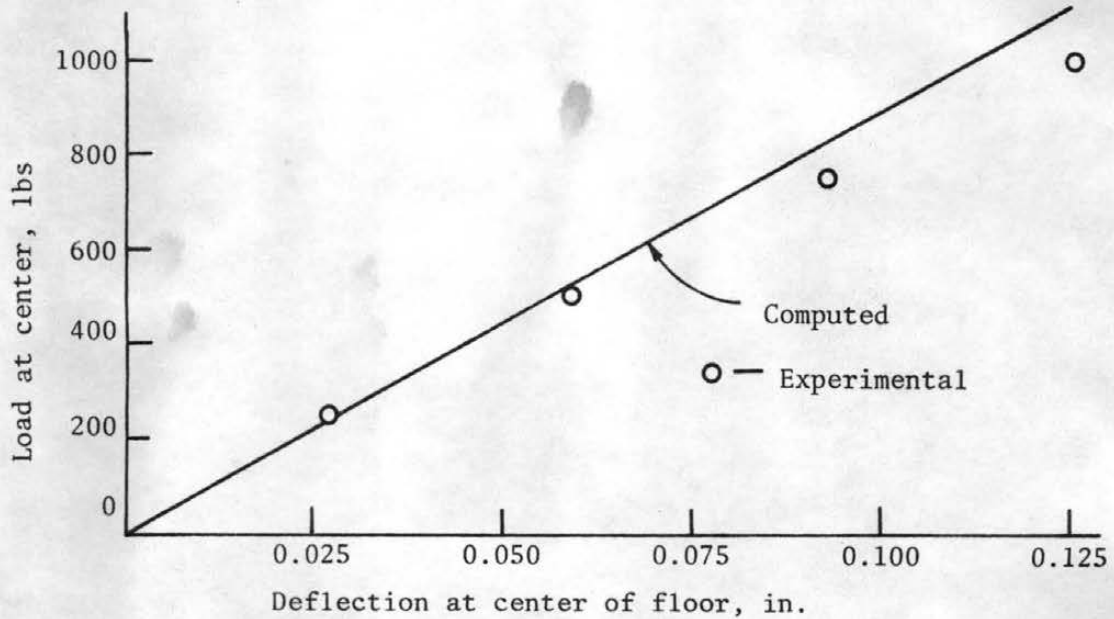


(b) Load-deflection behavior

Figure D.1 Computed vs Measured Results of Floor Specimen F3-8D16-1

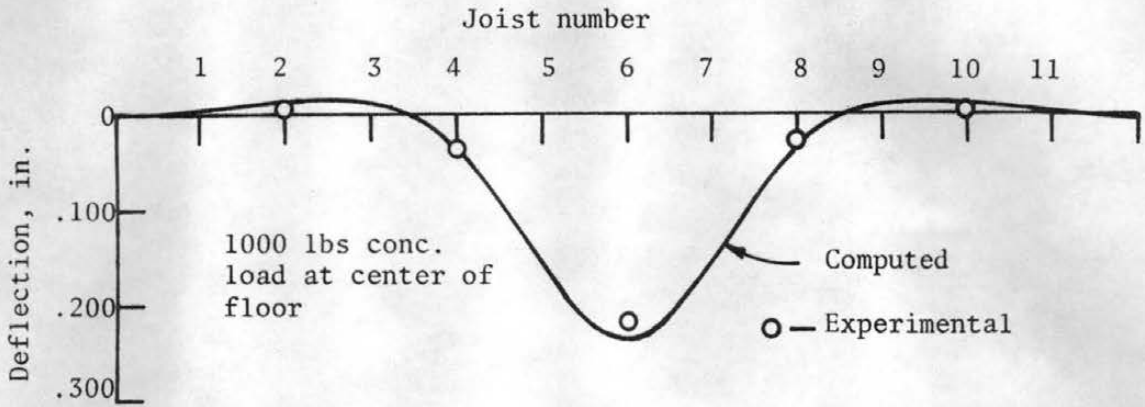


(a) Deflection profile at centerline of joists

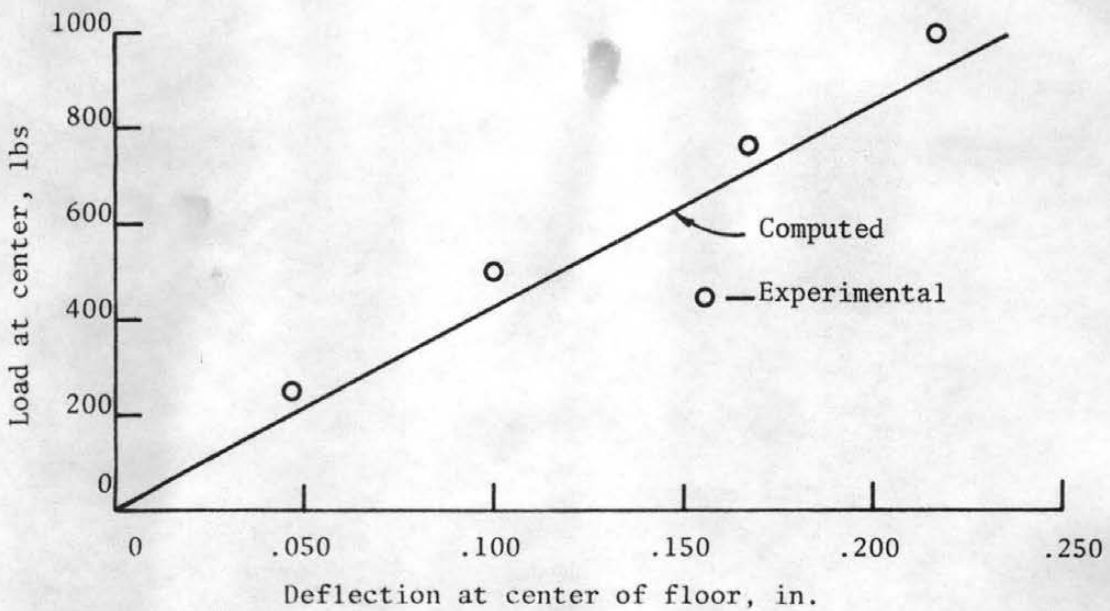


(b) Load-deflection behavior

Figure D.2 Computed vs Measured Results of Floor Specimen F4-8E16-1

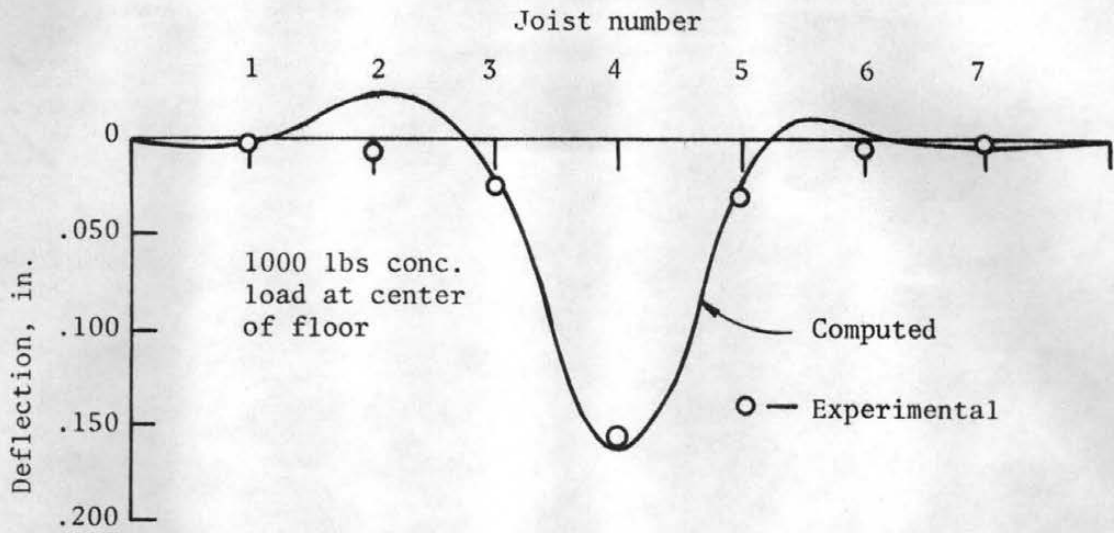


(a) Deflection profile at centerline of joists

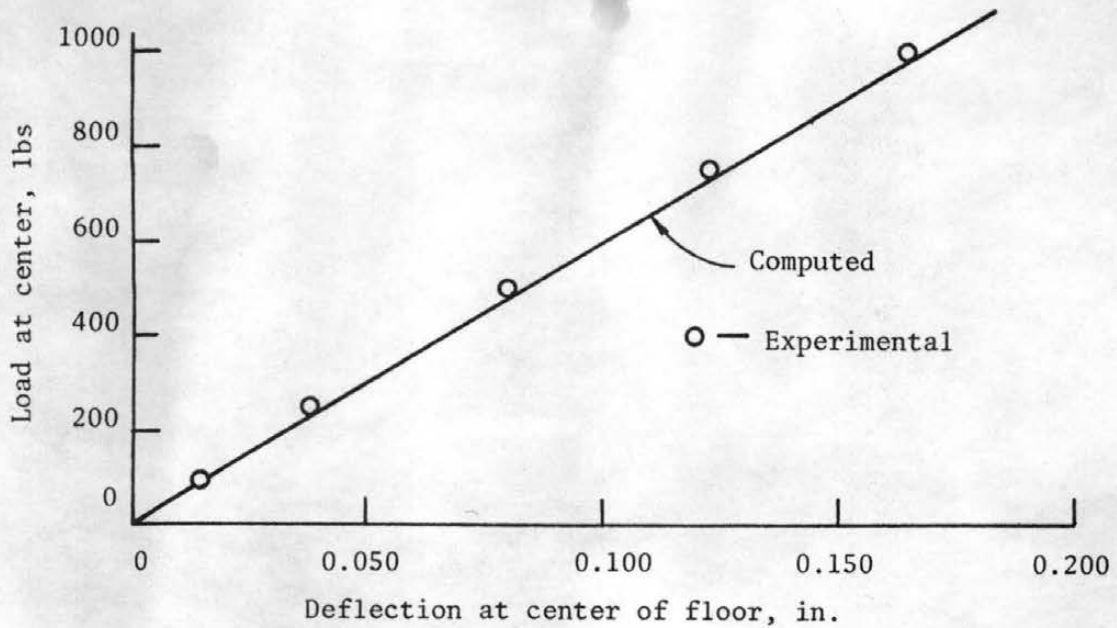


(b) Load-deflection behavior

Figure D.3 Computed and Measured Results of Floor Specimen F5-8D16-1

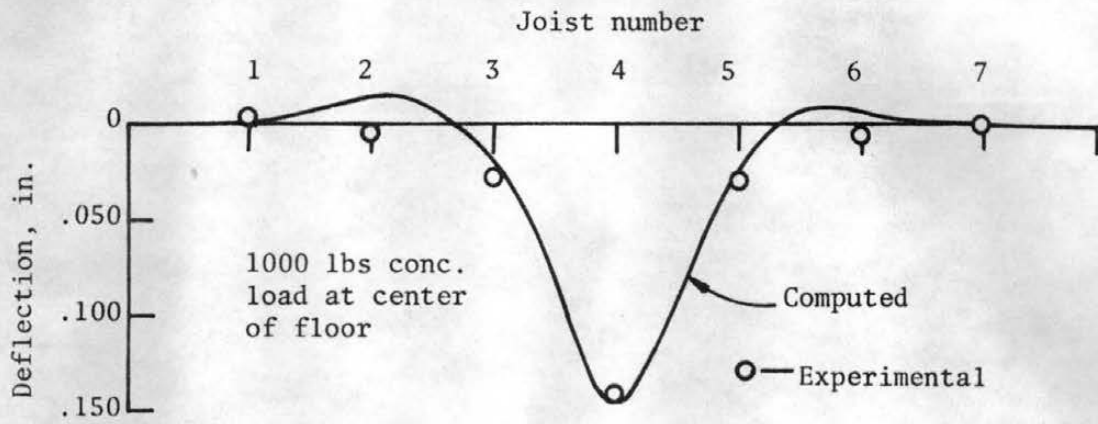


(a) Deflection profile at centerline of joists

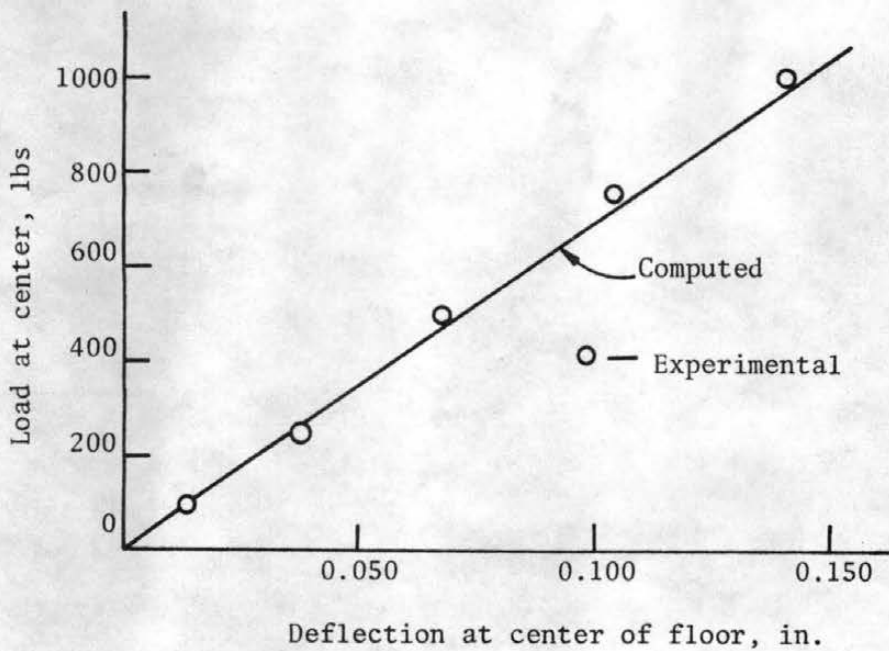


(b) Load-deflection behavior

Figure D.4 Computed vs Measured Results of Floor Specimen F7-12D24-1

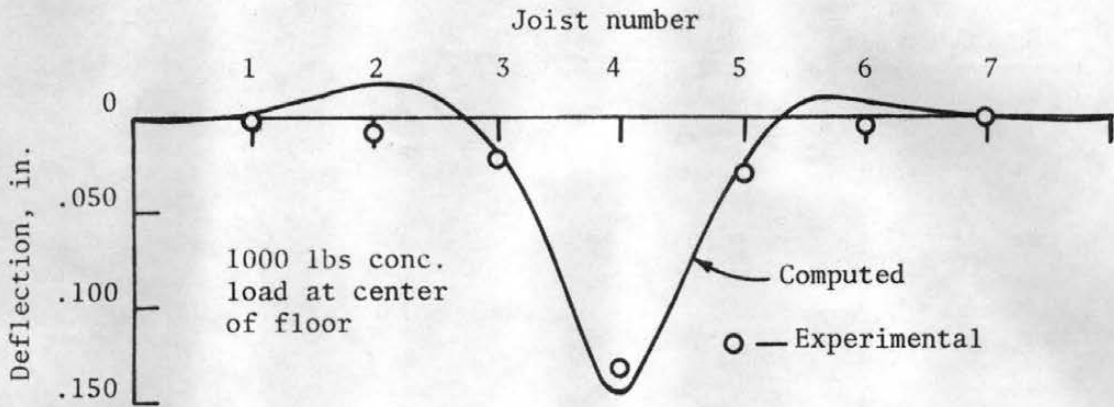


(a) Deflection profile at centerline of joists

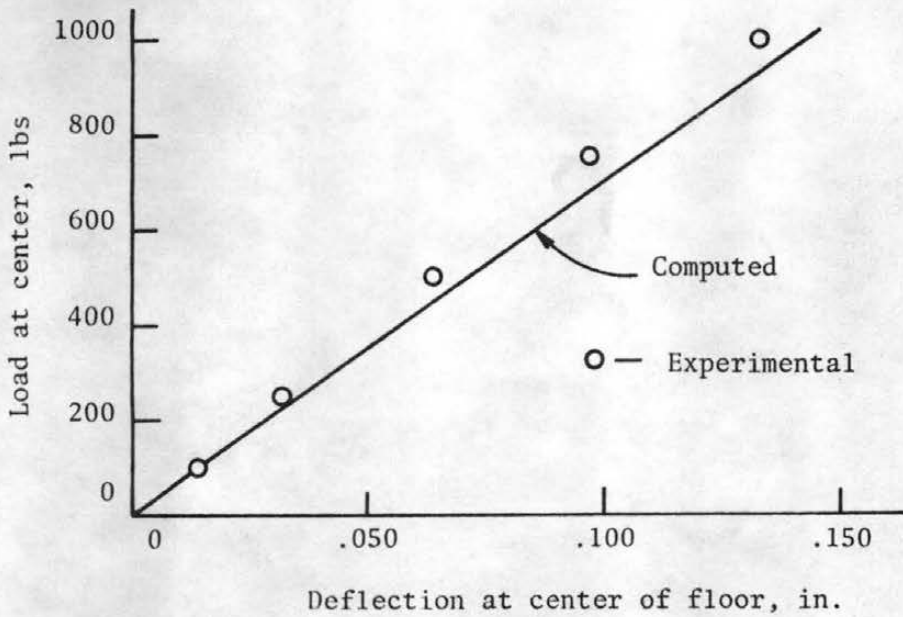


(b) Load-deflection behavior

Figure D.5 Computed vs Measured Results of Floor Specimen F7-12D24-2 (Nails of Top Layer Not Driven into Joists)

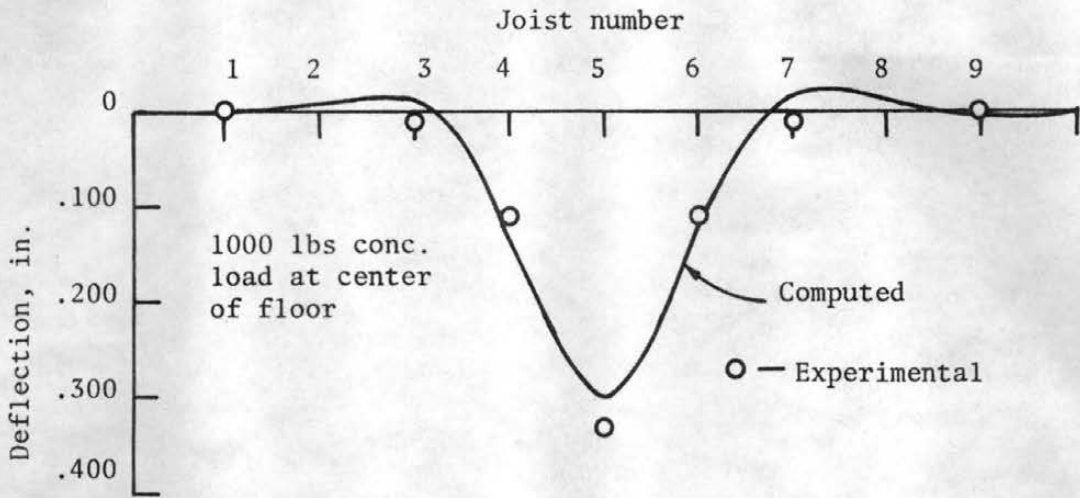


(a) Deflection profile at centerline of joists

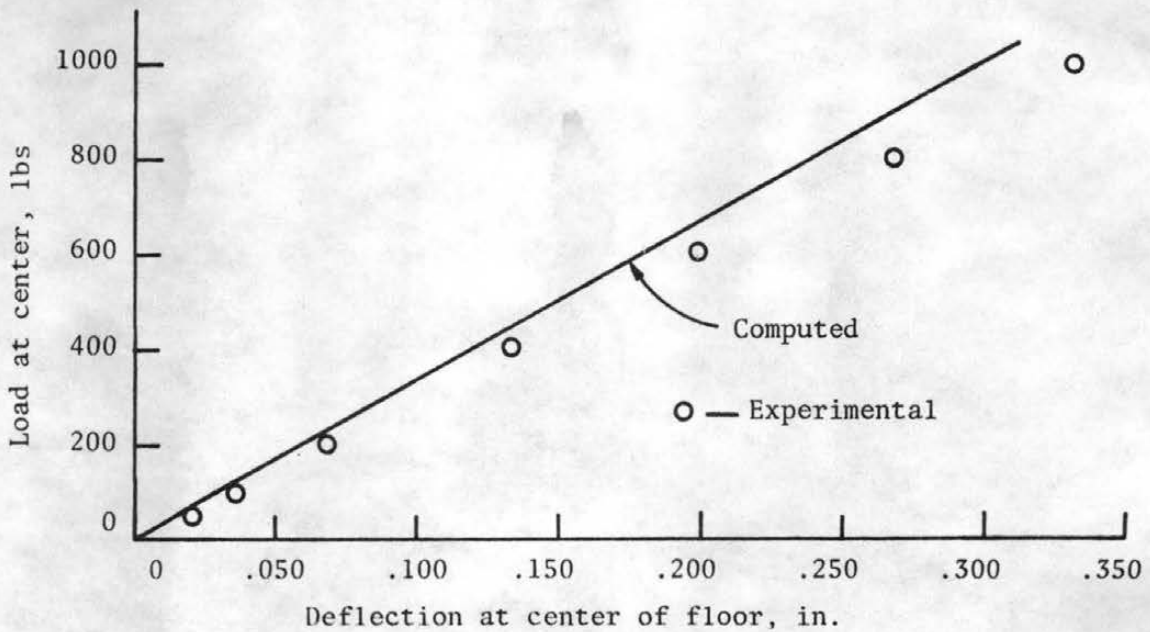


(b) Load-deflection behavior

Figure D.6 Computed vs Measured Results of Floor Specimen F7-12D24-2 (Nails of Top Layer Driven into Joists)

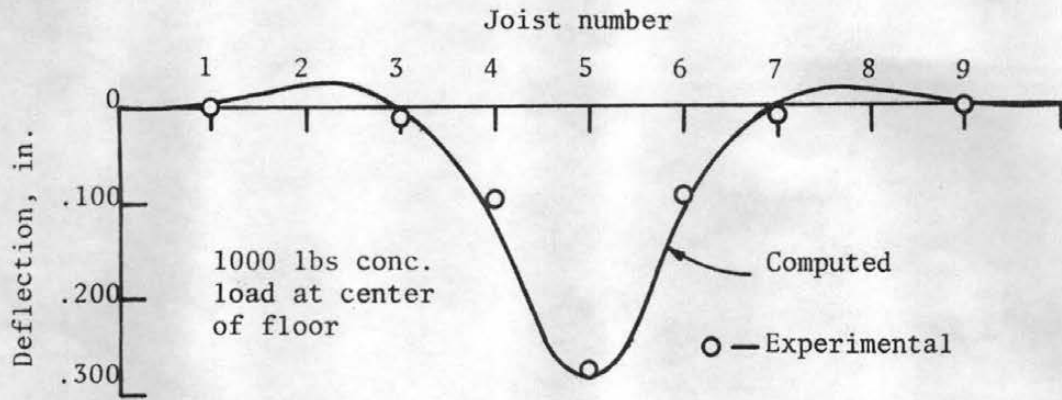


(a) Deflection profile at centerline of joists

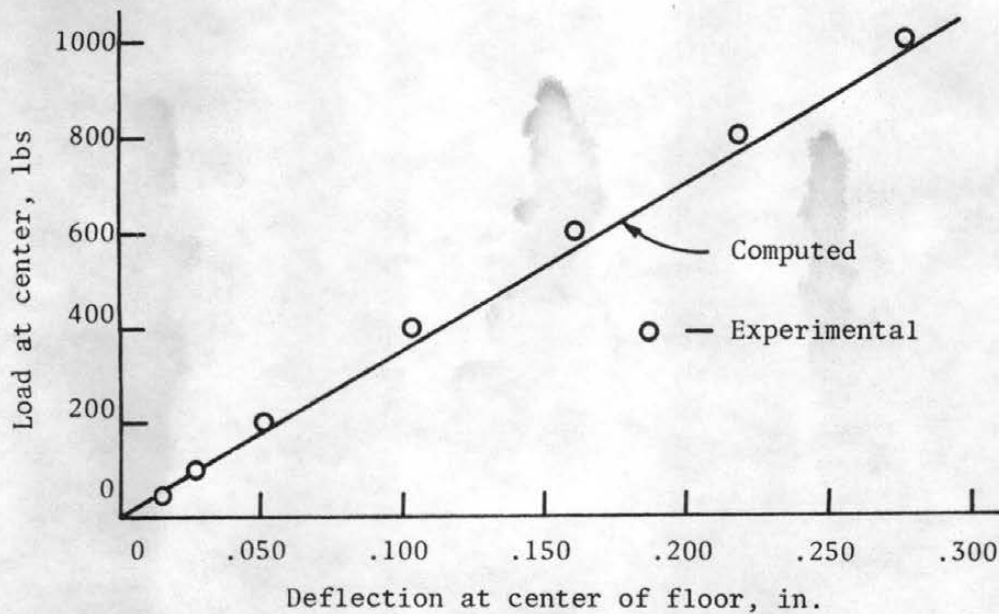


(b) Load-deflection behavior

Figure D.7 Computed vs Measured Results of Floor Specimen F8-8D19.2-1

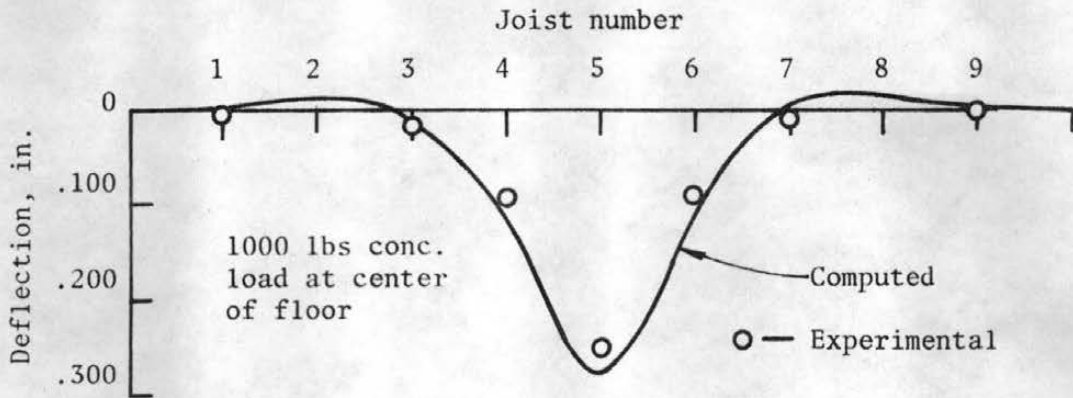


(a) Deflection profile at centerline of joists

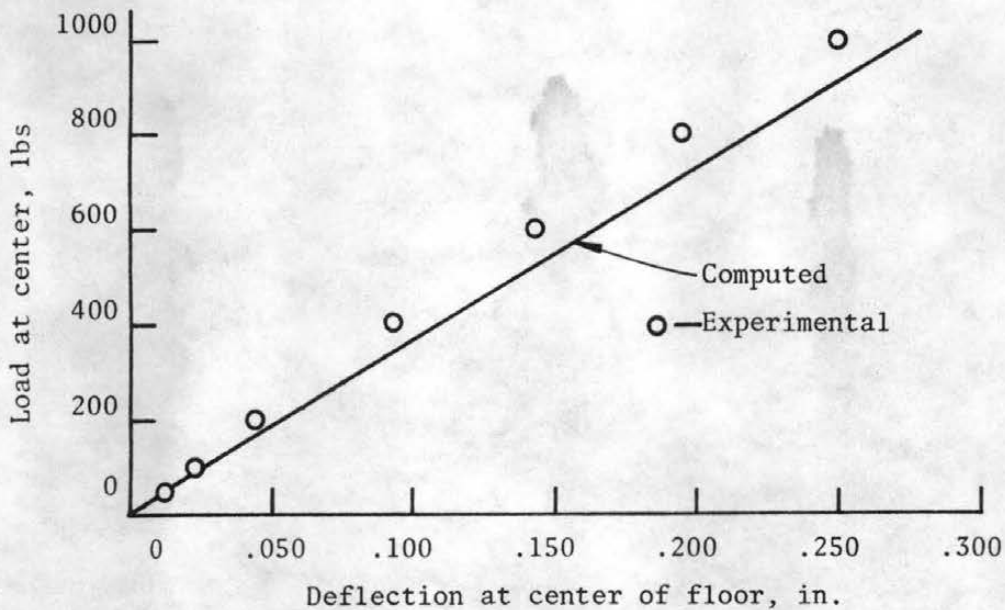


(b) Load-deflection behavior

Figure D.8 Computed vs Measured Results of Floor Specimen F8-8D19.2-2  
(Nails of Top Layer Not Driven into Joists)

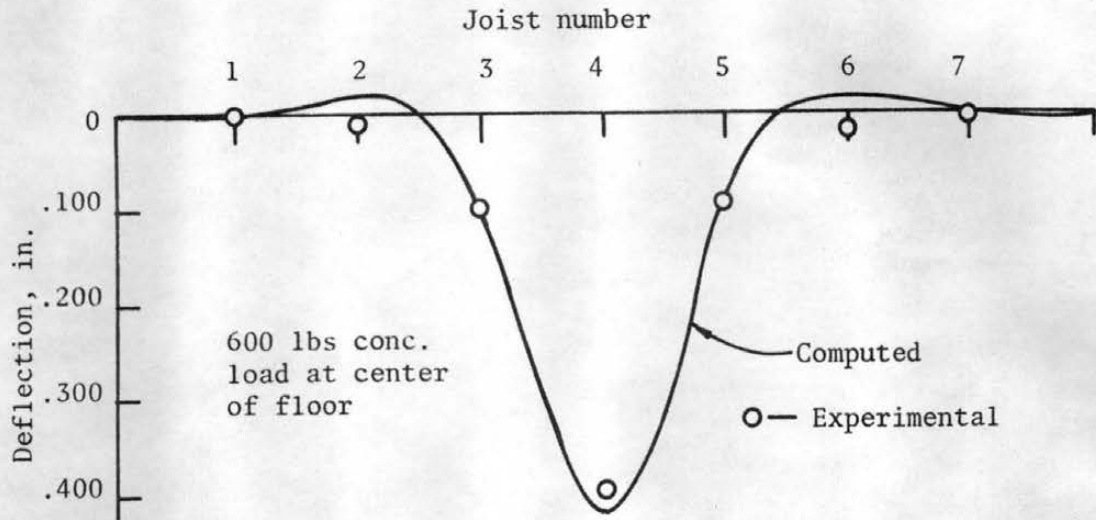


(a) Deflection profile at centerline of joists

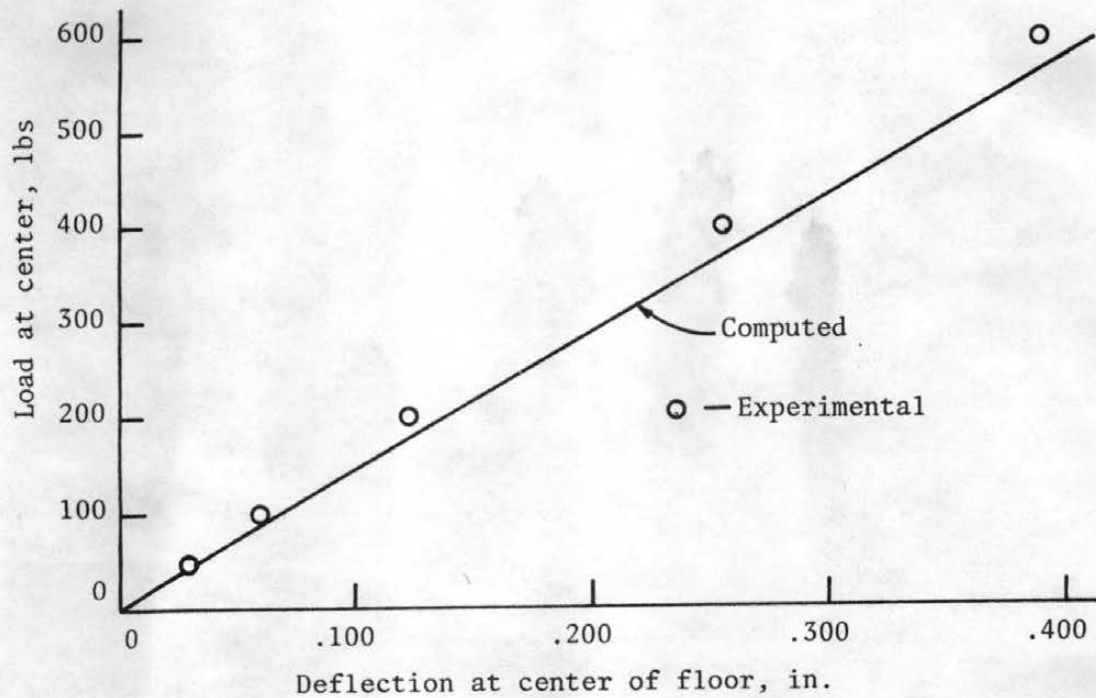


(b) Load-deflection behavior

Figure D.9 Computed vs Measured Results of Floor Specimen F8-8D19.2-2 (Nails of Top Layer Driven into Joists)

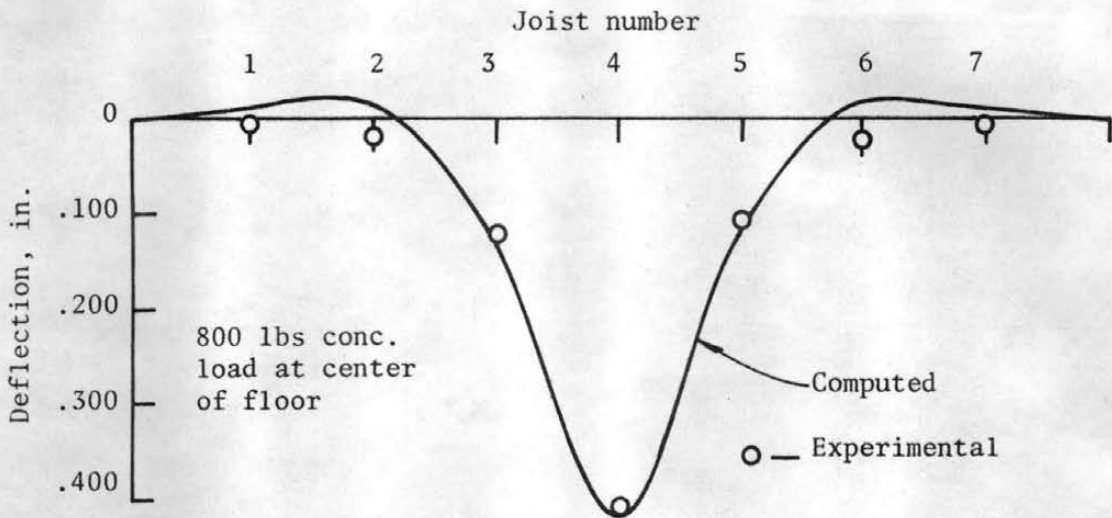


(a) Deflection profile at centerline of joists

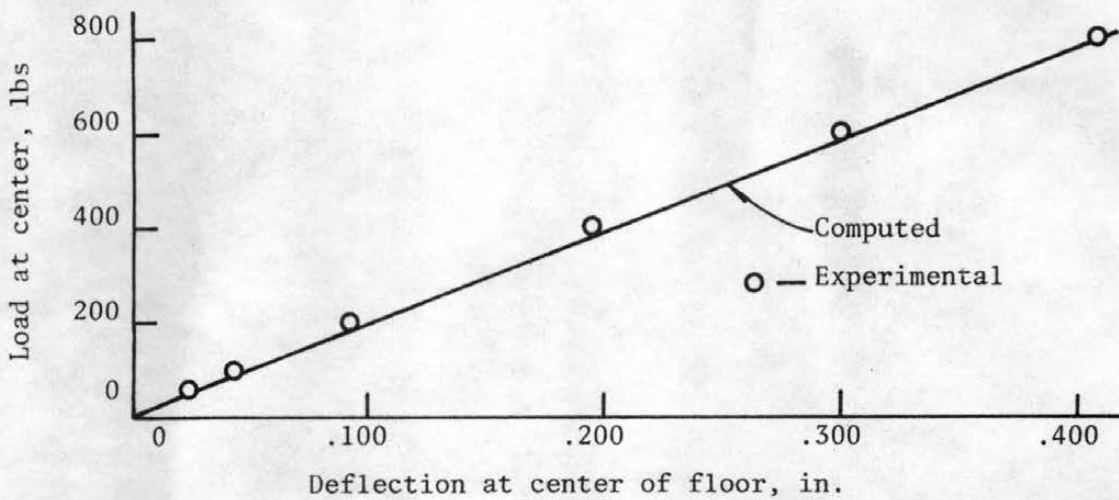


(b) Load-deflection behavior

Figure D.10 Computed vs Measured Results of Floor Specimen F9-8E24-1

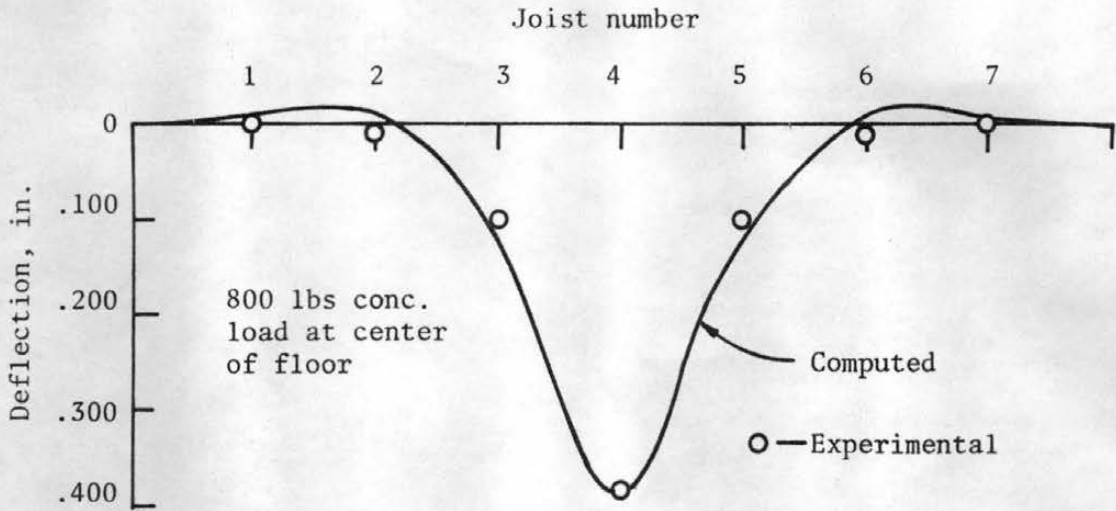


(a) Deflection profile of centerline of joists

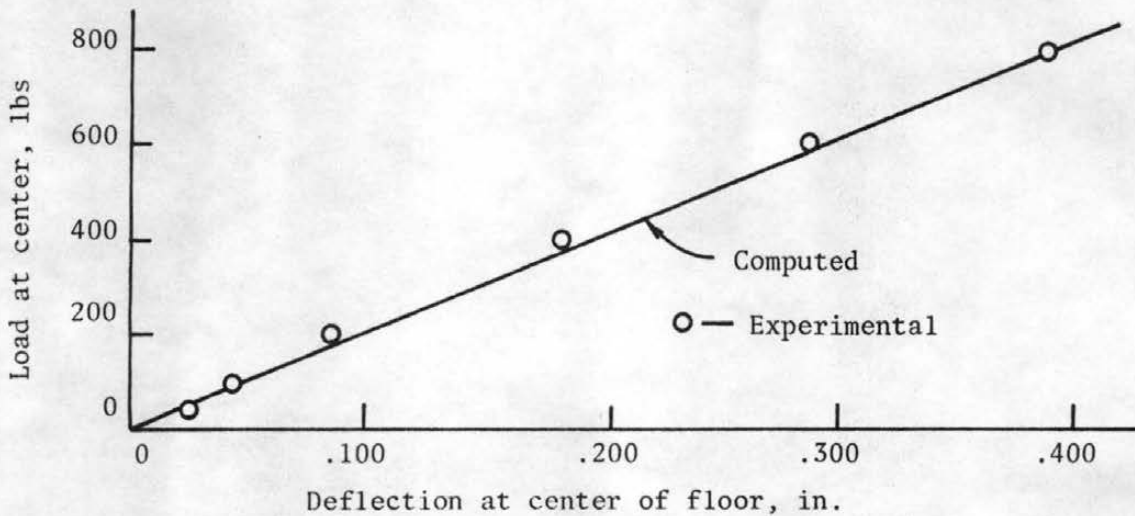


(b) Load-deflection behavior

Figure D.11 Computed vs Measured Results of Floor Specimen F9-8E24-2 (Nails of Top Layer Not Driven into Joists)

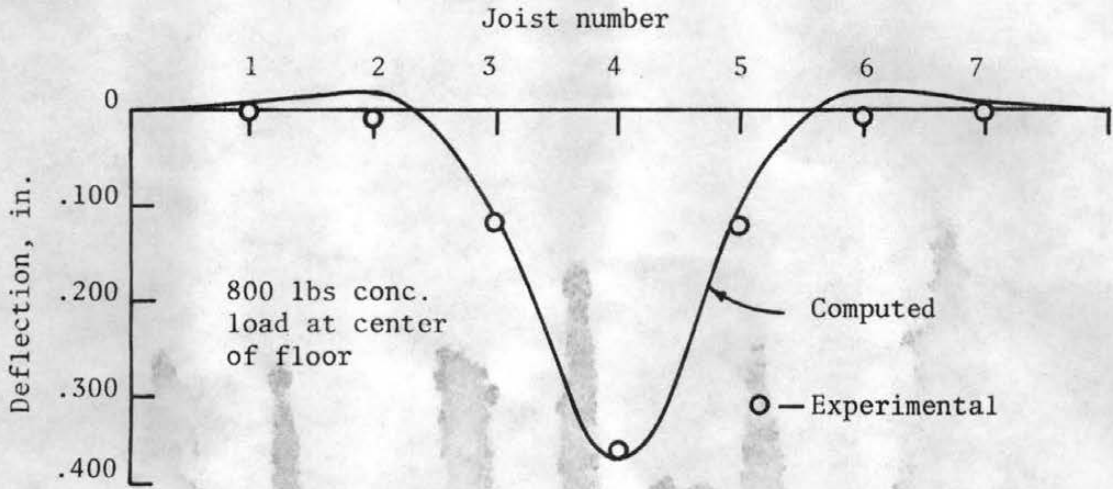


(a) Deflection profile at centerline of joists

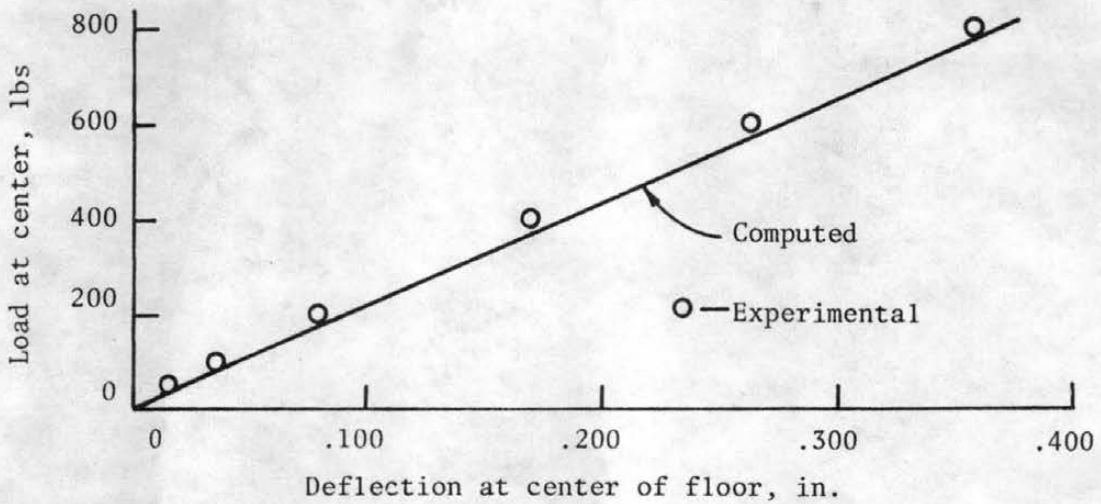


(b) Load-deflection behavior

Figure D.12 Computed vs Measured Results of Floor Specimen F9-8E24-2 (Nails of Top Layer Driven into Joists)

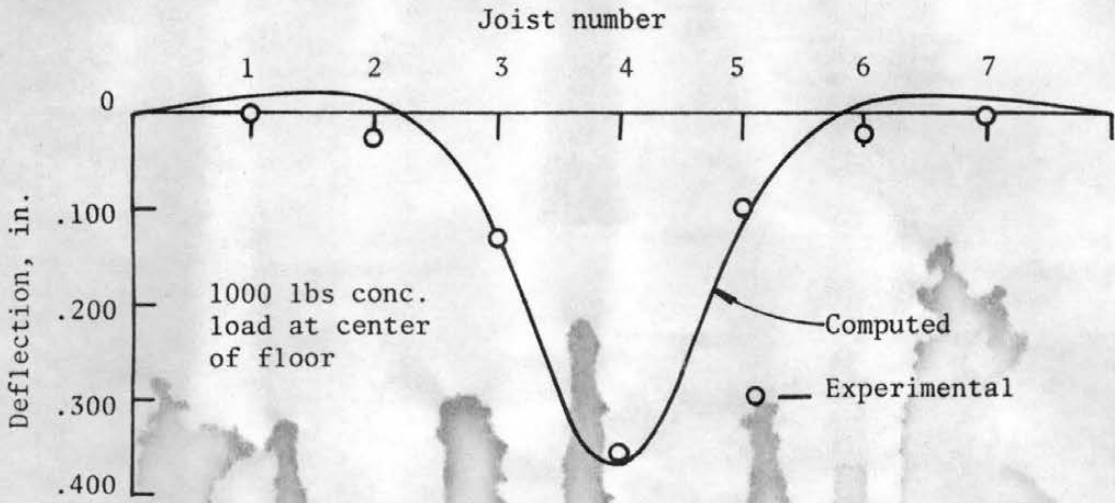


(a) Deflection profile at centerline of joists

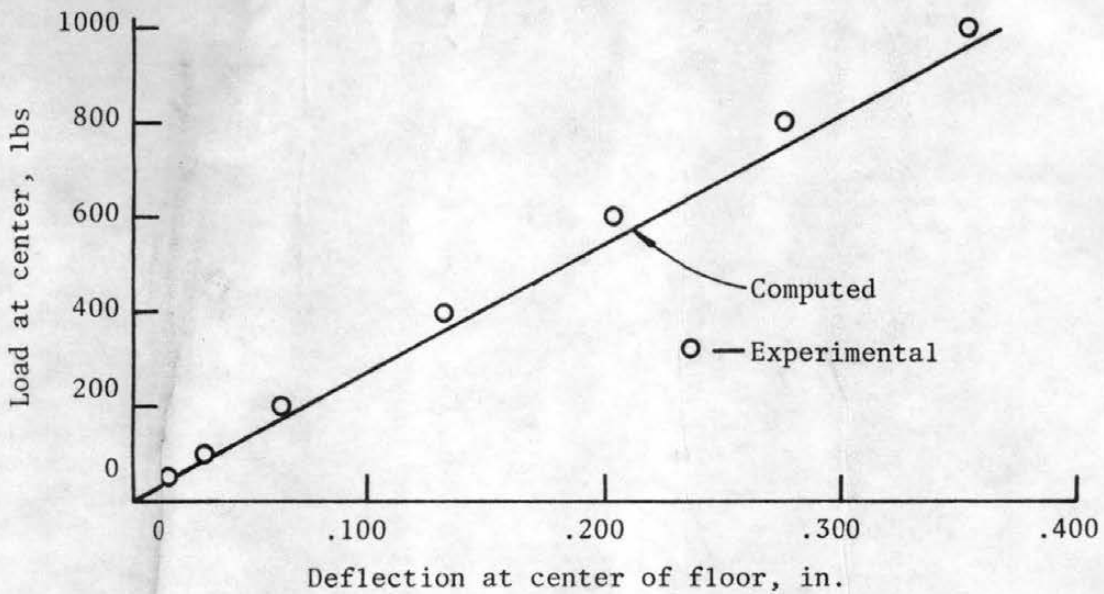


(b) Load-deflection behavior

Figure D.13 Computed vs Measured Results of Floor Specimen F10-8E24-1

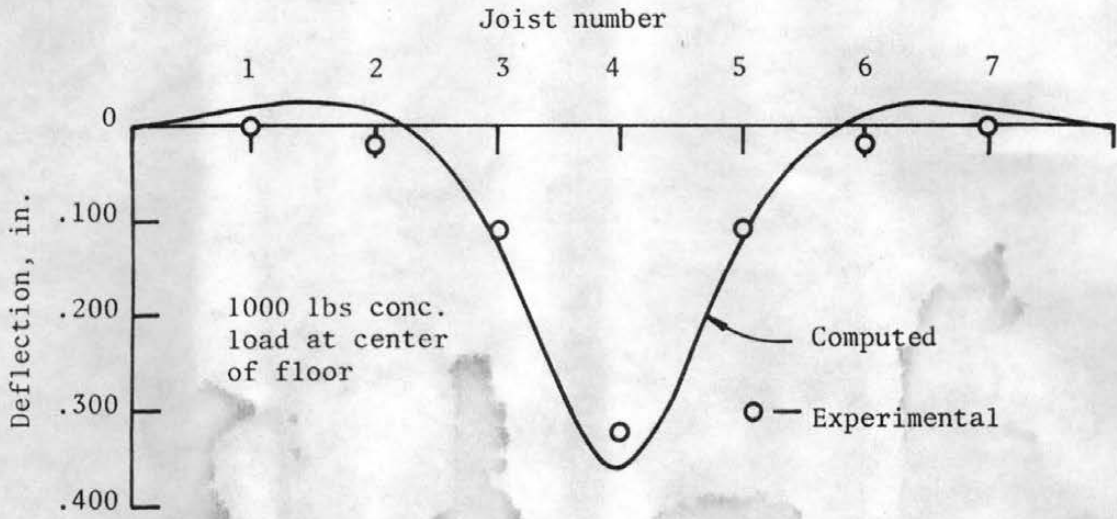


(a) Deflection profile at centerline of joists

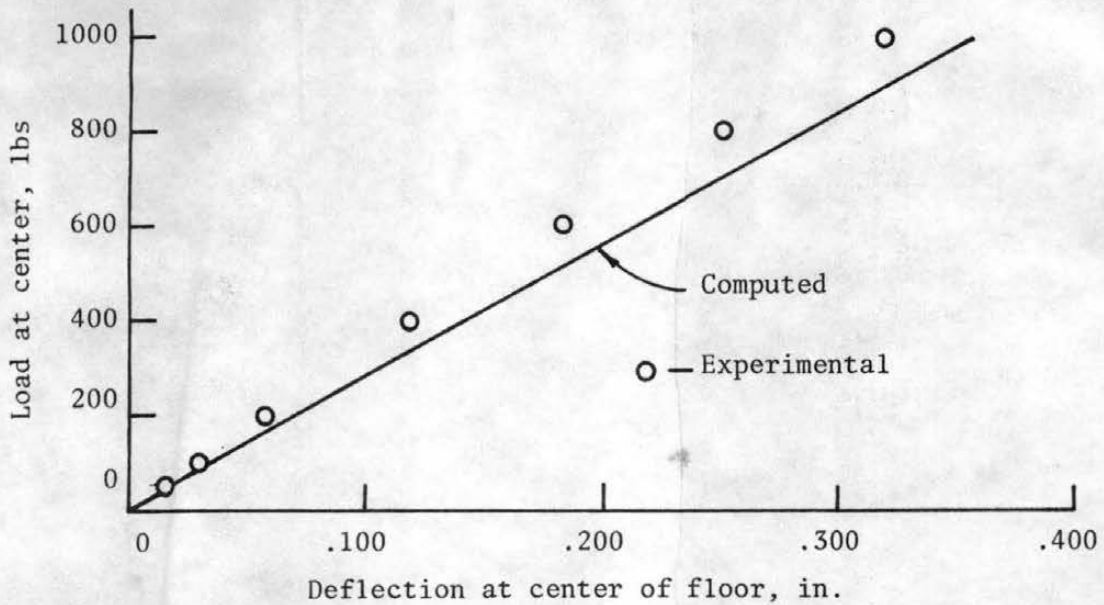


(b) Load-deflection behavior

Figure D.14 Computed vs Measured Results of Floor Specimen F10-8E24-2  
(Nails of Top Layer Not Driven into Joists)

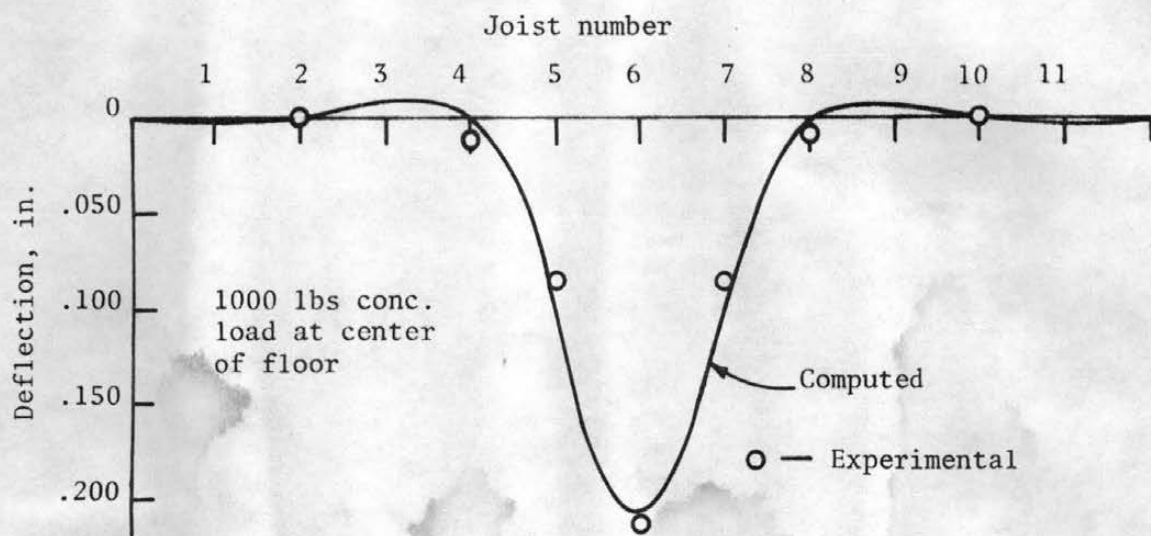


(a) Deflection profile at centerline of joists

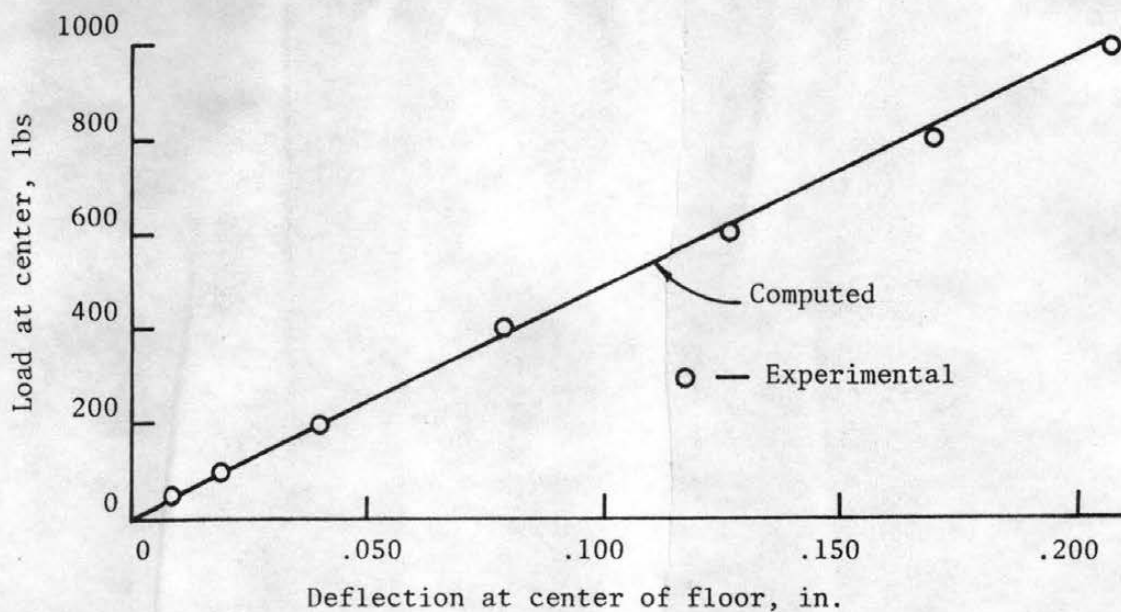


(b) Load-deflection behavior

Figure D.15 Computed vs Measured Results of Floor Specimen F10-8E24-2 (Nails of Top Layer Driven into Joists)



(a) Deflection profile at centerline of joists



(b) Load-deflection behavior

Figure D.16 Computed vs Measured Results of Floor Specimen F11-8D16-1

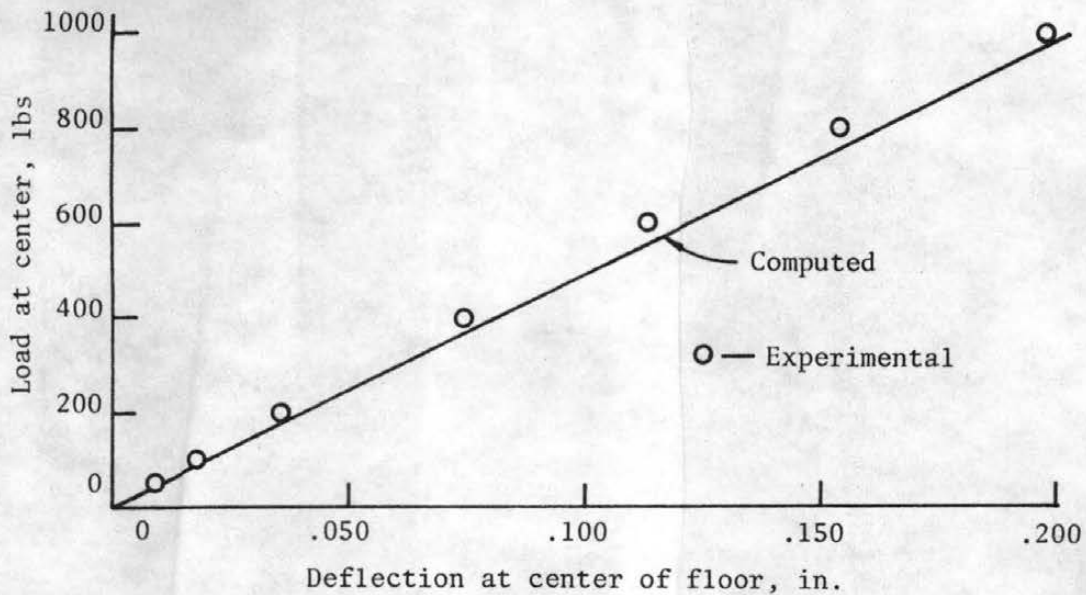
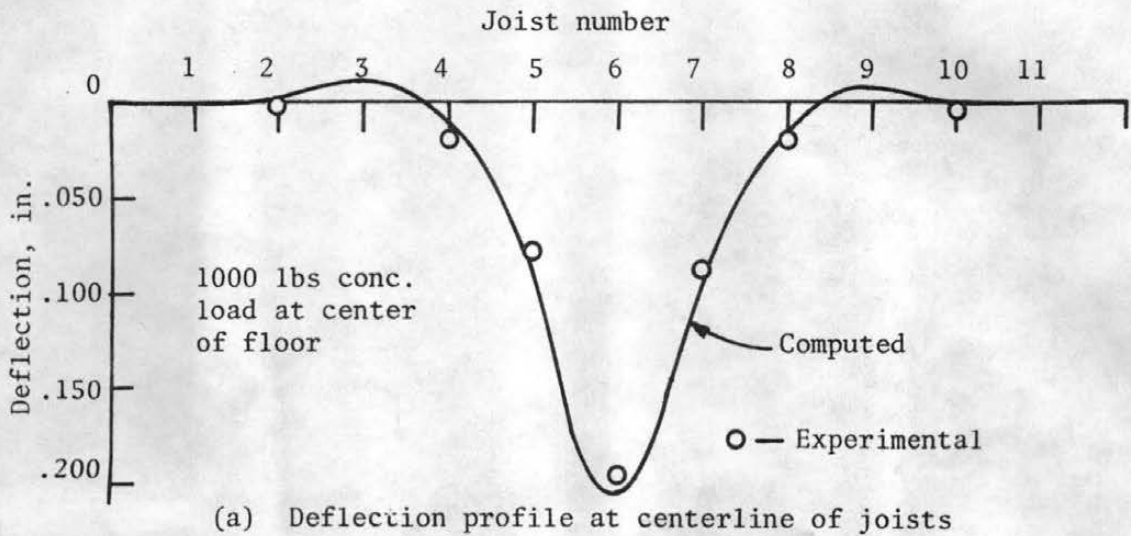
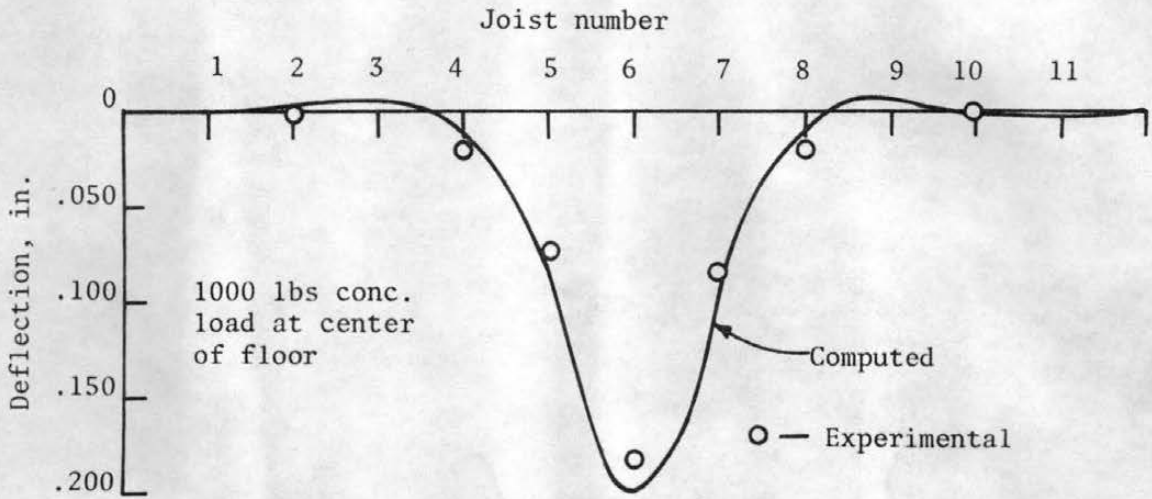
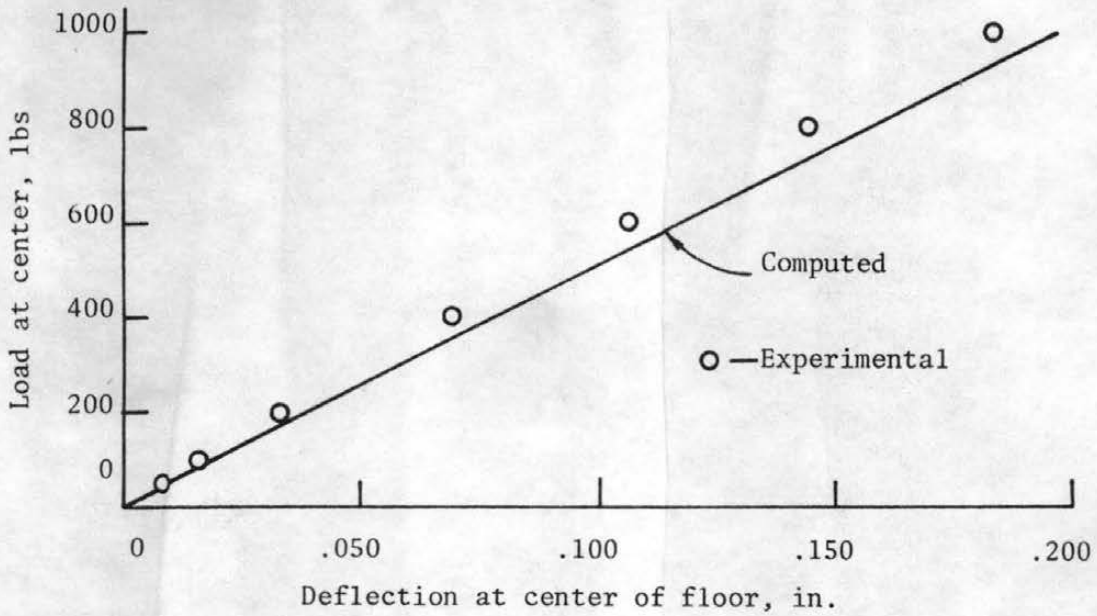


Figure D.17 Computed vs Measured Results of Floor Specimen F11-8D16-2 (Nails of Top Layer Not Driven into Joists)



(a) Deflection profile at centerline of joists



(b) Load-deflection behavior

Figure D.18 Computed vs Measured Results of Floor Specimen F11-8D16-2 (Nails of Top Layer Driven into Joists)

APPENDIX E

LISTING OF A COMPUTER PROGRAM FOR  
EVALUATING EFFECTIVE FLANGE WIDTH OF  
T-BEAM SYSTEMS

```

FTN.
LGO.
000000000000000000000000
PROGRAM EFLANGE
1 (INPUT,OUTPUT,TAPE5=INPUT,TAPE6=OUTPUT)
REAL K,LOAD,NU,LAM1,LAM2,LM1,LM2,NROW,I1,I2,KSTR,MNT(100)
DIMENSION W(100),P(100),Q(100),CH1(100),CH2(100),SH1(100),SH2(100)
1      ,D(100),PQ1(100),PQ2(100),CH11(100),CH22(100),SH11(100),
2      SH22(100),CF(100),CG(100),CR(100),CS(100),FS(100),CH(100)
3      ),EFW1(100),SIGX(20),CH1Y(100),CH2Y(100),SH1Y(100),
4      SH2Y(100)
C
C
C READ IN AN ALPHANUMERIC HEADER CARD. PLACE 1 IN COLUMN 1 OF HEADER CARD.
200 READ(5,300)
300 FORMAT(80H
1
IF (EOF(5)) 100,50
C
C
C READ IN MATERIAL PROPERTIES, CONNECTOR PROPERTIES, AND GEOMETRIC DIMENSIONS.
C E1X = MODULUS OF ELASTICITY OF TOP LAYER IN BEAM DIRECTION.
C E1Y = MODULUS OF ELASTICITY OF TOP LAYER IN FLANGE DIRECTION.
C E2X = MODULUS OF ELASTICITY OF BOTTOM LAYER IN BEAM DIRECTION.
C G = SHEAR MODULUS IN FLANGE PLANE.
C NU = POISSON'S RATIO OF TOP LAYER FOR PASSIVE STRAIN IN FLANGE DIRECTION,
C DUE TO ACTIVE STRAIN IN BEAM DIRECTION.
C K = CONNECTOR SLIP MODULUS.
C S = CONNECTOR SPACING.
C NROW = NO. OF ROWS OF CONNECTOR.
C H1 = THICKNESS OF TOP LAYER.
C H2 = DEPTH OF BOTTOM LAYER.
C W1 = WIDTH OF TOP LAYER.
C W2 = WIDTH OF BOTTOM LAYER.
C NMAX = NO. OF TERMS IN A SERIES TO BE SUMMED UP.
C LOAD= CONCENTRATED LOAD AT MID-SPAN IN LBS OR UNIFORMLY DISTRIBUTED LOAD
C IN LBS/INCH.
50 READ(5,400) E1X,E1Y,E2X,G,NU,K,S,NROW
READ(5,410) SPAN, H1, W1, H2, W2, KSTR, LOAD, NMAX
400 FORMAT(8F10,2)
410 FORMAT(7F10,3,I10)
C
C
C COMPUTE GEOMETRIC CONSTANTS.
E1STR = KSTR*E1X
A1 = H1*W1
A2 = H2*W2
I1 = W1*H1**3/12.
I2 = W2*H2**3/12.
C12 = 0.5*(H1 + H2)
C
C
C COMPUTE CONSTANTS INVOLVING MATERIAL PROPERTIES BUT INDEPENDENT OF NO.
C OF TERMS N.
E1 = E1X*I1 + E2X*I2
ALFA = 0.5*E1X/G - NU
BETA = E1X/E1Y
LAM1 = SQRT(ALFA + SQRT(ALFA**2 - BETA))
LAM2 = SQRT(ALFA - SQRT(ALFA**2 - BETA))
GAMA = E1X/G - NU
CP = LAM1/LAM2*(LAM1**2-GAMA)/(LAM2**2-GAMA)
LM1 = 0.5*(LAM2 + LAM1)
LM2 = 0.5*(LAM2 - LAM1)

```

```

C BUILD IN CONSTANTS.
  PIF = 3.14159265
  EXPO = 2.71828183
C
C HEAD IN NO. OF NODE POINT WHERE THE EFFECTIVE FLANGE WIDTH AND BEAM
C DEFLECTION ARE TO BE COMPUTED.
C KEY = 1 FOR CONCENTRATED LOAD AT MID SPAN OF BEAM.
C KEY = 0 FOR UNIFORMLY DISTRIBUTED LOAD.
  READ(5,501) NOSX,KEY
501  FORMAT(2I10)
      ANOSX=NOSX
C SPNG = SPACING BETWEEN NODE POINTS.
C NOP = NO. OF NODE POINT.
  SPNGX = SPAN/ANOSX
  NOPX = NOSX - 1
C
C PRINT HEADINGS AND INPUT DATA.
  WRITE(6,300)
  WRITE(6,510)
510  FORMAT(/** MATERIAL AND CONNECTOR PROPERTIES*)
  WRITE(6,520)
520  FORMAT(/**
      E1X      E1Y      E2X
      NU      K      S      NROW*)
  WRITE(6,530) F1X, E1Y, E2X, G, NU, K, S, NROW
530  FORMAT(8(3X,F12.2))
  WRITE(6,540)
540  FORMAT(/** GEOMETRIC DIMENSIONS*)
  WRITE(6,550)
550  FORMAT(/**
      SPAN      H1      W1      H2
      W2*)
  WRITE(6,560) SPAN,H1,W1,H2,W2
560  FORMAT(5(4X,F10.3))
  WRITE(6,580) KSTR
580  FORMAT(/** KSTR = *F10.4)
  WRITE(6,600) SPAN,NOSX
600  FORMAT(/** PIECE LENGTH = *F4.0*. THIS PIECE IS DIVIDED INTO *I3*
  ISPACING(S.*)
  DO 20 M=1,NOPX
    AM = M
    X = AM*SPNGX
    SUM1 = 0.0
    SUM2 = 0.0
    MNT(M) = 0.0
    EFWM(M) = 0.0
C EFWM(M) = EFFECTIVE FLANGE WIDTH AT NODE POINT M.
C
C BEGINNING OF DO LOOP TO EVALUATE CONSTANTS INVOLVING NO. OF TERM N.
  DO 10 J = 1,NHAX
    N = 2*J - 1
    AN = N
    W(N) = AN*PIE/SPAN
    P(N) = 0.5*LAM1*W(N)*W1
    Q(N) = 0.5*LAM2*W(N)*W1
C
C CHI=COSH(P(N))
C CH2(N)=COSH(Q(N)).
C SH1(N)=SINH(P(N)).
C SH2(N)=SINH(Q(N)).
    CHI(N) = 0.5*(EXPO**P(N) + EXPO**(-P(N)))
    CH2(N) = 0.5*(EXPO**Q(N) + EXPO**(-Q(N)))
    SH1(N) = 0.5*(EXPO**P(N) - EXPO**(-P(N)))
    SH2(N) = 0.5*(EXPO**Q(N) - EXPO**(-Q(N)))
  
```

```

PQ1(N) = P(N) * Q(N)
PQ2(N) = P(N) - Q(N)
C
C CH11(N) = COSH(PQ1(N)).
C CH22(N) = COSH(PQ2(N)).
C SH11(N) = SINH(PQ1(N)).
C SH22(N) = SINH(PQ2(N)).
  CH11(N) = 0.5*(EXPO**PQ1(N) + EXPO**(-PQ1(N)))
  CH22(N) = 0.5*(EXPO**PQ2(N) + EXPO**(-PQ2(N)))
  SH11(N) = 0.5*(EXPO**PQ1(N) - EXPO**(-PQ1(N)))
  SH22(N) = 0.5*(EXPO**PQ2(N) - EXPO**(-PQ2(N)))
C
C CF(N) = A(N)/D(N)
C CG(N) = B(N)/D(N)
  CF(N) = (LM2*CH11(N) - LM1*CH22(N) + LAM2*CP)/(CP*(LM2*SH11(N) -
  1 LM1*SH22(N)))
  CG(N) = (LAM1 - CP*(LM2*CH11(N) + LM1*CH22(N)))/(CP*(LM2*SH11(N) -
  1 LM1*SH22(N)))
C
C CR(N) = W(N)**2*(CF(N)*(LAM1**2 + NU) + CG(N)*(LAM2**2 + NU))
C CS(N) = W(N)*((CF(N)*SH1(N)-CH1(N)/CP+1./CP)*LAM1 + (CG(N)*SH2(N)
  1 +CH2(N)-1.)*LAM2)
C FS(N) = FOURIER COEFFICIENT OF MOMENT EXPANDED IN SINE SERIES.VARIES
C WITH LOADING CONDITIONS.
  IF(KEY .EQ. 1) GO TO 303
  FS(N)=LOAD*64R00.*(1.-COS(AN*PIE))/(AN*PIE)**3
  IF(KEY .EQ. 0) GO TO 404
  FS(N)=LOAD*360.*SIN(AN*PIE*0.5)/(AN*PIE)**2
303 CONTINUE
404
C CH(N) = D(N)/FS(N).
  CH(N) = C12/EI/(CR(N)/E1STR + 2.*H1*CS(N)*(1./A2/E2X + C12**2/EI *
  1 W(N)**2*S/K/NROW))
  D(N) = CH(N)*FS(N)
  MNT(M) = MNT(M) + FS(N)*SIN(AN*PIE*X/SPAN)
  SUM1 = SUM1 + 2.*D(N)*CS(N)*SIN(W(N)*X)
  SUM2 = SUM2 + D(N)*W(N)**2*(CF(N)*LAM1**2 + CG(N)*LAM2**2)*SIN(
  1 W(N)*X)
  SUM = SUM1/SUM2
  EFW1(M) = SUM
CONTINUE
10 WRITE(6,700) M, EFW1(M), J, MNT(M)
700 FORMAT(//* BEAM NODE POINT = *12*, EFFECTIVE FLANGE WIDTH = *
  1 G10.5*, NO. OF TERMS = *13*, MOMENT = *G10.3)
20 CONTINUE
GO TO 200
100 CONTINUE
STOP
END

```